Development of Methods for Characterizing Ankle Ligament Viscoelastic Properties

Alexander T. Berardo-Cates

A thesis

submitted in partial fulfillment of the

requirements for the degree of

Master of Science in Engineering

University of Washington

2019

Reading Committee:

Joseph Iaquinto, Chair

Ashley Emery

Nathan Sniadecki

William Ledoux

Program Authorized to Offer Degree:

Department of Mechanical Engineering

University of Washington

Abstract

Development of Methods for Characterizing Ankle Ligament Viscoelastic Properties

Alexander Berardo-Cates

Chair of the Supervisory Committee:
Dr. Joseph Iaquinto
Department of Mechanical Engineering

The goal of this work is to develop methods for determining the viscoelastic properties of ankle ligaments. The tibiocalcaneal ligament was used for the method development and for the preliminary mechanical testing presented in this work. This document focuses primarily on the development of several novel approaches to: morphological length and cross-sectional area measurements, *in situ* pose maintenance during ligament extraction and testing, and automated mechanical testing. Additionally, preliminary ligaments are mechanically tested using an exhaustive battery to determine their strain rate-dependent properties. Traditional caliper length (CL) measures are augmented by novel ligament linear length (LL) measures determined by a straight line between the centroids of insertion surfaces, and iterative length (IL) measures which refine the LL to define a length that wraps about the center of the ligament body along its

longitudinal axis. Cross-sectional area was estimated from an elliptical and rectangular fit to caliper measurements and from computed tomography (CT) scans. The mechanical properties from these length estimates are compared to caliper length measurements. Caliper length estimates were ~ 25% > LL and IL which were similar in length (≤ ~10%). There was ~80% variation in cross-sectional area measurements. This resulted in ~8-15% average change in modulus of elasticity. Peak force and hysteresis increased by 80% and 250% respectfully between length estimate strain levels. Ligament differed from *in situ* pose by about 23^{o} (± 6.6^{o}) and 1.4 mm (± 4.13 mm). Minimal loading rate-dependent differences in stiffness, modulus, and peak force were measured. However, a general rate dependent modulus change was observed from the plotted relationship. Temperature was maintained within ± 1.3 ^{o}C of the target temperature (37 ^{o}C) and specimens remained moist for the duration of mechanical tests. A quasi-linear viscoelastic (QLV) model was successfully fit to the data with minimal error (RMSE < 0.1) in most tests. There was a notable challenge relating to the mechanical testing system that led to the actuator not reaching the intended strain level at higher strain rates. This is a common challenge with mechanical testing, and additional steps are proposed to address this limitation in ongoing, further testing is required to determine the mechanical characteristics of these ligaments.

TABLE OF CONTENTS

LIST OF FIGURES

LIST OF TABLES

ACKNOWLEDGEMENTS

I would like to thank and acknowledge Dr. Joseph Iaquinto, Dr. William Ledoux, and my fellow lab mates for their help and guidance, the VA for funding this research project, and my family for their support. Each have played a vital role in the completion of this work. Thank you.

Chapter 1. INTRODUCTION

1.1 OVERVIEW

Articular ligaments provide structural support essential for joint stability and mobility. Ligaments are a connective tissue comprised of collagenous fibrous bundles that bind together bones of the body and cross joints. The mechanical function of articular ligaments is to maintain joint alignment by supporting desired motions between bones and inhibiting undesired motions. Thus, understanding the native function and potential for injury is critical for healthy joint function since ligamental structures can disrupt the balance between joint stability and joint mobility.

Some ligaments are recognizable structures as dense white bands of connective tissue, while others blend into the joint capsule and appear to be thickening of the capsule (i.e., glenohumeral ligament). Like ligaments, tendons also connect to bone and are mechanically similar connective tissues. However, ligaments have a variable orientation of collagen fibrils making them slightly less resistant to tensile stress but better able to function within a range of loading directions without damage [1]. The collagen fibers have a varied arrangement that enable the ligament to resist forces from more than one direction. For example, in the medial collateral ligament (MCL), the posterior fibers are under tension during knee extension, while the medial fibers are under tension during knee varus. The fibers are aligned in a direction parallel to the imposed forces of joint segment motion to resist tensile force applied to the ligament. There are additional examples to follow that highlight the various functions that ligaments take on in the body based on their location.

The ligaments of the foot and ankle are abundant and unique as the bones have many articulations to accommodate complex foot shapes. These ligaments are small relative to others in

the body, but large proportional to bony anatomy. Many of the foot ligaments are either thin flat structures with broad insertion sites, or thick cord-like structures with superficial and deep insertions to multiple bones. It is also common to see connections between fibers of multiple ligaments, forming a web of connected tissue. Some of these ligaments wrap over bony anatomy, while others exist within the joint space (known as interosseous ligaments). It is also common to see variations of ligaments between specimens, some of which differ from published anatomical descriptions [2]. This highlights the diversity in ligament shape.

Mechanical properties of ligaments are not typical of engineered solids. Instead, ligaments will strain for a period before enduring a significant stress, this phenomenon is known as a "toe region" on a stress strain plot. After the toe region, tissue relaxation causes a non-proportional stress-strain relationship until yielding. In addition to differences in stress and strain relationships, ligament tissue begins to relax when held a constant displacement. Therefore, characterizing the mechanical behavior of ligament tissues requires non-Hookean material laws. Viscoelasticity provides such material laws by introducing the standard linear model consisting of a linear spring in parallel with a spring and dashpot in series. From this model, a differential equation can be derived to describe the mechanical characteristics of the tissue. Further, this model can be linearized by considering the relaxation time for constant strain; this technique is described in quasi-linear viscoelasticity (QLV) theory [3].

Despite this knowledge, ligament tissue mechanical modeling limitations are prevalent in the literature as this modeling is dependent on techniques that are technically challenging to achieve. After determining the appropriate theoretical viscoelastic modeling approach, specimen harvest and preparation must be considered to ensure that measurements are true to the intact anatomy and the *in vivo* environment. During mechanical testing, considerations are made about

the composition and anatomy of the tissue while respecting native environmental conditions. Finally, theoretical modeling limitations and repeatability should be considered when analyzing and using experimental data.

Considering the limitations above, and with respect to the previously described complexity of ligaments, this work aims to address some of the limitations to yield detailed characteristics of foot and ankle ligament tissues. Before ligament characteristics can be determined, considerable thought should be given to the harvesting of ligament samples while preserving *in situ* strain and tissue orientation. Comprehensive measurements of ligament length and cross-sectional area are necessary as they are critical to experimental testing. Additionally, an exhaustive set of mechanical tests must be performed to measure the parameters of the QLV models. The variability of these models should be considered in order to improve the application of ligament characteristics to mechanical models. This work addresses these considerations in an effort to improve the quality of ligament viscoelastic characteristics.

1.2 Ligament Anatomy of the Foot and Ankle

The foot and ankle contain numerous bones and joints, supported by ligaments, which bear the weight of the entire body and are capable of motions such as eversion, inversion, and circumduction, in addition to plantarflexion and dorsiflexion. These joint functions require unique ligament support capable of enduring bodyweight during each of these movements. Thus, ligaments contribute to healthy foot function during gait and other foot loading activities. The ankle is critical to mobility and the function of its parts is dependent on the anatomy of the ankle joint complex [4].

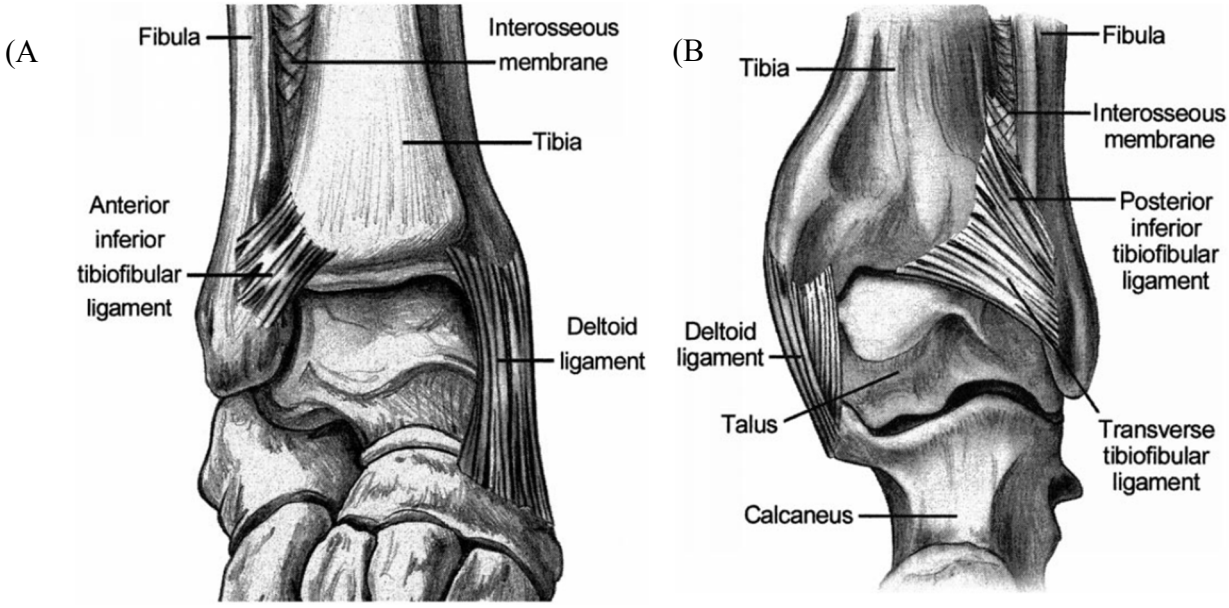

Figure 1: (A) anterior inferior tibiofibular syndesmosis and the (B) posterior inferior tibiofibular syndesmosis (image from Norkus, et al.) [4]

The ankle joint complex is comprised of the tibia, fibula, talus, and calcaneus articulating to form the tibiotalar joint (ankle) and the talocalcaneal joint (subtalar). Proximal to the ankle joint complex is the syndesmosis joint (high ankle).

The high ankle joint is a fibrous joint formed by the tibia and fibula (Figure 1). These two bones are held together distally by the anterior and posterior tibiofibular ligaments which assist with ankle function, as well as the tibiotalar syndesmosis. This articulation helps to maintain proximal integrity between the tibia and fibula with the interosseous membrane and tibiofibular ligaments holding the fibula and tibia together [4]. During dorsiflexion the wider anterior portion of the talus "wedges" between the medial and lateral malleoli, occupying much of the space in the ankle [5]. This position increases ankle joint stability but places increased demand on the tibiofibular ligaments of the high ankle. When the foot moves from plantarflexion to dorsiflexion, the syndesmosis joint widens by approximately 1 to 2 mm [5], [6].

The tibiotalar or ankle joint has been referred to as a mortis and tenon joint [4], which primarily serves the dominate motions of the ankle, plantarflexion and dorsiflexion (Figure 3). The mortis is formed from the distal end of the tibia and fibula, which articulates with the dome-shaped proximal talus (the tenon) to form the predominate ankle motions of dorsiflexion and plantarflexion in the sagittal plane (Figure 2A) [7]. The mortis is stabilized by the syndesmosis

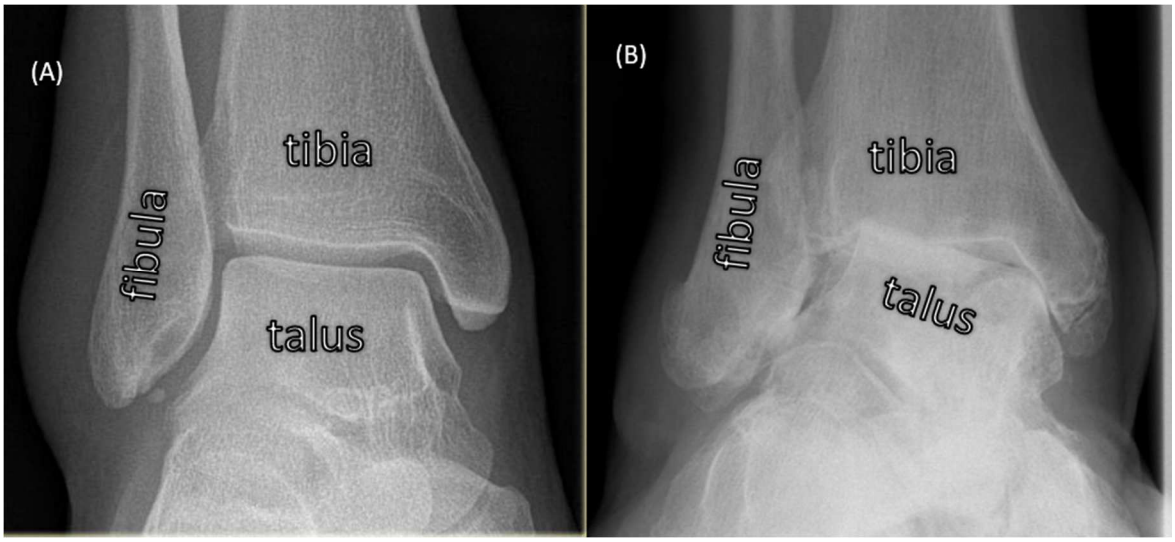

Figure 2: (A) X-ray image of a mortis formed by the tibia, fibula as they articulate with the talus in a healthy foot. (B) Talus everted from flat foot deformity (images from www.radiologyassistant.nl and from *The Bone School* [http://52.62.202.235/]).

joint which permits normal ankle function but limits motion such as transverse plane rotation, which can force the tibia and fibular apart [6]. Excessive lateral motion of the talus within this mortis can produce high strain of the tibiofibular ligaments at the proximal anterior and posterior aspects of the ankle joint [4], [6]. The medial aspect of the ankle joint is supported by the fan shaped tibiocalcaneal (deltoid) ligament which arises from the tibial malleolus and inserts onto the navicular anteriorly as well as the talus and calcaneus distally and posteriorly. The deltoid resists valgus forces from calcaneal eversion when the ankle is loaded through the tibia (Figure 3). On the lateral aspect of the ankle, the peroneus muscles and lateral ligaments of the ankle resist varus stresses from calcaneal inversion [2].

The talocalcaneal or subtalar joint is formed from the meeting of the talus and the calcaneus. This is a multi-facet synovial gliding joint. This joint primarily allows for ankle joint complex inversion and eversion and is comprised of the fan shaped talocalcaneal ligament, and three cord-like ligaments known as the posterior talofibular, calcaneofibular, and anterior

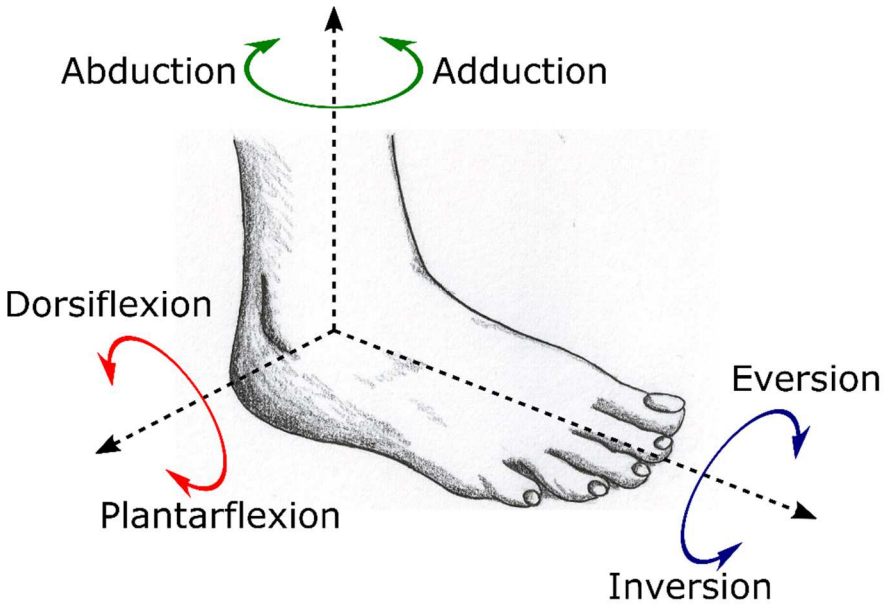

Figure 3: Anatomical terms of ankle motions of the ankle (image from *The foot and ankle in Rheumatology*)

talofibular ligaments [2]. The anterior and posterior ligaments run almost horizontal when the foot is in anatomical position, while the calcaneofibular ligament is nearly vertical in the same pose. Generally, the lateral ankle ligaments are weaker and more susceptible to injury than the medial ligaments [7]. Therefore, both the calcaneofibular and tibiofibular ligaments are commonly injured, often resulting in reduced ankle function.

Moving beyond the ankle joint complex, the ligaments of the foot help to determine its shape which influences the alignment of the ankle and therefore determines how loads are transferred proximally. The longest ligament of the foot is the plantar fascia which is located along the plantar surface of the foot, originating on the anterior, inferior aspect of the calcaneus, and courses distal to form a complex interaction of insertions into the toes, musculature, and skin of the forefoot [2]. The plantar fascia also helps to support the medial arch of the foot, which is vital to dynamic, weight bearing foot function [8]. The plantar fascia is aided by the plantar calcaneonavicular (spring) ligament (SPL) and the calcaneocuboid ligament. Together these ligaments help to maintain the shape of the hindfoot by preventing calcaneal inversion and eversion. The plantar fascia and SPL maintain the medial longitudinal arch of the foot by preventing calcaneal eversion; if these ligaments become lax a flatfoot deformity can result. If severe, this can evert the talus within the talocrural joint (Figure 2B), thereby misaligning articulations at the ankle [9].

1.3 Ligament Microstructure and Composition

Load bearing tissues are comprised of microstructures that are adept at enduring loads in their anatomical orientation. Regions mainly consisting of uncalcified fibrocartilage and collagen constitute most of the ligament body, often referred to as the midsubstance. At the macroscopic

scale, as the ligament approaches bone, it forms an enthesis, or osteoligamentous junction. Due to the non-uniform nature of tension within ligaments, and the morphology of ligaments and bone at the enthesis, this junction exhibits areas of stress concentration [10]. At the microscopic scale (Figure 4), a ligament enthesis is comprised of the subchondral bone surface in the calcified fibrocartilage region, and the uncalcified fibrocartilage region which is interconnected with the ligament tissue [10]–[13]. The demarcation between the calcified and uncalcified fibrocartilage regions is known as the tidemark and is differentiated by the cellular composition of calcified cells in these regions. The area immediately surrounding the bone contains cartilage-like (chrondrocyte-like) cells supported by a dense collagen network continuous with the ligament tissues. In this region, the connective tissue surrounding the bone (perichondrium tissue) is composed of elongated bone and cartilage stem cells (mesenchymal cells) that are mostly aligned directionally [10]. As the ligament begins to embed into the bone the matrix architecture changes as perforations

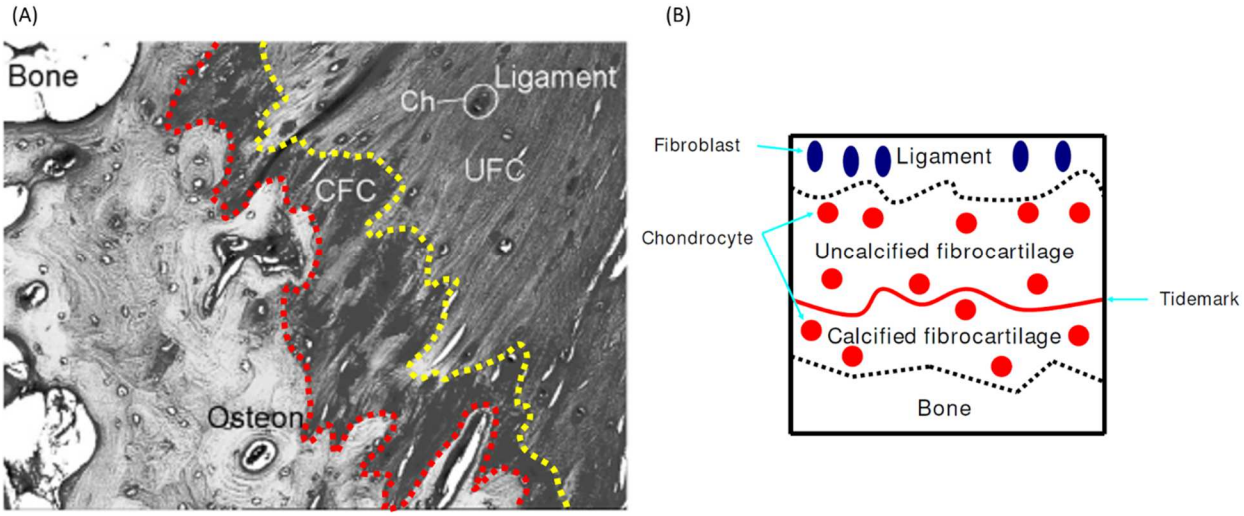

Figure 4: (A) Illustration of the enthesis zones (osteoligamentous junction) superimposed on a histological section of a posterior cruciate ligament (PCL). On the left side of the image is bones with visible osteons, the right side are collagen fibers with chondrocytes (Ch). Between the calcified fibrocartilage (CFC) and the uncalcified fibrocartilage (UFC) is the is the tidemark (yellow dotted line). Between the bone and the CFC is the cement line. (B) Schematic representation of the osteoligamentous junction (images from Submit, D, et al., 2008 & Sakane, M, et al., 2009).

of fibrous tissue cement into the bone forming Sharpey's fibers. These fibers connect the soft tissues to the periosteum to the bone.

Visible in the microstructure of ligaments and enthesis are the cellular content, fiber orientation, and calcification zone, but ligaments are more compositionally complex than this. Ligaments are heterogeneous structures primarily comprised of extra cellular matrix (ECM; 80-90% of tissue volume) and a small amount of cells (10-20% of tissue volume), mainly fibroblasts [7]. Ligaments are 65% to 70% water, of the remaining dry weight, approximately 70% to 80% is type I collagen. The remaining ligament dry weight other than collagen is comprised of proteoglycans (~3%) [14], elastin (5% to 7% dry weight), glycoproteins, and other proteins. In summary, the fiber component of the ECM is mostly comprised of type I collagen and varying amounts of elastin.

The collagen content is responsible for the stiffness and strength of the material composition of ligament tissues. Collagen is abundant, accounting for 25% to 30% of all protein in mammals [15]. The biological content of the extracellular matrix of ligaments consists primarily of fibroblasts arranged in rows between bundles of parallel collagen fibrils [16]–[19]. The basic building block of collagen is the triple helix of three polypeptide chains called the tropocollagen molecule (Figure 5). Like other fiber proteins, it is synthesized in the rough endoplasmic reticulum of the fibroblasts [20]. Elastin, a molecular constituent of tissues that provides an elastic response, is similar to collagen in molecular composition but forms only a single alpha-like strand without a triple helix. The alpha-like strands are crosslinked to each other to form rubber-like, elastic fibers for which the material is named. Under tension, elastin uncoils only to return to its alpha-like structure when the load is removed [21]. Ligaments with

high elastin content have been shown to be less stiff and undergo larger strains before failure as compared to ligaments with lower content elastin [22], [23].

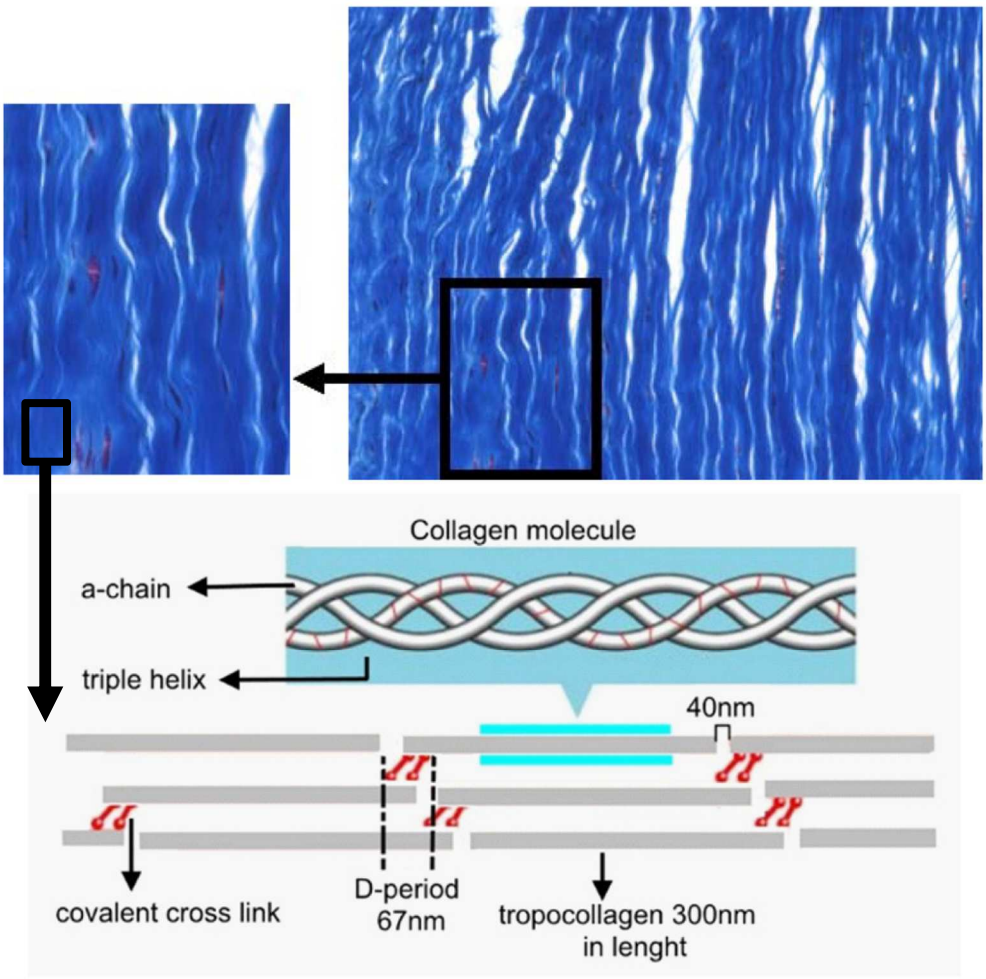

Figure 5: (above) Organized collagen fiber bundles (stained blue) and spindle shaped fibroblasts (stained purple) from histology of a rabbit medial collateral ligament. (below) A graphical representation of collagen fiber bundles comprised of tropocollagen molecules (Images modified from Hsu et al., 2010 & Berillis, 2015)

As a complete structure, ligaments resemble the parts of a rope (Figure 6). Collagen is attracted to other tropocollagen molecules to form microfibrils. The microfibrils form subfibrils that combine to form fibrils which are stabilized and strengthened by intermolecular crosslinks of glycosaminoglycans (GAGs). The GAGs have been shown to contribute to ligament mechanical properties (namely increasing stress relaxation ~2% and modulus ~3.5%; see Mechanical Behavior section for more about stress relaxation and modulus) [24]. The fibrils combine to form fascicles,

which combine to form fibers [25]. In ligament tissue these relaxed fibers appear wavy under a microscope. This wavy configuration found in the tertiary molecular structure and is often referred to as a crimp [18], which straightens when the fibers are loaded. It has been hypothesized and confirmed through computational modeling that the helical organization of fibrils within the fiber would result in a larger Poisson's ratio in ligaments [26]. This has implications for the transverse loading properties of ligaments.

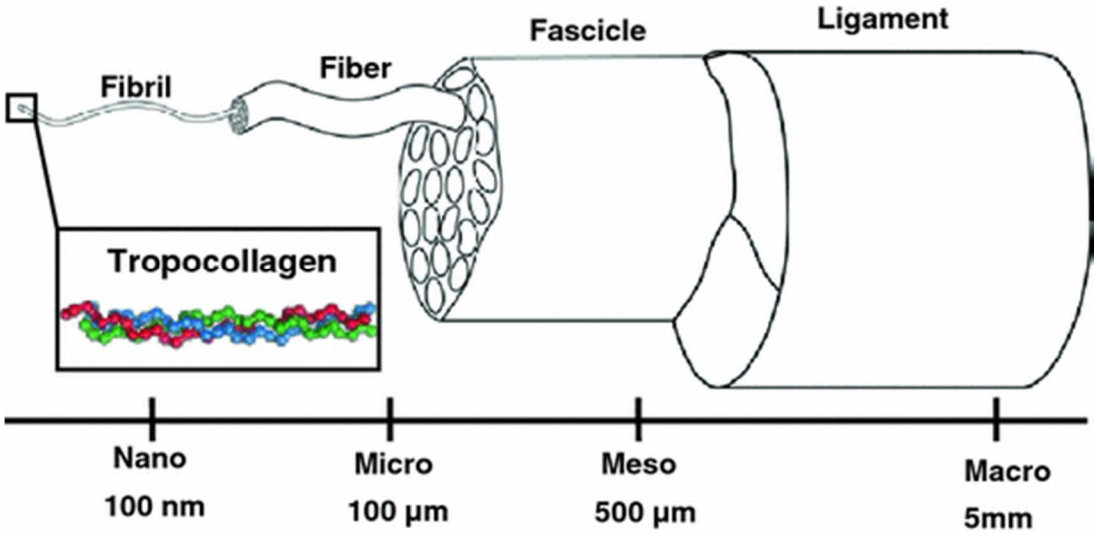

Figure 6: Structural hierarchy of ligament (image from Reese & Weiss, 2015)

1.4 MECHANICAL BEHAVIOR

The anatomy and composition of ligaments determine how these structures respond to external loads of the body. Foot and ankle ligaments are uniquely designed to endure the loads associated with articulations of the insertion bones. The mechanics of materials is a subject that describes the behaviors of solid materials, such as ligaments, subjected to these loads.

Ligaments of the body are biological solids that exhibit different mechanical behavior than engineered solids [27]. Consider applying a tensile load to an engineered material such as a taut

steel cable (Figure 7). Almost as soon as a load is applied, the cable begins to deform. The relationship between the stress (σ; force/area) and the strain (ε; initial length/deformed length) are linearly proportional until the steel cable permanently deforms at a point known as yielding. Before yielding, the cable will return to its initial length with minimal energy loss. After yielding, the cable does not return to its original length and suffers a larger energy loss as a result of stored elastic energy breaking atomic bonds that permanently deform the steel. At this point, the steel will continue to permanently deform with applied loads in a behavior called plasticity. The physical mechanisms and material behavior within the plastic region vary widely between samples. However, biological solids such as ligaments exhibit quite a different mechanical behavior (Figure 7B). Instead of a linear relationship between stress and strain, ligaments exhibit an exponential relationship. Additionally, these materials behave like other highly deformable materials in that they will strain for a period before experiencing substantial stress. When describing the stress strain relationship, this is an area known as the toe region. For ligaments, this is due to the uncrimping of the collagen fibers described in the previous section (Figure 8). The differences, however, are minimal between the plastic deformation of the steel cable and that of the ligaments. Individual fibers of the ligament tend to fail suddenly in a pattern that can resemble that of individual steel strands. However, the non-destructive mechanical behavior of biological tissues such as ligaments is notably different than that of engineered materials and therefore requires a unique mechanical model.

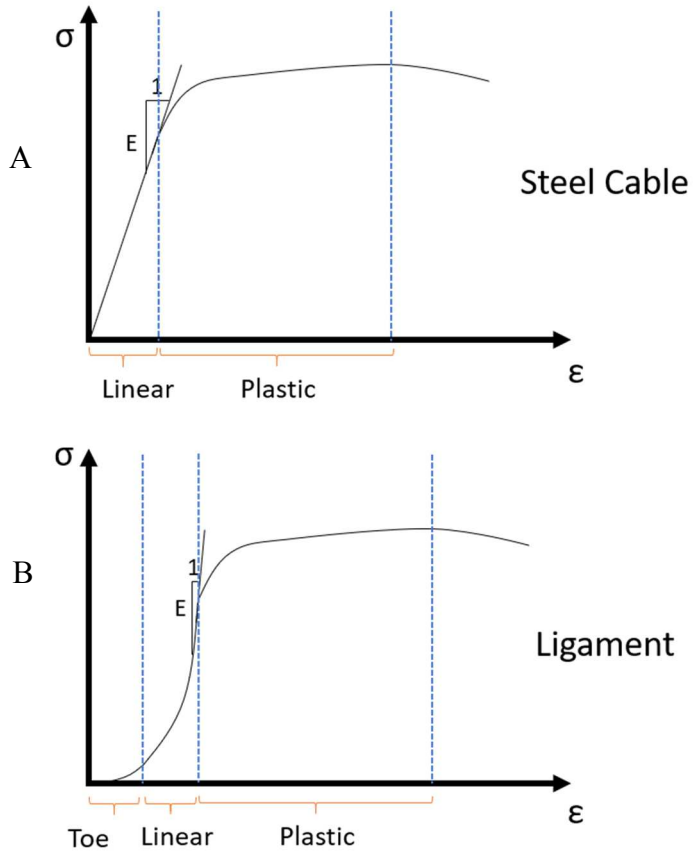

Figure 7: (A) Theoretical representation of a stress (σ) strain (ε) relationship of a steel cable undergoing constant strain. (B) stress strain relationship of a viscoelastic body undergoing a constant strain. Each plot displays Youngs modulus (E) extrapolated from the linear region.

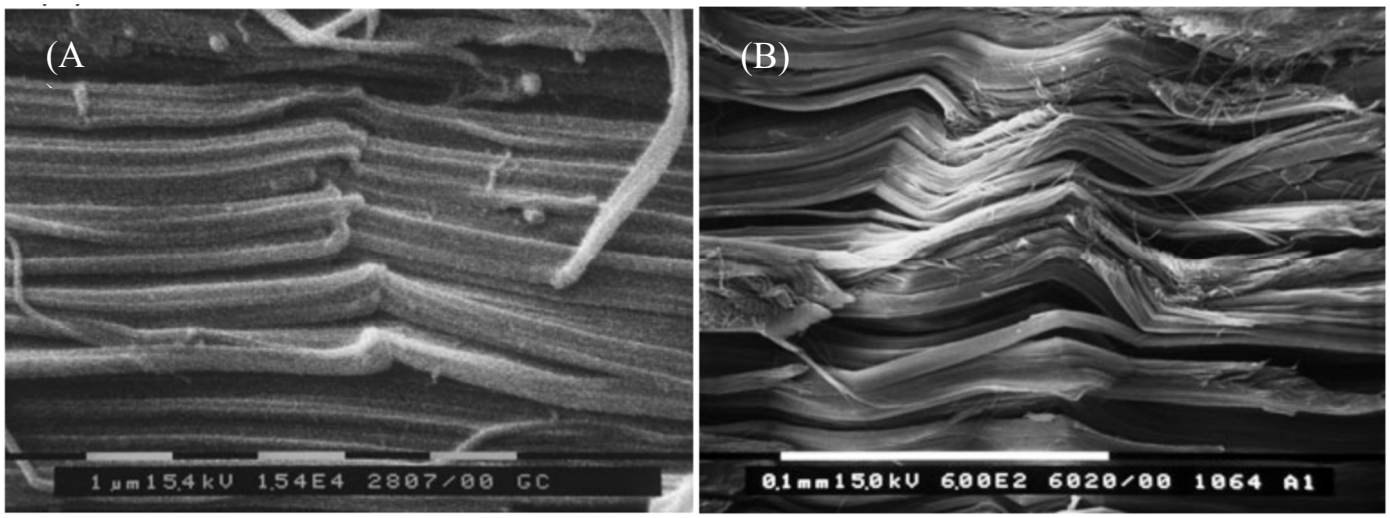

Figure 8: Scanning electron microscopy (SEM) of the frontal section of the collagen from a rat Achilles tendon (A) under load and (B) unloaded

1.5 VISCOELASTICITY

As these ligaments vary in location, composition, and geometry it is necessary to find a framework for which mechanical behavior can be determined and compared. The properties of all materials are specified by using constitutive equations which serve to model relationships between two physical quantities specific to a given material. Consider three simple idealized stress-strain relationships, namely: Newtonian viscous fluids, non-viscous fluids, and Hookean elastic solids; these can be used as a good description of the behavior of many materials in our world and in our bodies. While these models of material behavior are generalizable to many tissues in the body, they also serve an important role to standardize material behavior characterization between tissues and experimenters. However, it should be acknowledged that these models are not perfect representations of biological tissue behavior. In fact, these stress-strain relationships describing material behavior breakdown outside a limited range of temperature, stress, and strain. Blood for example, is a non-Newtonian fluid and therefore does not follow Newton's law of viscosity. Yet,

it is commonly modeled as a Newtonian fluid with a nominal viscosity of about 3.5 cP [28]. Additionally, almost all solid materials are Hookean in a specific range of stresses and strains, beyond that range, Hooke's law no longer applies. It is common knowledge however, that under a sufficiently large stress or strain, solid materials can be broken (fractured), however, in doing so these materials are violating Hooke's law. Therefore, no material is known to behave exactly like one of these idealized stress-strain relationships.

Instead, a combination of stress-strain relationships can be used to describe many materials adequately. Viscous materials resist shear flow and strain linearly over time when exposed to an applied load, when load is removed viscous materials do not recover their initial state. Elastic materials strain when a load is applied, to an amount proportional to the load, and immediately return to their original state once the load is removed. Materials that exhibit the properties of both viscous and elastic characteristics when undergoing deformation are known as viscoelastic materials. The features of these materials are hysteresis, stress relaxation, creep, and rate-dependence [3]. A stress relaxation test, or relaxation for short, describes a body that is suddenly strained, and that strain is maintained for a period of time while the corresponding stresses decrease. A body subjected to a fixed stress exhibit a gradual strain (known as creep behavior). If a body is subjected to cyclic loading, the loading-unloading profiles are not identical (i.e., hysteresis). The energy under the loading portion of the stress strain curve is greater than the energy of the unloading portion. Viscoelastic materials differ from Hookean elastic materials on atomic levels as well. Rather than stretching of atomic bonds along crystallographic planes exhibited in ordered solids, viscoelastic materials exhibit diffusion of atoms or molecules inside an amorphous material [29]. Therefore, viscoelastic materials exhibit both time-dependent strain and a degree of recovery from deformation.

Mathematical models developed from elements relating to mechanical objects such as springs and dashpots (viscous friction dampers) are often used to discuss the viscoelastic behavior of materials. There are three such models commonly used: the Maxwell body, Voigt body, and the standard linear model. This work will focus on the standard linear model (Figure 9) since it is simplest model that predicts both creep and stress relaxation. This model is comprised of linear springs with a spring constant E and dashpots with the coefficient of viscosity η. The linear spring produces instantaneous deformation proportional to load and the dashpot produces a velocity proportional load. Thus, if there is a force F acting in tension on the spring and u is the displacement of the standard linear model body, then $F = \mu u$. If the same force is acting on the dashpot it will produce a velocity $\dot{u}$, and $F = \eta\dot{u}$. From the standard linear model, we can derive the time dependent force function $F(t)$ (eq. 1.1) as well as the time and position dependent stress $\sigma(x,t)$ (eq 1.2) (see Appendix A and Appendix C)

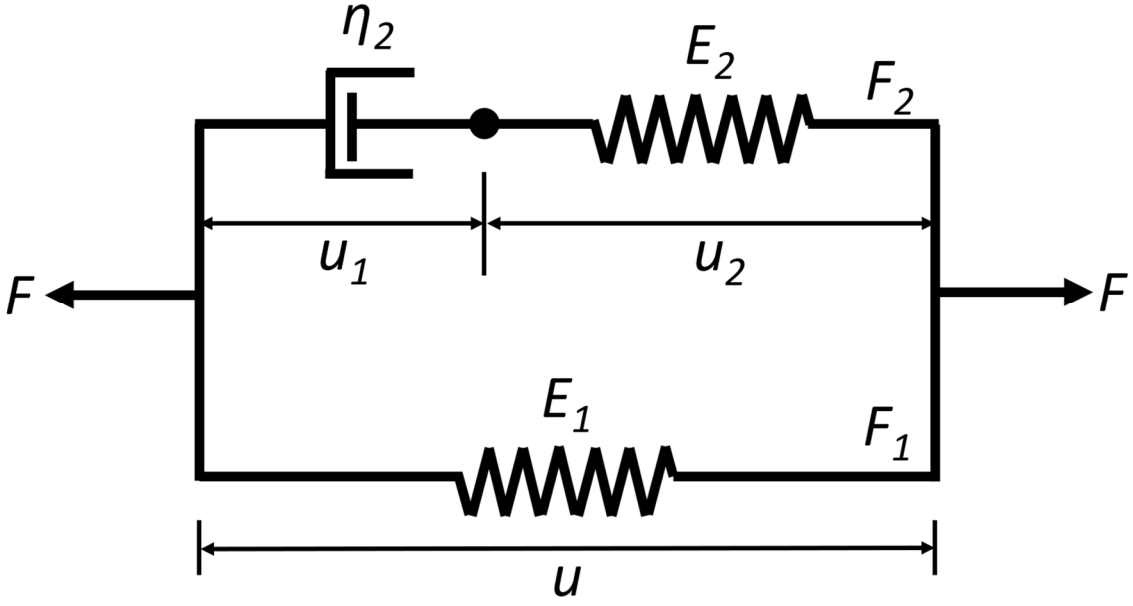

Figure 9: The standard linear model

$$\sigma(x,t) = \int_{-\infty}^{t} G(x,t-\tau)\frac{\partial \varepsilon}{\partial \tau}(x,\tau)d \tag{1.1}$$

Where k is the relaxation function, du is the change in length, G is the relaxation function for tension, and $\partial\varepsilon$ is the strain tensor.

Like other biological tissues, ligaments are viscoelastic solids which exhibit a stress-strain relationship that is rate and history dependent [3], [18], [30]–[32]. Thus, appropriate testing parameters must be considered when determining ultimate strength, ultimate strain, and modulus of elasticity. One such parameter is the strain rate, where higher strain rates result in a higher stress and strain at both yield and failure, as well as increased elastic modulus [18], [33]. Additionally, the energy loss from hysteresis is likely due to frictional forces converting energy to heat, some of which flows to surrounding tissues. For most tendons and ligaments a steady state is achieved after 10-20 cycles [18]. Therefore, when testing cyclical non-destructive properties, the tissue is often subjected to a set of preconditioning cycles to achieve this steady state.

To characterize ligament viscoelastic behavior, one must relate viscoelastic theory to experimental data. After identifying the appropriate constitutive relationship, a mathematical model of the viscoelastic behavior can be developed. The material constants (material parameters) are determined by curve fitting the mathematical model parameters to experimental data consisting of stress relaxation and cyclical loading tests to measure relaxation and hysteresis. Since the creep and relaxation functions are directly related in the Laplace domain ($s\overline{J}(s)\overline{G}(s) = 1$), it is only necessary to measure one of these experimentally. Once the material parameters have been solved by curve fitting the mathematical model to experimental data, this model can be used to characterize the biomechanical behavior of the tissue. Due to the errors associated with curve fitting and constitutive modeling, developing methods to improve parameter estimation is critical for characterizing ligament function.

1.6 Quasi-Linear Viscoelastic Theory

The nonlinear time and history dependent viscoelastic behavior of collagenous tissues has been described by the quasi-linear viscoelastic (QLV) theory formulated by Fung [27]. The QLV parameters can be estimated by fitting an exponential function to the stress-strain data from the loading phase of a stress-relaxation test, and the relaxation function to the normalized stress data during the hold phase of a stress-relaxation test. Ideally, a QLV curve fitting requires an instantaneous step function, as this separates the nonlinear elastic and time-dependent viscoelastic behavior. However, it is impossible to achieve this in practice since we are limited to finite time ramp displacements experimentally. As a result, during the finite ramp displacement, the specimen undergoes some unknown amount of relaxation. During a stress-relaxation test, the relaxation during loading effectively reduces the total amount of relaxation seen during the constant strain phase of the stress-relaxation test and can lead to parameter estimation errors. However, in practice it is difficult to achieve an accurate ramp displacement at a high loading rate, even with the most state-of-the-art materials testing equipment. To mitigate this fact, hysteresis is often used to determine the complex modulus which can be fit to a linear function ($S(\tau)$) consisting of the relaxation time for constant strain and relaxation time for constant stress.

1.7 Overview of Experimental Limitations

Modeling ligament mechanical behavior mathematically is dependent on accurate experimental data that is often expensive, technically difficult, and prone to errors. The challenges begin with designing a mechanical testing protocol that ensure viscoelastic modeling is possible. Then specimen preparation must be considered to ensure that measurements are true to the anatomy and the *in vivo* environment. The mechanical testing and subsequent analysis should

consider the composition and anatomy of the tissue and the environmental characteristics of the sample. Finally, theoretical modeling limitations and experimental repeatability must be considered when analyzing data. Attempting to address these considerations requires specialized equipment, expertise, and time.

1.8 Preparation Limitations

Unlike other collagenous structures such as tendons, ligaments of the body are loaded in various directions under physiological conditions, therefore should ideally remain in anatomical positions during mechanical testing. An effort has been made to mechanically test partially dissected joints retaining the *in situ* position with multiple ligaments and bony anatomy intact [8], [34]. These methods often move the joint through a range of motion, then remove one ligament at a time by cutting or changing the alignment of the ligaments before retesting. The contributions of the cut ligament are inferred from kinematic and kinetic comparisons of the joint motion before and after a ligament was removed. While these experiments can provide valuable information about the contributions of each ligament to the whole joint, they do not control the loading direction of individual ligaments which might alter the measured mechanical characteristics. More commonly, ligaments are excised and potted so that the ligament can be mechanically tested in a machine that is constrained to uniaxial tension [30], [32], [35]. These techniques rely on visual alignment of ligament fibers and ensure that fibers are in-line with the applied load from the actuator. It is difficult to ensure alignment due to the irregular shape of the ligaments and bone surfaces. Additionally, there is no certainty that the orientation of the potted ligament is relevant to *in vivo* loading conditions when using visual fiber alignment techniques.

The micro and macro composition of ligaments and their length estimation both contribute to the quality and interpretation of experimental data. Ligament stress and strain fields are

inhomogeneous, yet most studies are forced to model ligaments as a set of discrete homogeneous points. Factors such as contact area, insertion definition, and cross-sectional area are extremely difficult to measure experimentally. It is common therefore to determine ligament length by averaging caliper measurements of the outer ligament fibers [36], [37]. This technique introduces subjective error when estimating the ligament boarder and location of measurement sites. For long ligaments with more uniform shapes, the percent error introduced might be less since the variability is small compared to the overall length. However, this is not the case for small irregularly shaped ligaments such as those found in the foot and ankle. Bertozzi et al. [38] found that knee laxity is extremely sensitive to variations in reference length. This study simulated variations in cruciate ligament length during a drawer test (moving the tibia anteriorly or posteriorly with the knee flexed at 90^{o}) and found that a 1% change in length resulted in laxity values outside of experimental range. Additionally, Bloemker et al. [39] simulated variations in the initial length (zero-load length) of the major knee ligaments (ACL, PCL, LCL, MCL) from 75% to 95% of measured length and showed that tibia to femur kinematics (orientation and translation) could change by a factor of approximately two.

Cross-sectional area is estimated in several ways, some of which include taking a thickness measurement and estimating the cross sectional area as a rectangle [40], [41], estimating the area as an ellipse from two principal diameters [37], using specialty equipment such as an area micrometer with a load cell in line (Figure 10) [35], using imaging [42] and laser scanning [43], [44] to map the 3D shape, or molding and casting [45]. To the authors knowledge, there are no studies examining the effects of cross-sectional area uncertainty on mechanical properties.

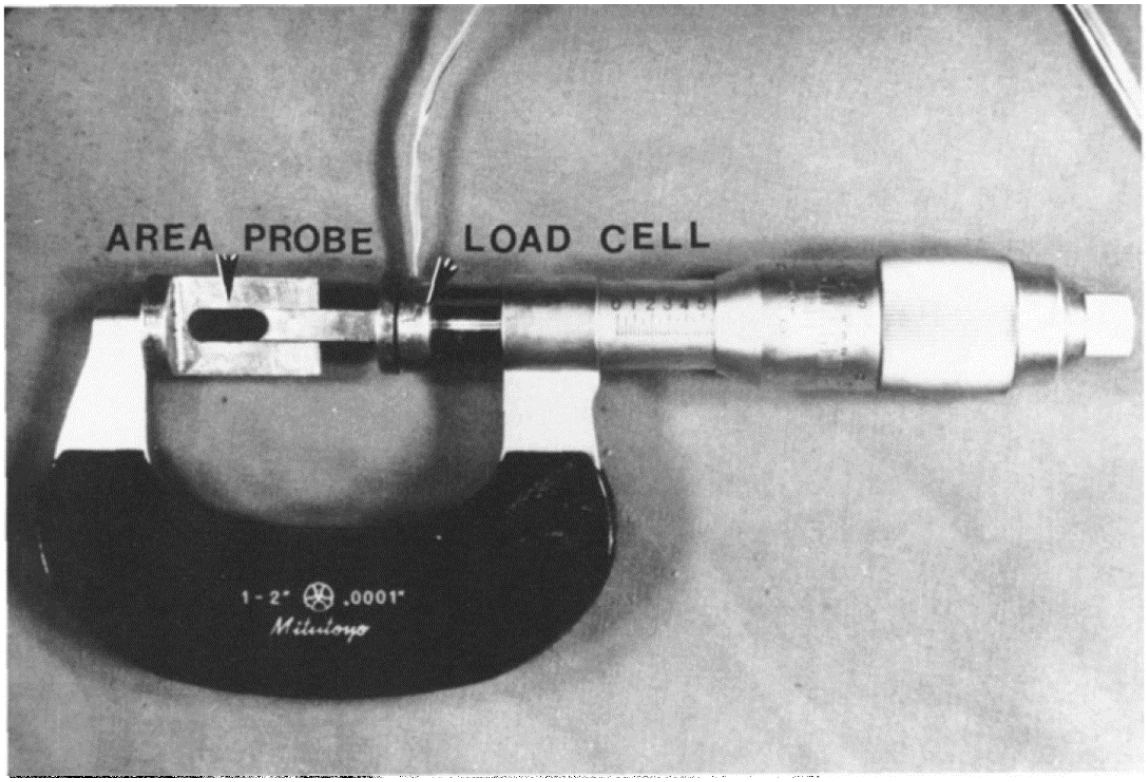

Figure 10: Area micrometer used by Siegler et al. (1988) to measure cross-sectional area of ligament specimens.

1.9 MECHANICAL TESTING LIMITATIONS

Several methods have been employed to ensure specimen hydration during mechanical testing and produce consistent results. One of the more commonly used hydration solutions is phosphate buffered saline (PBS), however, a 0.15 M PBS increases the tissue's water content causing a decrease in tensile stiffness by over 70% [46]. Solution exposure over a long duration causes solutes from the buffer to diffuse into the tissue and interact with its structure and mechanics [47]. Solute diffusion can also be measured with high concentrations of saline solutions (25% NaCl/volume) after long-term (8hr) incubation periods resulting in slight increases in cross-sectional area (~8%) and about a 24% decrease in stiffness [47]. No change in stiffness or

relaxation has been shown for a 0.9% NaCl/volume saline solution. However, small increases in cross sectional area have been measured [47]. Conversely, dehydration can cause reductions of up to 52% as well as up to a 50% reduction in creep rate and storage compliance [48]. Therefore, it is important to consider tissue exposure to hydrating solutions and weigh that against tissue dehydration and degradation, each of which can alter mechanical properties.

In classical mechanics of materials modeling, the constitutive equations are stated for a specific temperature with deviations resulting in erroneous measurements. The viscosity of a fluid and the elastic modulus of a solid varies with temperature. Therefore, the viscosity coefficients of a Newtonian fluid, and the elastic strain tensor vary in the constitutive equations. Additionally, the pressure in an ideal gas is related to the density ρ and the temperature T by the equation

$$\frac{p}{\rho} = RT \tag{1.3}$$

Where R is the gas constant and p is pressure. The effects of temperature therefore influence several aspects of the constitutive equations. It is common to use heated baths of saline during mechanical tests. While these baths often ensure a heated and hydrated specimen environmental conditions, this method also causes tissue swelling which can influence mechanical testing results as mentioned above [47]. Additionally, these chambers create challenges in strain field optical measurements due to light refraction through the viewing window and solution.

It is ideal to test unaltered and unpreserved tissues from cadaveric specimens, however it is often necessary to freeze the tissues at some point increasing the chance of degradation due to freezing. This is most often done in transit and in preparation of mechanical testing. Studies have shown ligaments that have been frozen are about 17% stiffer than those that are fresh [49]. However, no significant difference was found in the load to failure of fresh and frozen specimens. These changes are likely the result of mechanical damage from freezing and thawing which can

result in a slight cross-sectional area decrease in ligaments [50]. The mechanical effects of freezing and thawing are primarily expressed in hysteresis area and Young's modulus (Figure 11) [50], [51]. The differences in fresh and frozen hysteresis were pronounced in the first few cycles (decrease of ~63%) but no significant difference has been found after about 10 cycles [50]. Therefore, the effects of hysteresis are mitigated in most studies by preconditioning tissues before preforming mechanical tests. Moon et al. examined the effects of refreezing specimens [52]. In this study no measurable difference in mechanical properties was measured between subsequent freeze thaw cycles. It is unclear from the results of this study whether freezing affects the properties of ligaments. Some studies indicate no change in mechanical properties due to freezing while others show significant differences in stiffness and hysteresis, as well as damage to the tissues from a single freeze cycle [49]–[52]. It is important to be consistent and report the frequency of freezing and thawing for all specimens tested within a study.

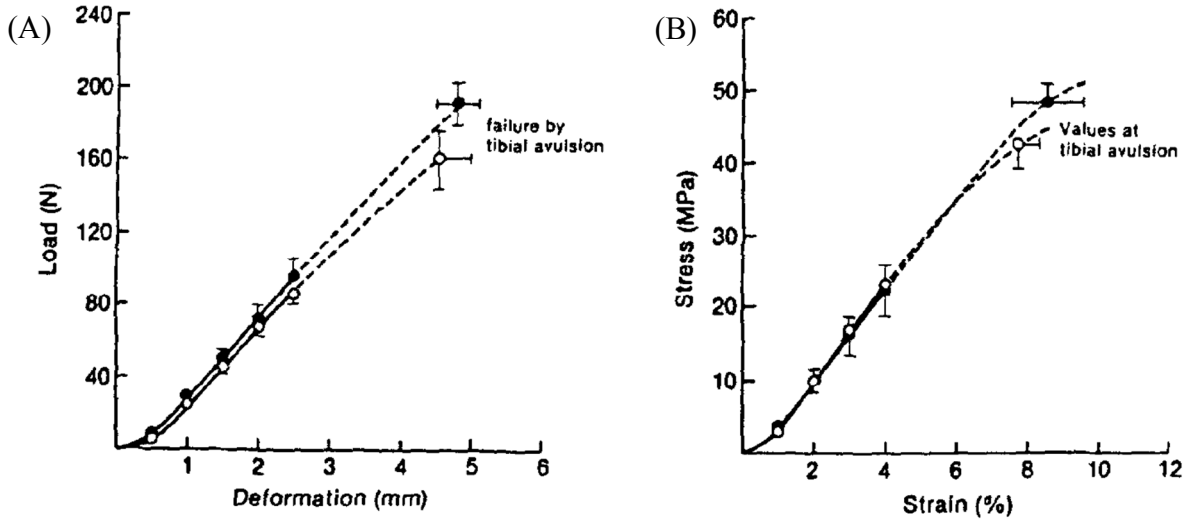

Figure 11: Comparison of structural properties of (A) MCL-bone complex and the mechanical properties of the (B) MCL substance from the fresh and frozen rabbit knees. (Woo, S et al., 1986)

To ensure that the strain history from the previous mechanical test is not introducing errors on the subsequent test, a zero-stress state is maintained for a period of time to allow tissues to

recover. During mechanical testing, hysteresis causes tissue relaxation which influences stress measurements. The reported zero-stress times vary from 10-30 minutes [37], [53] up to one hour [40], [54]. Recent work by Funk et al. [30] and VanDommelen et al. [32] reports using a zero-stress period of 1,000 seconds (~16 minutes) between non-destructive cyclical triangle or sine wave tests. These studies outline a test duration and environmental conditions similar to the work proposed here.

1.10 Analysis Limitations

Foot and ankle ligament strain data is challenging to determine due to the complex shape of the structures and the challenges associated with measuring *in situ* strains. There is little data available quantifying the *in situ* strains causing many investigators to assume a uniform initial strain [30], [40], [54]. Some studies have developed methods for predicting *in situ* strains using model optimization techniques [55], [56] with results that are often physiologically unrealistic. In their knee joint contact model, Blankevoort et al. were not able to determine a ligament stiffness that would produce a realistic joint contact force without causing the femur to move too far anteriorly past 60^{o} of flexion due to the uncertainty of experimental ligament strains. Additionally, ligaments *in vivo* respond differently based on various anatomical and physiological events. Ligaments *in vivo* often wrap around surrounding anatomical features (such as native bone geometry) thereby influencing mechanical behavior that differs from a purely point to point idealistic loading. This causes soft tissue load to be transferred to surrounding tissues other than the insertion sites, altering the direction of the load transferred to the bones. These transferred loads can be distributed to neighboring collagen fibers in varied orientations, therefore, altering ligament mechanics. Additionally, bony anatomy can act as a lever changing mechanical efficiency throughout the range of motion. Wrapping can also occur because of soft tissue

obstructions. In some cases, surrounding tissues can apply compressive forces which can result in ligament tensile loads in otherwise unloaded positions. It is important, but extremely challenging, to control for these events as much as possible while mechanical testing cadaveric specimens.

Having a large, representative sample of specimens improves the ability to generalize experimental data. While some ligament mechanical testing studies have relatively large sample sizes ($N \geq 20$) [23], [35], most have moderate ($10 \leq N < 20$) [8], [41], [57] to small sample sizes ($N < 10$) [36], [39]. This is likely due to the high cost and labor time required to conduct such experiments. However, the small sample size makes it difficult to interpret findings. Both Weiss et al. [58] and Baldwin et al. [59] "advocate performing sensitivity studies, especially when applying population averages to subject-specific models [39]." The uncertainty due to stochastic variations of biological tissue mechanical modeling parameters can make interpretation of experimental data challenging. Efforts have been made to determine the uncertainty of joint mechanics models [38], [60] and finite element analysis [61] using sensitivity analysis. Hamdia et al. [62] used sensitivity analysis to show how the microstructural and nanoscale properties effect collagen mechanical properties. Findings from this study showed that fiber crimp amplitude and intermolecular cross-link stiffness density were the dominating parameters influencing rat tail tendon fiber modulus, stress, and molecular deformation. However, this group did not use this information to make recommendations about steps that can be taken to minimize variability. Sensitivity analysis has been used to make estimations of sample size in other fields where sample size can influence outcomes. Some examples include determining the sample size of a trial for alcohol interventions of HIV-infected patients [63], and for the treatment of hypertension [64]. To the authors knowledge, there is no study reporting recommendations about sample sizes based on

the variability of modeling parameters. However, results from small sample sizes are more sensitive to changes in experimental data values and sample biasing.

Now that the anatomy, composition, viscoelastic modeling, and potential limitations have been described, let's explore why these tissues are necessary by examining some of the ways in which they become injured.

1.11 Ligament Injury

The importance of understanding and overcoming the numerous limitations above is underlined by the impact and application of accurate material behavior models. Understanding ligament injury for example, requires an accurate delineation between the behavior of intact, healthy structures, and diseased or injured tissues. The difference between these states, and within the severity of a specific injury, can be very small. Errors from the limitations above can easily mask the difference between injured and uninjured tissues.

Foot and ankle ligaments can undergo yielding or ultimate failure which can present in several ways. Sprains occur when ligaments have endured excessive strain or rupture which is often slow to heal. Ankle sprains occur when ligaments that connect the primary bones of the ankle (tibia, fibula, talus, and calcaneus) undergo yielding or ultimate failure. Sprain severity is classified based on the extent of damage to the ligament: Grade I is a mild sprain with possible mild tearing usually resulting in soreness without instability, Grade II is a moderate sprain usually resulting in moderate pain and some joint instability, and Grade III is a severe sprain with gross joint instability and possible ligamentous rupture. A related ligament injury is an avulsion fracture which can occur when excessive ligament strain causes a bone fracture near the insertion site.

There are three general categories of ankle sprains: syndesmotic, eversion, and inversion sprains. The syndesmotic sprain occurs in the joint that is formed by the tibia and fibula. This type

of ankle sprain occurs when the talus translates laterally pushing the fibula away from the tibia. The eversion sprain occurs when the foot is excessively everted causing damage to the deltoid ligament (Figure 5B). Although rare, syndesmotic sprains and eversion sprains are often associated with fibular fracture [65]. The inversion sprain is the most common ankle sprain (Figure 12A), occurring when the ankle is excessively inverted causing excessive strain on the calcaneofibular ligament. After enduring an acute ankle sprain, around 40% of patients suffer long term residual discomfort such as pain and swelling, and about 70% of these patients do not return to a preinjury level of activity [65]. One of the largest risk factors of an ankle sprain is a history of a previous ankle sprain [65]. In response to an excessive strain, muscles that are stretched beyond a certain point might engage in a reflexive action known as the stretch reflex where sensory neurons (afferent neurons) send a signal to the spinal cord which returns a motor neuron signal (efferent neuron) that causes the stretched muscle to contract. This can protect the foot and ankle from further injury in the case of absent or damaged underlying ligaments.

Ankle sprains are common and result in a considerable monetary cost. In the US ankle sprains are one of the most common injuries in active populations and occur in approximately 30% of sports injuries [66]. Foot and ankle injuries are prominent among U.S. Active-Duty Army making one of the largest proportions of lower leg injuries. The Department of Defense (Air Force, Marines, Army, and Navy) have substantially greater rates of ankle sprains than the general population with 34.95 per 1000 persons-years versus 2.15 per 1000 person-years for the general public. This results in an estimated 2 million ankle sprains each year in the United States civilian population [66]–[69]. In the United States, each trip to the emergency department for ankle sprain treatment can cost between $914 and $1008 [70], resulting in a $2 billion cost to the health care

system annually and can result in considerable disability compensation in up to 60% of patients [66], [70].

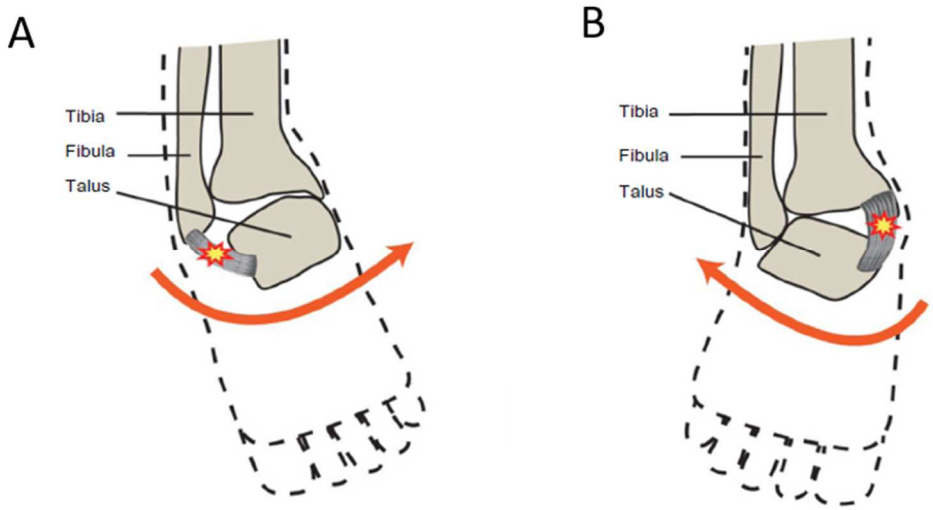

Figure 12: (A) a typical inversion injury of the ankle causing to damage of the lateral ligaments. (B) A typical ankle eversion injury, resulting in damage to the medial ankle ligaments. (image adapted from Blalock et al., 2014)

Once injured, ligaments are slow to heal in part because of poor tissue perfusion. The calcaneofibular ligament is perfused with the primary blood supply coming from the anterior and posterior branches of the peroneal artery [71]. The tibiocalcaneal ligament which is supplied by the medial malleolar branches of the posterior tibial artery. However, it is common to damage this blood supply during ligament injury which detrimentally affects healing causing relatively avascular watershed areas. Healing times can be slow due to the relatively avascular nature after injury, the severity of the sprain, and the level of activity. Some patients will go on to develop chronic ankle instability despite adequate rest, rehabilitation, or surgery.

When healing does occur, it follows a complex process that effects the composition of the ligament tissue. Following the initial injury, fibroblasts proliferate and produce a matrix of proteoglycan and collagen to bridge between torn ends. After about 6 weeks, an increasingly

organized matrix of type I collagen proliferates. Finally, the collagen fiber alignment improves producing an increased collagen matrix maturation that can continue for years [72], [73]. Thus, healing ligaments continue to be abnormal even after one year. These ligaments contain large amounts of extracellular matrix (proteoglycans) and fewer collagen crosslinks [74]. Often the number of collagen fibrils increases (~ 140%), but the diameters of the fibrils decreases (~ 40%) to those of uninjured ligaments [75], [76].

Since ligaments are viscoelastic, they gradually strain when under a constant load (known as creep behavior) and will eventually return to their original shape when the load is removed. However, ligaments loaded beyond their yield point or beyond a point for a sustained period, cannot return to their original shape. Using a common physical examine known as an anterior drawer test, it has been shown that sprained ankles within 1 year exhibited significantly lower viscous response than uninjured ankles [77]. This results in a greater amount of creep for a given load. Additionally, healing ligaments have been shown to dissipate more energy, have longer recovery times upon removal of load, and reach an earlier long-term plateau during a stress-relaxation test [76].

Ankle instability is sometimes the result of joint laxity from weak or damaged ligaments. Although the exact cause of chronic ankle instability is not well understood, 10-20% of patients exhibit chronic ankle instability following an ankle sprain. This is one reason why joints that are sprained or dislocated can become chronically unstable and prone to future dislocations. Joint instability as a result of ligament injury can alter joint kinematics, load distributions on the articulating bone surfaces, and injury to other musculoskeletal tissues. Chronic ankle instability is a clinical problem involving various complicated mechanical and neuromuscular factors. The two hypothesized causes of chronic ankle instability are mechanical instability and functional

instability. Mechanical instability is defined as ankle is movement beyond the physiological range of motion limit, where functional instability is the subjective feeling of ankle instability and/or a recurrent symptomatic ankle sprain due to neuromuscular and proprioceptive deficits [78]. Patients with chronic instability have a history of multiple instability events, often resulting in pain [79]. Mechanically instability is diagnosed with a physical examination (anterior drawer or a varus stress test). Functional instability occurs when no clinically reproducible dysfunction is found, yet the patient feels as though the ankle will "give out" [80]. It has been shown that while physical therapy does result in improvements in the short term, it lacks long term follow-up success for patients with chronic ankle instability [81]. Repair to ligament tissue is difficult. Remodeled ligament tissue is morphologically and biomechanically inferior to normal ligament tissue [17] (Figure 13). This results in ligament laxity and can eventually lead to degenerative joint disease, the most common of which is osteoarthritis. After at least 6-12 weeks of therapy, a patient might opt for one of several surgical interventions. The most common of which involves fixation of the anterior talofibular (anterior deltoid) ligament and mobilizing the inferior extensor retinaculum. However, one of the risk factors for this procedure is poor tissue quality, sometimes from a failed anatomical repair. It is difficult to predict the quality of the tissue preoperatively and often an allograft is preferred. This donor tissue is fixed in place with screws and guided through a tunnel drilled into the bones [80].

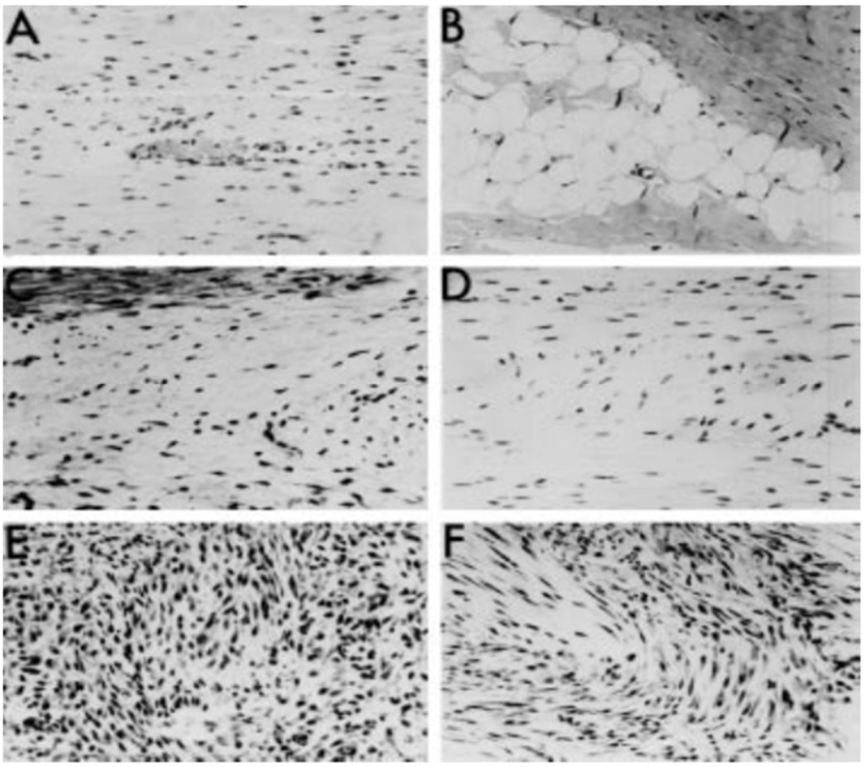

Figure 13: Histological analysis (x 125 magnification) of rabbit MCL scars showing various defects whin the new matix: (A) blood vessels, (B) fat cells, (C) loose collagen, (D) disorganized collagen, (E) inflammatory site, (F) a combination of all. (images taken from Hauser et al.)

Injuries to ligament structures earlier in life that become unstable can sometimes results in damage to the articulating cartilage, referred to as osteoarthritis (OA). Joint laxity from prior injury has been established as a cause of OA due to poor bony alignment resulting in uneven joint loading and articular cartilage trauma [82]–[84]. OA is the most common form of joint disease and is characterized by, among other things, a loss of articular cartilage and a thickening of the joint capsule [85]. The common symptoms of OA are joint pain and stiffness, however other symptoms may include joint swelling, and decreased range of motion. These symptoms can affect work and daily activities, which can cause a decrease in muscle tone [85]. If pain from OA becomes unbearable, in some cases a total ankle arthroplasty (TAA; ankle joint replacement) is required.

Understanding the underlying mechanics of ligaments can inform joint health and the progression of foot and ankle pathologies. Additionally, modeling ligament behavior can provide tools to evaluate the effects clinical interventions, determine the effects of injuries or morphology on ankle structure and function, and help to evaluate the effects of various orthoses on joint function.

1.12 Ligament Mechanical Property Applications

As in the prior section on ligament injury, the limitations of experimental testing described earlier also have a tremendous impact on the utility of our knowledge about ligaments. Considering the various applications that can make use of ligament mechanical behavior, it will become apparent in the sections that follow that many of these techniques are completely dependent on an accurate understanding of how ligaments respond.

The use of computational methods for the study of joint mechanics can yield information about the function of ligaments that is difficult or impossible to obtain through experimental measurements [58]. We have already seen some of limitations associated with viscoelastic modeling characterization and experimental measurements. When applying viscoelastic material properties to a mechanical model, considerations are made about the tissue level (molecular, cellular, tissue) and the level of modeling detail. A simple 1D model can consist of applying ligament viscoelastic characteristics to a simple spring truss or beam element. A more complex model might consist of 3D elements used to model ligament response (Figure 14) [86]. Therefore,

it is important to carefully consider the ways in which ligament viscoelastic properties have been derived.

Developing a mechanical model that is relevant to anatomy is challenging due to the discrepancies between the ways in which tissues are mechanically tested as compared to how they are modeled. Often the fibers are visually aligned and with the actuator of the mechanical testing machine to maximize the number of collagen fibers that are in tension during a test [34], [40], [87], [88]. There are even examples of ligaments being cut into dog-bone shapes to more closely

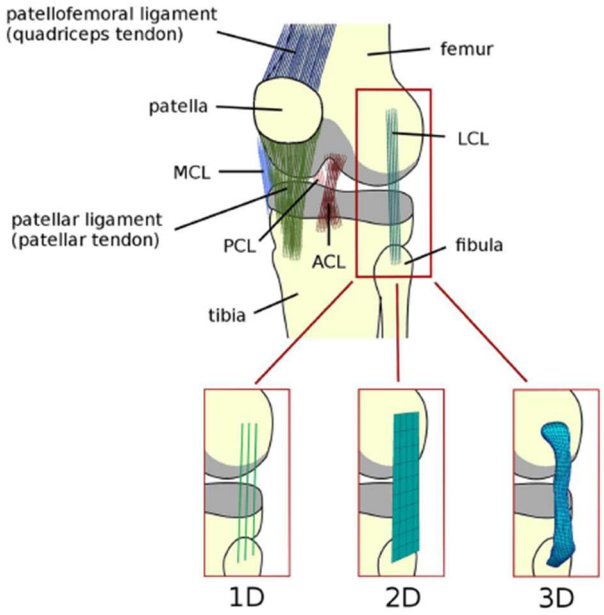

Figure 14: Schematic representation of knee joint complete with ligaments and articulating cartilage. Examples of the lateral collateral ligament (LCL) represented as a 1D (springs, trusses, and beams), 2D (shell and membrane), and 3D elements (solid) used to model viscoelastic characteristics (image from Galbusera et al. 2014).

approximate standards set by the American Society for Testing and Materials (ASTM) [88]. However, these experimental protocols do not consider the *in situ* loading orientation of these tissues. For tissue samples that are removed from the bone and clamped into the mechanical testing

machine, the mechanics of the enthesis and bone at the insertion site are not measured. Mechanical models using viscoelastic material models can benefit from experimental data that considers the mechanical properties of ligaments loaded in anatomically relevant orientations. With enough experimental data of this nature, a mechanical model could even be used to predict where and how a ligament might fail (i.e., the likelihood of an avulsion fracture, or the likelihood of a failure site along the ligaments length).

To develop an understanding of how ligaments function, accurate stress and strain measurements must be made. There has been an effort to perform length and cross-sectional area measurements using calipers with the ligament exposed in a cadaveric specimen [32], [49], or with the ligament in a mechanical testing machine under a preload [34], [37], [40]. Each of these measurement techniques will yield different initial lengths and cross-sectional area measurements. This variation influences the experimental data since the length is used to determine strain and the strain target, while the area is used to estimate tissue stress. Furthermore, length measurements using the caliper technique might be overestimations since caliper measurements are taken from the outer most ligament fibers. Additionally, the cross-sectional area measurements are possibly over estimations due to geometric shape assumptions (rectangular or elliptical) of cross-sections. The measurement uncertainty of the ligament length and cross-sectional area will influence the stress and strain relationship variability. To the authors knowledge, there has been no attempt to characterize the cross-sectional area along the length of a ligament in anatomical position prepared for mechanical testing. A through estimation of regional cross-sectional area and regional strain estimation could provide data to better validate mechanical model outcomes.

Mechanical testing environmental conditions can also influence stress and strain relationships making it challenging to interpret experimental data. While it has been shown that

ligaments need to remain hydrated during mechanical tests [50], [52], [89], there are variations in how this is achieved. The evidence discussed [47] shows the effects of mechanical properties for ligaments in different bathing solutions. There is variability in the duration of mechanical tests performed and therefore exposure to the different solutions. This also makes interpretation of mechanical properties difficult to relate between studies. Additionally, there are differences in the testing temperatures of these tissues. Some tests are conducted at room temperature [32], [34], [87] while others are tested at body temperature (37^{o}C) [50], [52], [54]. Mechanical models can lose fidelity by applying viscoelastic ligament properties from a variety of different studies using different ligament *in situ* orientations, length and cross-sectional area measurements, environmental temperatures, and hydration solutions.

Independent of their source, it should not be assumed that mechanical modeling inputs are absolute known quantities [58]. Instead, material property coefficients are based on several subject-specific measurements. Therefore, models that consider the uncertainty in the coefficients due to the inherent errors in experimental measurements, yield improved modeling outcomes. The uncertainty can often be derived from the standard deviations of the reported experimental data. Using sensitivity analysis can provide important insight into the physics of the model, and therefore, improve the confidence of the model predications.

1.13 OBJECTIVE OF CURRENT WORK

Ligaments are challenging to experimentally measure and mathematically model. As a result of this, reported mechanical properties can differ based on the methodology used. Therefore, there is a need for improved experimental methods that set a new standard to improve model accuracy.

To achieve this, mechanical tests should be performed in their *in situ* position. Maintaining the anatomical ligament positions during mechanical tests helps to ensure that the resulting mechanical characteristics will more closely reflect an *in vivo* response. It is important to not only maintain ligament pose when excising the ligaments form cadaveric specimens, but also to track the ligament insertion positions during testing. Tracking these positions can help offset any misalignment of the ligament during potting and ensure that actuator strain is congruent with the insertion-to-insertion strain. This work will present methods for mitigating these limitations by fixing the *in situ* anatomical position before excising the ligament and tracking the insertion sites during mechanical tests.

Stress and strain values are predicated on accurate length and cross-sectional area measurements. However, there is little consistency in these measurements [30], [35], [37], [40], which can result in challenges when interpreting viscoelastic characteristics. Overestimations in ligament length can decrease the reported strain targets, resulting in underestimations of stiffness. Likewise, overestimations of ligament cross-sectional area can result in lower stress measurements which can also result in underestimations of stiffness. Novel methods to measure length and cross-sectional area based on ligament anatomy will be presented in this work.

Viscoelastic solid materials such as ligaments exhibit loading rate dependent stiffness properties which can be challenging to test experimentally. Mechanical testing protocols that test at one loading rate are not able to capture the stiffness changes as they correspond to various loading frequencies. Additionally, it is difficult to determine if the ligament strain targets have been loaded beyond the toe region causing some to test ligaments at multiple strain targets [30], [35]. Recall that the viscoelastic model requires experimentally data consisting of stress relaxation or creep response, as well as the hysteresis response. It can be time consuming to conduct the

multitude of mechanical tests required to measure this experimental data, especially when considering the time for zero-strain periods necessary for tissue recovery. Meanwhile, specimen hydration and temperature must be maintained during testing. It is possible to perform the testing over multiple days, however, this requires additional freezing cycles which would alter mechanical properties [50]–[52]. Therefore, it is desirable to determine ligament behavior at various loading rates and strain targets, however, this poses several logistical challenges. To overcome these challenges, a mechanical testing protocol that subjects each ligament to several physiological loading frequencies (0.5, 1, 2, 3, 5, 10 Hz) at several strain targets, will be presented in this work. However, this testing protocol is long (~6 hours/ligament) and maintaining precise timing and testing order is tedious, exacting work. The nature of this protocol increases the chances of making a mistake, therefore, a semi-automated mechanical testing system will be introduced to execute the testing protocol. To reduce ligament damage during testing, a custom environmental chamber will be introduced to maintain a constant temperature ($37^{o}C \pm 1^{o}$) and regularly bathe the specimen in a saline solution.

In summary, what is presented here is a comprehensive methodology to mechanically test ligaments which draws from state-of-the-art approaches which overcome many historical testing limitations. To provide evidence of the utility of this method, a small sample size of human foot and ankle ligaments were evaluated using these methods.

Chapter 2. METHODS

2.1 OVERVIEW

As it encompasses test system development, and characterization of the mechanical properties of foot and ankle ligaments, this project is broken into two major parts. The first part will focus on the development of a ligament testing methodology that overcomes previously mentioned limitations by using state-of-the-art measurement and automation techniques, the product of this effort is an improved way to measure ligament tissue properties. The second part will use this methodology to evaluate several important foot and ankle ligaments, the product of this effort is in providing the research community with the most accurate and biofidelic ligament mechanical characteristics possible with current techniques, for the ligaments we have chosen to study. Chapters 2 and 3 are presented in manuscript format and comprise the bulk of the methods and results of this thesis.

2.2 INTRODUCTION

Ligaments are stiff connective tissues which behave as elastic elements while simultaneously exhibiting time dependent stress in response to strain history and are additionally dependent on tissue temperature and hydration. Ligaments therefore exhibit viscoelastic properties which are predicated on accurate measurements of ligament morphology and control of environmental conditions during mechanical tests. Length and cross-sectional area are the bases

for stress and strain measurements used to set actuator targets and measure tissue response. Errors in these measurements can lead to inconsistent mechanical characteristics. Additionally, soft tissue temperature and hydration influence tissue stress and strain history and contribute to further errors in material characterization. Finally, with our increased understanding of the rate dependent response of tissues, there is an acknowledgement that evaluating tissue performance using a single loading rate is inadequate for anything beyond very simplistic evaluation. This opens the challenge of how to execute a comprehensive battery of tests on a ligament tissue to capture a broader range of its rate- and displacement point- dependent response. Large test batteries are complex, prone to user error and can take substantial time – limitations that are well suited to automation. Therefore, precise measurements of ligament morphology and control of environmental conditions during a battery of mechanical tests aided by an automated testing regiment, is vital to ensure the accuracy of ligament mechanical characterization.

2.2.1 Ligament Measurement

It is challenging to determine ligament length due to the nature of the fiber network at the insertion surfaces, the wrapping orientation of the tissue, and the typically irregular 3D geometry of ligaments (Figure 17). One convention for measuring ligament length is to average manual caliper measurements of the superficial ligament fibers (Figure 15) at several locations as they insert into bone [34], [36], [87], [90]. While this convention has been used consistently from early studies to papers being published in 2019, the method has challenges with consistent placement of calipers in specific anatomical locations to achieve repeatable measurements. Additionally, the superficial fiber lengths may not reflect the entire tissue behavior and may instead overestimate

length in ligaments with concave insertions and underestimate length in ligaments with convex insertions. To overcome this, other studies have used laser scanners [43], [44], [52], [91], [92] and imaging tools [42], [93], [94] to measure the irregular 3D geometry of the ligament. While high resolution is common among these imaging techniques, not all are well suited for differentiating ligament from surrounding tissues. Regardless of imaging methods, ligament length has been derived in several ways once geometry is obtained. Techniques vary from fitting a straight line to the ligament shape [43], to taking virtual linear measurements of the superficial ligament surface edges at several anatomical locations in a method akin to caliper measurements in physical space [94]. Independent of the measurement technique, ligament length has been shown to change with joint position and the measured length can differ when the ligament wraps around bony anatomy [2], [43], [94] (Figure 15). While it is infrequently addressed, isolating bone-ligament-bone specimens for 3D geometric measurements can alter the *in situ* pose of the ligament. Additionally, such specimens are scanned in a very low load state, which may not be characteristic of a ligament pose while standing. The inability to recover physiological orientation during mechanical tests has been explicitly addressed as a limitation in several studies [45], [95], [96]. Methods for determining ligament measurements vary between studies—some studies will apply a 5N load [45], while others will measure *in vivo* [94], [97].

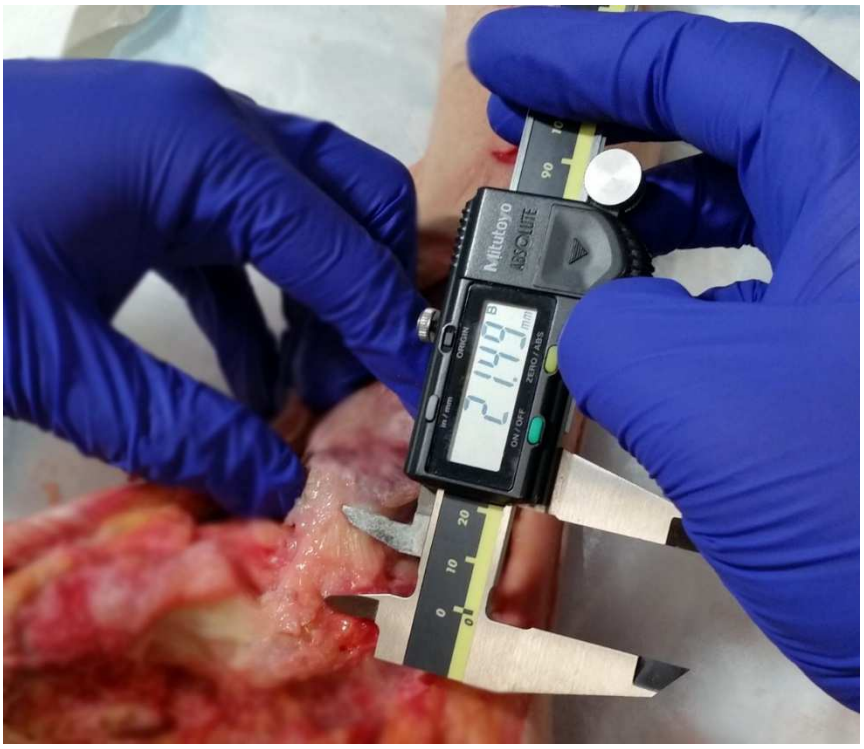

Figure 15: Caliper length measurement of the middle fibers of the deltoid ligament

Measuring ligament cross-sectional area is also challenging as it changes considerably along the length of the ligament, includes concavities of the ligament surface, and deforms dynamically with joint position. To measure cross-sectional area, the width and thickness have been measured using calipers [37], [40], [41], [98], specialized micrometers [35], or imaging tools [45], [93], [97], [99] at the approximate mid-length and fit to either a rectangle [40], [41] or an ellipse [37], [98]. However, this method simplifies the shape of the cross-section and therefore may not best represent ligament morphology (Figure 16). To mitigate these measurement errors, an effort has been made to accurately capture ligament cross-sectional area via molding and casting [45]. With this technique, a cross-section is cut from a bone-ligament-bone casting and the area of the irregular shape is measured from a high-resolution, high-contrast photograph. While this technique captures the concavities of the ligament surface and is accurate within 0.334 mm^2, it poses challenges in practice due to the estimation of ligament center, the loss of material from the

cut, and the experimenter's ability to cut normal to the ligament surface. Additionally, this method is labor intensive, and the number of potential slices available varies based on ligament length. In a study by Fujimaki et al. (2015) cross-sectional area was measured using a laser scanner at varying *in situ* positions. This study found significant differences in ACL mid-substance cross-sectional area with changes in knee flexion angle. Additionally, the group found a small change (less than 5%) between knee loaded and unloaded conditions. Therefore, measurements of initial ligament length and cross-sectional area might differ depending on orientation and applied load.

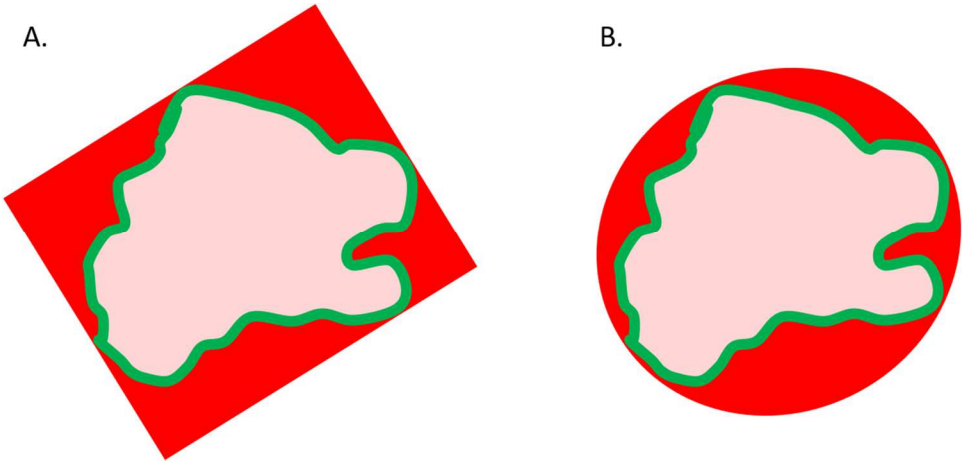

Figure 16: Representation of the (A) rectangular fit (Kwan et al.,1993; Hewitt et al., 2001) and (B) elliptical fit (Pioletti et al., 1999; Anderson et al.,2001) as compared to ligament cross-section measured from CT.

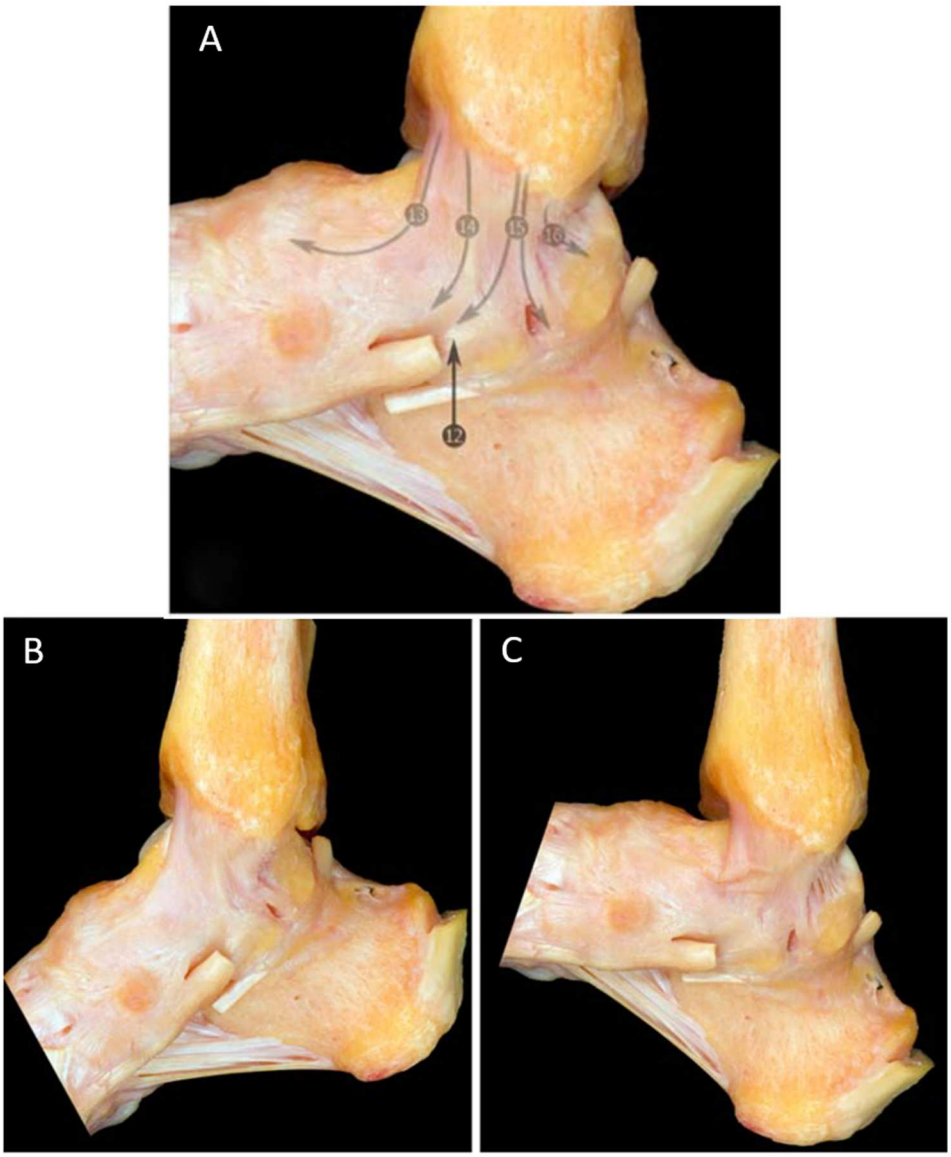

Figure 17: Medial aspect of the ankle showing the (A) fiber orientation of the different ligaments, including the deltoid (15) during (B) plantarflexion and (C) dorsiflexion. The deltoid ligament changes shape in each position. (image modified from Golanó, P, et al., 2016)

2.2.2 Ligament environmental conditions

As ligaments dehydrate they become stiffer, and the relaxation decreases [46], [48], [100], while increases in temperature result in hysteresis decreases, relaxation increases, and peak load decreases [49], [101], [102]. It is common therefore to submerge ligaments in heated saline

solutions when conducting mechanical tests for long periods [48]. However, long exposures (≥ 8 hours) to saline solutions causes an increase in cross sectional area and can produce a decrease in modulus as compared to short term exposures (~15 minutes) [47]. To improve mechanical characteristic accuracy, an effort has been made to control the effects of long exposures to saline solutions. An advantage to submerging ligaments in a bath of circulating saline is temperature regulation. There is some speculation that unregulated temperatures results in thermal contraction/expansion of the mechanical testing apparatus and specimen [102]. While some of these mechanical variations can be adjusted using the time-temperature superposition [103], [104], reliance on these mathematical models can make data interpretation vulnerable to numerical instability. Therefore, it is ideal to maintain ligament environmental temperatures while moderating exposure to saline solutions. Managing hydration and temperature over the necessary extended testing period in order to perform a battery of material tests becomes an increasingly challenging problem and another opportunity for an automation solution.

While the techniques described above provide a summary of existing limitations and have been established in attempts to minimize the errors in ligament mechanical characteristics, there is room for further improvement. Therefore, this work proposes new methods which are compared to common standard practices where possible. To evaluate foot and ankle ligament mechanics, the primary aims were to (1) determine how morphological ligament length and (2) cross-sectional area effect mechanical properties as compared to current conventions. Additionally, this work will outline a novel mechanical testing automation system which aims to (3) maintain environmental conditions in a repeatable and reliable fashion and (4) accommodate extensive testing batteries via hardware automation to improve repeatability and minimize user errors.

2.3 METHODS

2.3.1 Dissection

To evaluate the efficacy of the novel methods presented here, the middle portion of the tibiocalcaneal ligament was harvested from eight fresh-frozen cadaveric foot specimens (3 male/5 female, 57 ± 11.5 years, 168.7 ± 33.5 lbs., 26.3 ± 6.3 Body Mass Index). Foot specimens were stored at -20ºC until 24 hours before dissection at which time they were thawed at room temperature. Careful surgical dissection was used to remove skin/fat/muscle from immediately around the tibiocalcaneal ligaments, so that surrounding tissue was not in contact with the ligament and therefore the ligament was surrounded by air on all sides (Figure 18).

Figure 18: Dissection of the calcaneofibular ligament to highlighting the ligament (outlined with dotted line) isolated such that it is not in contact with any surrounding tissue.

2.3.2 Physiologic Ligament Pose

To replicate the pose and shape of these ligaments during stance, the cadaveric feet with an exposed tibiocalcaneal ligament were placed in a custom loading jig with a neutral ankle pose (leg ~90^{o} from long axis of the foot) that applied approximately 50lbs of compression through the residual tibia. While in this loading jig, the feet were imaged with a commuted tomography (CT) cone beam scanner (PedCAT, Curvebeam, Hatfield PA; 0.37 mm isotropic volume) (Figure 19). Following the CT scan, the loading jig was removed and the ankle was placed in approximately 90^{o}. Ligament caliper measurements were taken at 3 locations and averaged to measure ligament caliper length (CL), these data are captured to compare to novel length estimates via CT scans.

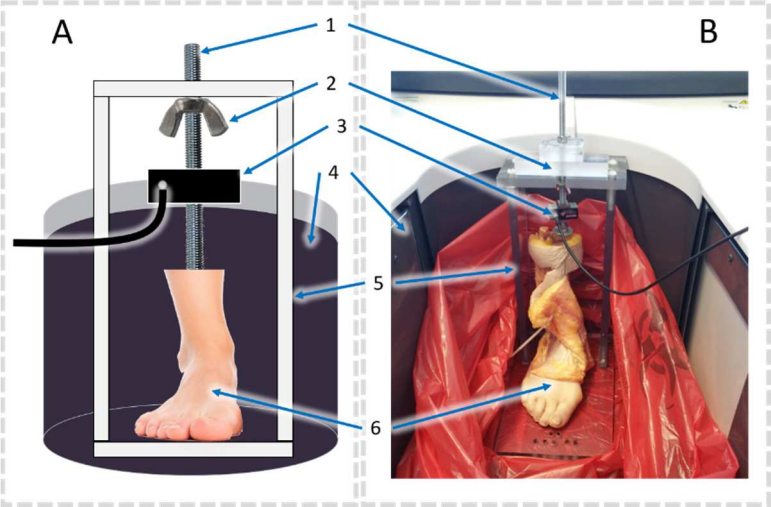

Figure 19: The illustration (A) and photograph of a data collection (B) of CT scanning with foot loading jig. The weight is loaded through a threaded rod (1) by applying tension to an acrylic box (5) via a wing nut (2). The load cell (3) monitors the applied load on the cadaveric foot (6) within a CT bore (4).

2.3.3 Ligament Removal

With the ankle still in approximately 90^{o}, the soft tissues remaining on the bone were dissected away from the ligament insertion sites and a 1mm drill bit was used to drill two holes into the bone, with care taken to avoid damaging nearby ligament fibers. 1mm wires were shaped into hooks and forced into the drilled holes. By twisting neighboring wires together, a small amount of tension was applied to the cortical bone by the hooks. A rigid wooden brace (tongue depressor) was attached to the wires, bridging the two insertion sites, and polyurethane adhesive (Gorilla glue, Cincinnati OH) was applied to the wooden brace and wires to form a rigid external brace. The bone-ligament-bone sample complete with wire and wood brace was then excised using a surgical saw (Stryker, Kalamazoo MI.) (Figure 20). The ligament preparation processes mentioned to this point of dissection, CT scanning, ligament fixation, and ligament removal took approximately 8 hours; when these steps were complete, the samples were stored at -20^{o}C overnight (freeze cycle 2).

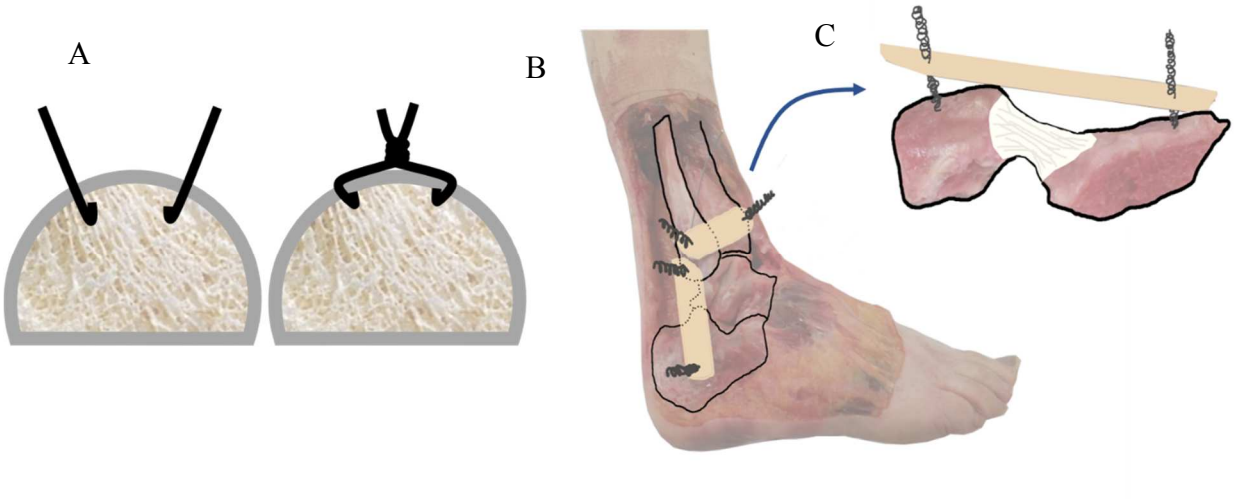

Figure 20: Ligament fixation starting with (A) bone cross-section of wires inserted into the bones and tensioned against cortical bone, (B) wooden brace fixing the joints within the foot pose, and (C) the excised ligament with external fixation.

2.3.4 Potting

After thawing a second time, the ligament was potted so that it could interface with the mechanical testing machine (Figure 21). Additional wire was coiled into drilled holes in the bony ends of the bone-ligament-bone sample to increase the surface area for potting. Bony ends were placed in an alignment jig which allow one bone end to be potted at a time while maintaining vertical and rotational alignment. Polyester resin and putty (Bondo; 3M, Maplewood MN) were combined (approximately 2-to-1 putty-to-resin) to maximize the flow around the bone thereby fixing the bone fragments and wire in the potting cups. These steps required approximately 5 hours after which the potted bone-ligament-bone sample still with external fixation were stored again at -20^{o}C until the day of mechanical testing (freeze cycle 3).

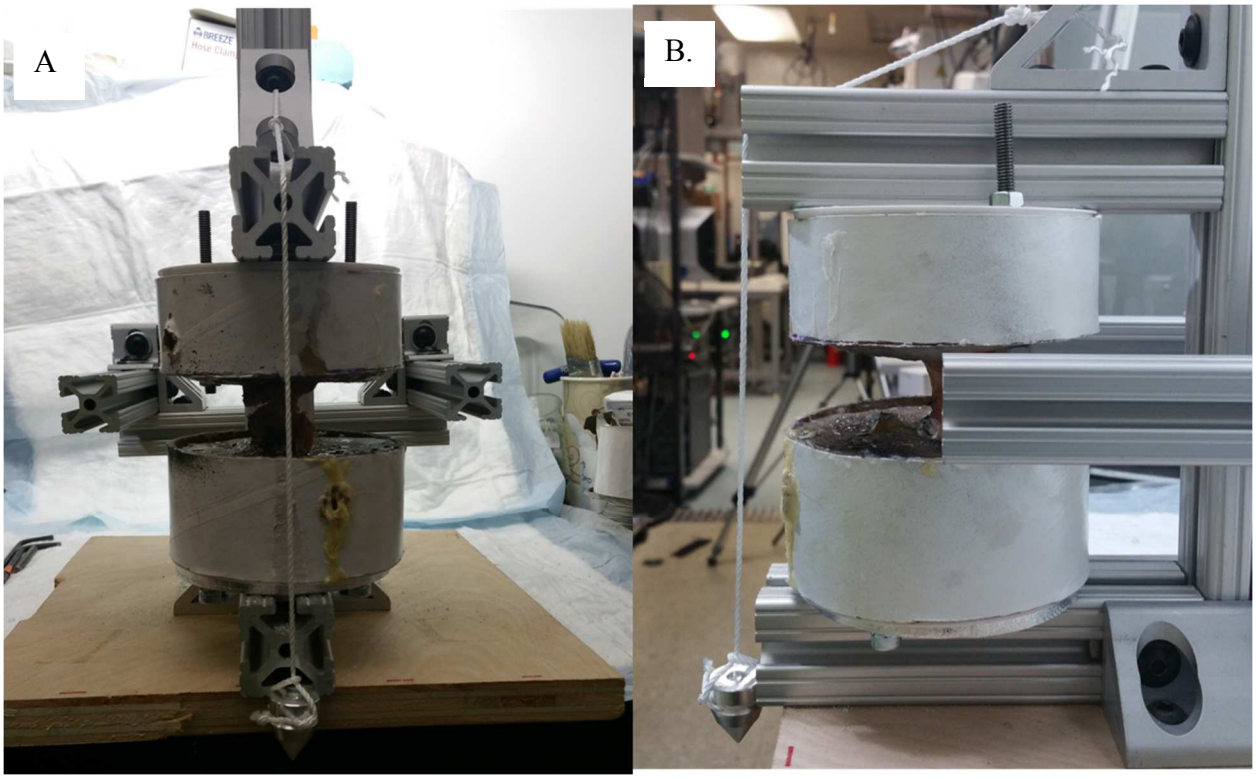

Figure 21: potting jig used to align the ligament in the center of the potting used to interface with the mechanical testing machine. (A) The view from the front of the potting jig and (B) the side of the potting jig.

2.3.5 Length and Cross-Sectional Area Measurements

Morphological ligament length and cross-sectional area estimates were made from segmented DICOM images in Mimics (Materialize, Leuven Belgium) of the weighted foot CT scans. The air surrounding the ligaments created a clear border between tissue and the air, the intensity difference between bone and ligament provided an additional border to separate tissues using thresholding tools in Mimics. The scans were visually inspected and adjusted as needed to correct any discrepancies. The segmentation yielded surface point cloud data, which was imported to Meshlab [105] where internal/duplicate faces and vertices were removed, surface mesh density and uniformity was increased using least squares subdivision surfaces (3 iterations, absolute threshold = 0.5 mm, threshold 1%) [106]. The resulting overlap between ligament and bone point clouds were used to create two insertion surfaces from closely neighboring ligament and bone points (within 1mm of one another) (Matlab, Natick, MA).

Once the segmented 3D bone-ligament-bone point clouds were created, several measurements were applied. Linear length (LL) was measured as the distance between the centroid of each ligament to bone transition surface (i.e., insertion site). To refine the initial LL and determine cross sectional shape over the length of the ligament, several steps were performed. First, the ligament length was divided into nodes at 1% intervals along the LL's vector thus converting the LL into a set of piecewise 3D lines (co-linear for now). Second, each node was adjusted to the ligaments cross-sectional center, based on the cross section at that node. To define these cross-sections, starting from distal moving to proximal, a plane orthogonal to the LL's vector at each node was created; then the points within 0.5 mm of that plane were projected onto the plane and alpha shapes ($3\frac{1}{3}$ mm radius) were used to determine the perimeter of the cross-sectional of the

ligament. Due to the process of fitting a circle to the 2D points, alpha shapes are able to find and connect the points along the perimeter and distinguish concave shapes (Figure 22) [107]. Once this is done, the centroid of the cross section can be calculated, and the node (and therefore also the piecewise 3D line segments between them) were adjusted for each node along the ligament's length. The piecewise 3D lines were then filtered with a low-pass Butterworth filter (4^{th} order, cut-off 10 Hz). This yields an updated ligament length which is defined as the sum of each 1% segment lengths. Third, after this initial pass, the process repeats in the proximal to distal direction. As the piecewise segments are no longer co-linear, the planes used to calculate the cross section are defined differently. To find the first cross-sectional slice plane, the LL vector (from proximal to distal this time) is used to define the normal vector as before. For subsequent cross-sectional plane slices, the previous 2 nodes are used to define the normal vector of the current cross-sectional slice plane. The center of the cross-sectional ligament area is used to refine location of the next node as before. The final point is the insertion which may be adjusted based on the 2D cross-sectional center determined in part by the previous 2 nodes (Figure 23). Fourth, after each such iteration, the updated length estimate is compared to the previous length estimate and the process iterates bi-directionally as described until the ligament length changes by less than 5%. At this convergence, the resultant iterative length (IL) is defined. This length considers both 3D ligament morphology and insertion shape.

2.3.6 Mechanical testing preparation

Following the digital analysis above, potted ligaments were thawed for the third and final time and prepared for mechanical testing. A fiducial marker cluster was fixed to each potted end using additional polyurethane adhesive. The bone-ligament-bone sample with external fixation, potting, and fiducial marker clusters were CT scanned for a second time for later registration of these marker clusters to the ligament insertion registration via segmented DICOM images in Mimics. The potted ligament position data is captured in this CT scan for a later comparison with the mostly intact weighted foot ligaments position. In the event that the ligament failed prematurely, a speckle pattern was applied to the ligament with black and white spray paint so that

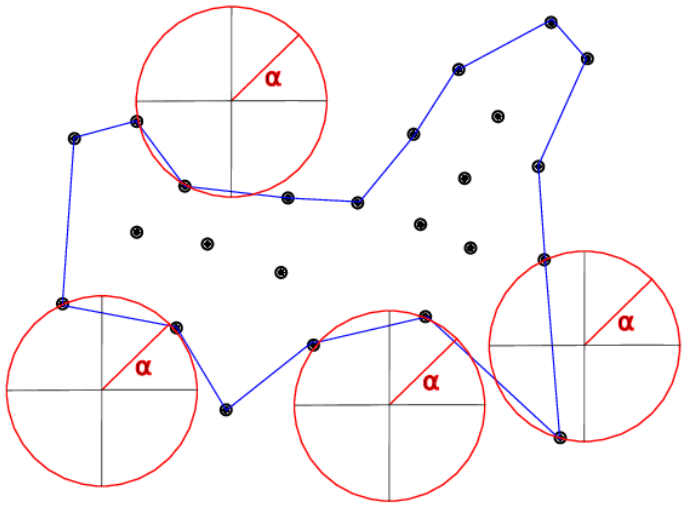

Figure 22: Schematic of the alpha shapes function. A circle with radius α is fit to each point and its nearest neighbor within a set of points on a 2D plane. If the circle does not contain a point inside, then the 2 points are classified as perimeter points and a line is drawn between them. Note how this function captures the concavities of the shape formed by the set of points.

digital image correlation (DIC) tracking could be used to characterize failure mechanics. While it is beyond the scope of this thesis project, surface strain analysis of non-destructive properties is also possible with DIC data. Speckle size and density was controlled to optimize DIC pattern recognition [108] by spraying compressed air through the aerosolized paint.

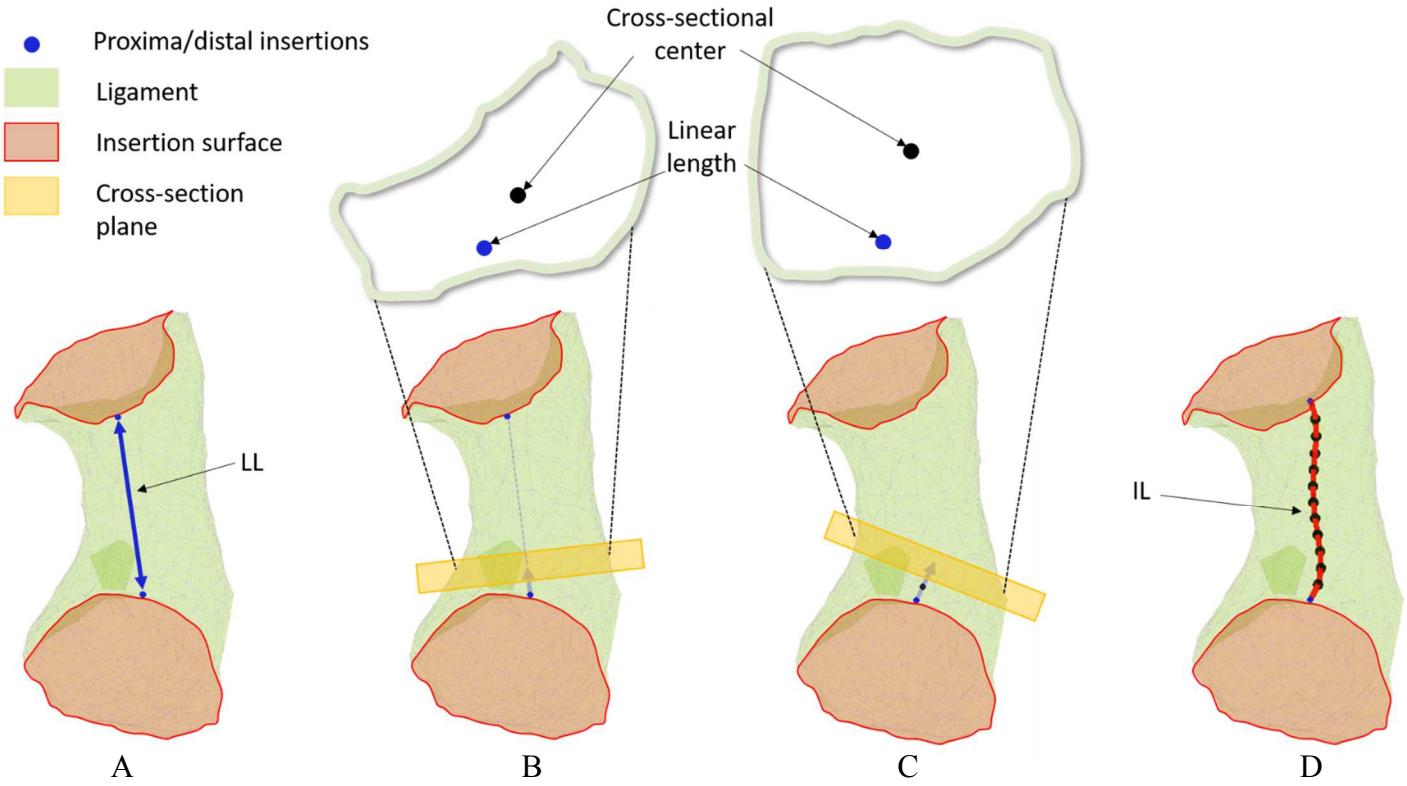

Figure 23: Illustration of ligament length estimation. (A) the Linear Length (LL) is a straight line (blue arrow) between insertion surface (red) centroids (blue points). The linear length is updated to the centroid of the cross-section (black points) defined at 1% intervals along the ligament length (points reduced in figure). (B) Cross-section shape was defined by a plane (orange) whose normal vector aligns with the LL vector for the first point. (C) Subsequent cross-sectional plane normal vectors were defined by the previous two points. (D) The Iterative Length (IL) estimate is defined after the cross-sectional area centroid is updated along the ligament length.

Following specimen preparation, the three length estimates (CL, LL, and IL) were used to define three separate actuator strain levels for a series of repeated mechanical tests in increasing strain order (LL, IL, CL). In each test, ligaments were subjected to 34 triangle waves of 6% strain (based on either CL, LL or IL) at physiological loading rates (1, 2, 3, 5, and 10 Hz) in randomized order. Following each of the triangle wave series, 15 minutes of zero stress was maintained to allow the ligament to rest. This entire test battery took about 12 hours.

2.3.7 Mechanical Testing and analysis

The first 30 triangle waves of each series served to precondition the tissue. The next 3 triangle waves were used to estimate stiffness, modulus, hysteresis, and peak force. The final cycle was collected as a buffer during test cessation.

The tibia of the partially dissected weighted foot was matched to the tibia of the potted ligament using iterative closest point matching (ICP; MeshLab) [105]. The LL was determined for the potted ligament using the methods described above. Next, the ligament angle and length differences were compared between the partially dissected weighted foot and the potted ligament using the vectors between insertion centroids (Figure 24).

A linear fit to the last 30% of the loading portion was averaged for the 3 triangle waves to measure stiffness and modulus. Hysteresis was measured by integrating the loading and unloading of those three waves.

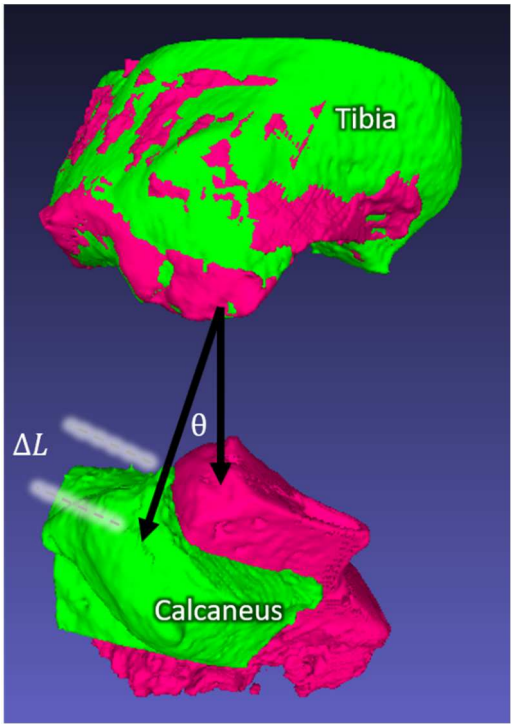

Figure 24: Comparison of calcaneus position after matching the tibia position in a partially weighted foot (green) before and after potting (pink). The difference in length and angle of the vector formed between insertion points is used to compare the ligament position.

2.3.8 Simulating Environmental Conditions

Temperature was monitored (1000 Hz) using 6 calibrated thermistors mounted circumferentially around the ligament and a ceramic heating element was used to maintain a constant temperature (37°C). Hydration was maintained by spraying the ligament with a 0.9% saline solution for 2 seconds every 15 minutes. The sprayer was interrupted during actuator motion so that a high-speed camera (240 Hz; Optitrack, Corcallis, OR) could record ligament strain. Fiducial markers were tracked with a 6-camera motion capture system (240 Hz; OptiTrack, Corcallis, OR) during actuator motion. Sprayer actions, temperature measurements, and camera

recordings were triggered throughout testing using the analog/digital BNC breakout. To capture misalignment between the ligament insertion points and the linear actuator motion, the registered fiducial markers were used to measure the angle offset and the true strain correction for all strain level conditions (Figure 25).

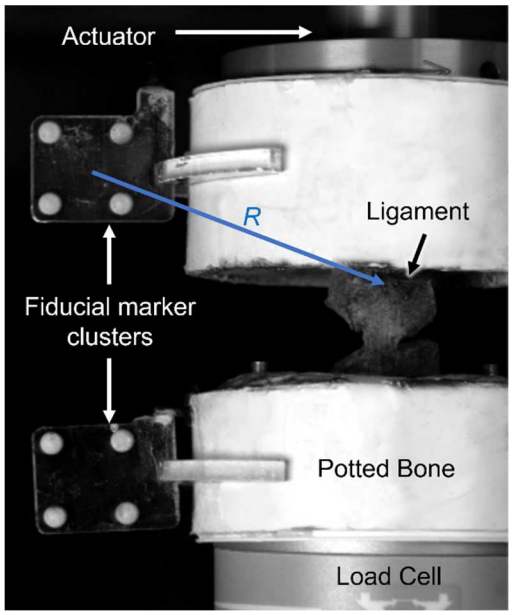

Figure 25: potted ligament with rigidly fixed fiducial markers registered to ligament insertions (R). By tracking fiducial markers during mechanical tests, the insertions can be determined.

2.3.9 Automated Testing

To mitigate errors during the long battery of tests and rest intervals, an automated mechanical testing system was designed to manage all of the components needed to perform the proposed testing battery. These components include: the mechanical testing machine (E3000 Instron, Norwood, MA) which was programmed to execute tensile tests while recording load and displacement data (WaveMatrix, Instron, Norwood, MA); the sprayer and heating elements whose function was controlled using an analog/digital BNC breakout (BNC 2090; National Instruments, Austin TX); motion capture cameras and a high-speed camera (OptiTrack, Corvallis, Oregon) to

record ligament strain and monitor the ligament (Figure 26); and a custom LabView program which monitored signal traffic between components and monitored the status of the mechanical testing machine.

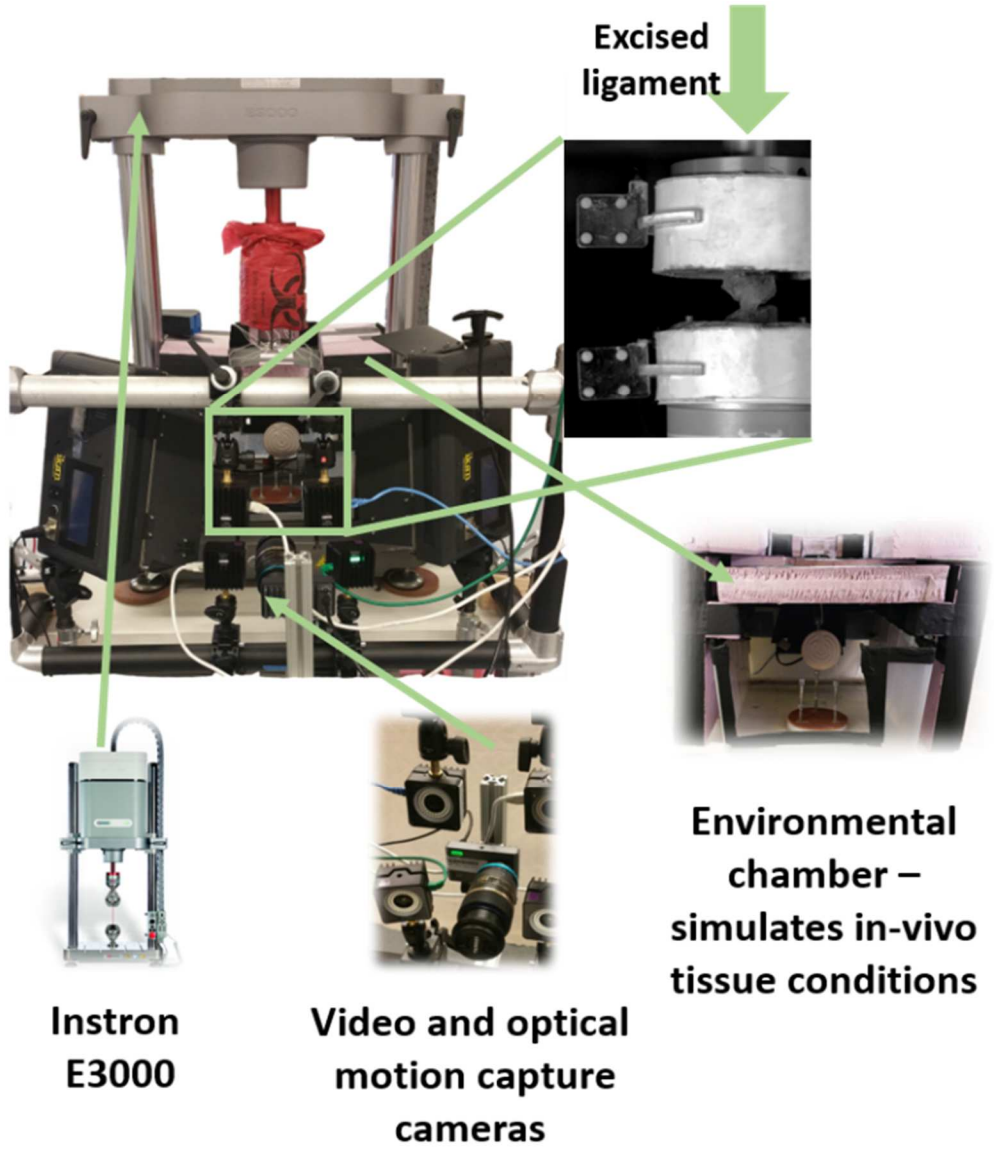

Figure 26: Experimental set-up of mechanical testing automation system.

The LabView program managed the actions of the motion capture cameras, high speed camera, heating element, and sprayers. Once the initiation of a mechanical test was detected, the system

would begin recording high speed and motion capture cameras and interrupt the sprayer function (to not obscure the video data). This data along with the load, displacement, and temperature data was saved with a consistent naming convention for improved file management. During testing, the sprayers and heating element were controlled by the automated system via relay switches. The automated system streamed and recorded backup load and displacement data for the duration of mechanical testing (Figure 27).

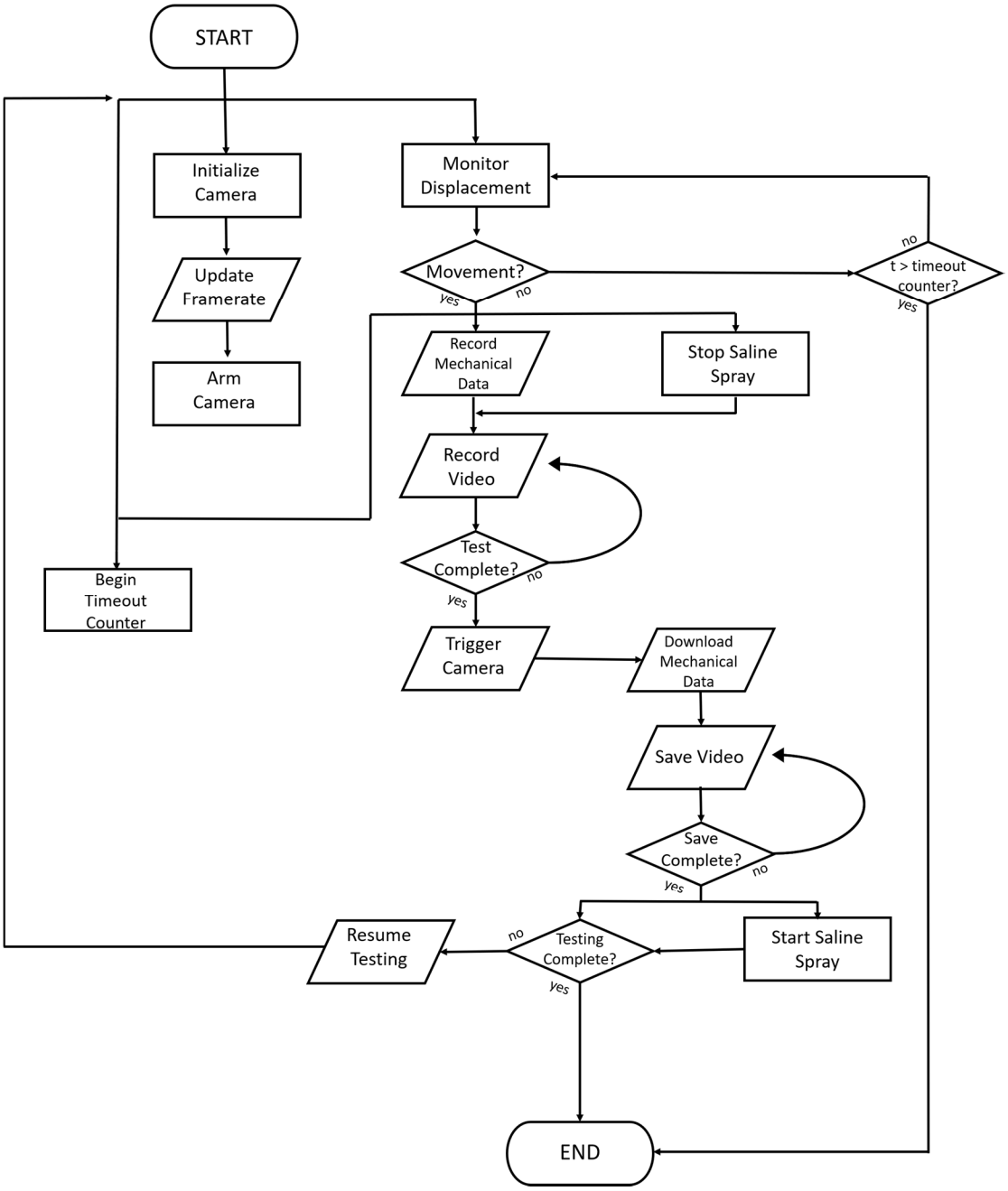

Figure 27: Flowchart summary of the automated mechanical testing system. This system monitored and controlled a mechanical testing machine which triggered cameras and maintained environmental conditions.

2.4 RESULTS

Data from six of the eight ligaments were used. One ligament (specimen 5) were excluded from the study due to very low loads during testing (< 5N for most tests). Data from another specimen (specimen 8) were excluded due to a bone fracture near the insertion cite which was discovered in the pretesting CT scan. During mechanical testing the target strain level was not achieved for the higher frequency triangle waves and during the stress relaxation test. For 10 Hz triangle waves, the strain levels were within about 50% of target strain.

2.4.1 Length

Length estimates for CL, IL, and LL, and displacement targets were measured for all specimens. The CL was largest measured length (~25% > LL and IL) as compared to LL and IL which were somewhat similar to each other in length (≤ ~10%).

Hz	Measurement	Length Estimate		
		CL	LL	IL
	Length (mm)	28.9 ± 2.6	19.78 ± 1.96	22.07 ± 1.756
	Displacement level	1.7 ± 0.2	1.19 ± 0.12	1.32 ± 0.11
0.5	Stiffness (N/mm)	44.3 ± 14.8	31.62 ± 8.05	37.78 ± 10.88
	Hysteresis	69.9 ± 23.3	28.74 ± 7.40	37.78 ± 10.88
	Peak Force (N)	55.1 ± 20.1	29.18 ± 7.03	37.69 ± 9.97
1	Stiffness (N/mm)	45.7 ± 16.3	31.56 ± 8.20	36.96 ± 10.60
	Hysteresis	68.3 ± 23.0	29.25 ± 6.57	36.96 ± 10.60
	Peak Force (N)	55.6 ± 20.7	29.50 ± 6.82	36.12 ± 8.61
2	Stiffness (N/mm)	45.8 ± 15.7	29.97 ± 7.70	35.91 ± 10.51
	Hysteresis	61.1 ± 18.2	26.07 ± 4.86	35.91 ± 10.51
	Peak Force (N)	52.8 ± 18.4	27.80 ± 5.69	34.25 ± 7.85
3	Stiffness (N/mm)	46.0 ± 17.1	29.90 ± 9.18	38.62 ± 12.30
	Hysteresis	60.7 ± 14.2	27.51 ± 7.87	38.62 ± 12.30
	Peak Force (N)	52.6 ± 17.0	28.40 ± 7.02	36.88 ± 8.01
5	Stiffness (N/mm)	43.6 ± 17.4	27.53 ± 8.08	35.68 ± 12.81
	Hysteresis	47.7 ± 12.7	24.27 ± 3.14	35.68 ± 12.81
	Peak Force (N)	46.7 ± 17.3	26.56 ± 4.94	33.65 ± 7.88
10	Stiffness (N/mm)	39.4 ± 15.6	25.68 ± 8.62	31.01 ± 13.85
	Hysteresis	35.3 ± 7.3	15.19 ± 4.76	31.01 ± 13.85
	Peak Force (N)	40.2 ± 13.0	22.13 ± 4.53	27.66 ± 6.27

Table 1: Variations in stiffness, hysteresis, and peak force as a result of changes in length estimate and triangle wave frequency for a 6% strain level.

2.4.2 Cross Sectional Area

There was ~ 80% variation in cross-sectional area when comparing the methods proposed to traditional rectangle or elliptical area fits. The largest measurement was typically seen using the rectangular fit, second largest for the elliptical fit, and smallest for the cross-sectional area measured from CT using the methods proposed. When determining the elastic modulus using each of those areas, variations in cross-sectional area estimates resulted in ~8% average change in modulus of elasticity between the elliptical fit and CT scan cross-sectional area estimates, and ~15% average change between rectangular fit and CT scan cross-sectional area estimates (Table 2 & Figure 28). However, cross-sectional area had less of an effect on modulus as the loading rate increased. It is expected that the differences in cross-sectional area measurement variation

influenced the stress and strain relations according to the relationship A^{-1}, where A is the cross-sectional area determined by measurement variability resulting in large changes in modulus. Therefore, the modulus decreases as the cross-sectional area increases.

Measurement		Tangent Modulus (E_T)		
		rectangle fit	ellipse fit	CT measurement
	Cross-Sectional Area (mm^2)	54.3 ± 30.4	42.7 ± 23.9	41.5 ± 22.4
E_T at Triangle Wave Hz (MPa)	0.5	23.4 ± 16.7	29.8 ± 21.3	27.4 ± 21.3
	1	23.1 ± 16.7	29.4 ± 21.2	27.0 ± 21.2
	2	22.2 ± 15.9	28.3 ± 20.2	26.1 ± 20.2
	3	23.6 ± 16.6	27.3 ± 18.6	26.6 ± 18.6
	5	21.8 ± 15.3	25.8 ± 18.2	25.1 ± 18.2
(MPa	10	18.9 ± 13.5	23.6 ± 17.5	22.8 ± 17.5

Table 2: Variations in modulus of elasticity as a result of changes in midpoint cross-sectional area estimates and test frequency.

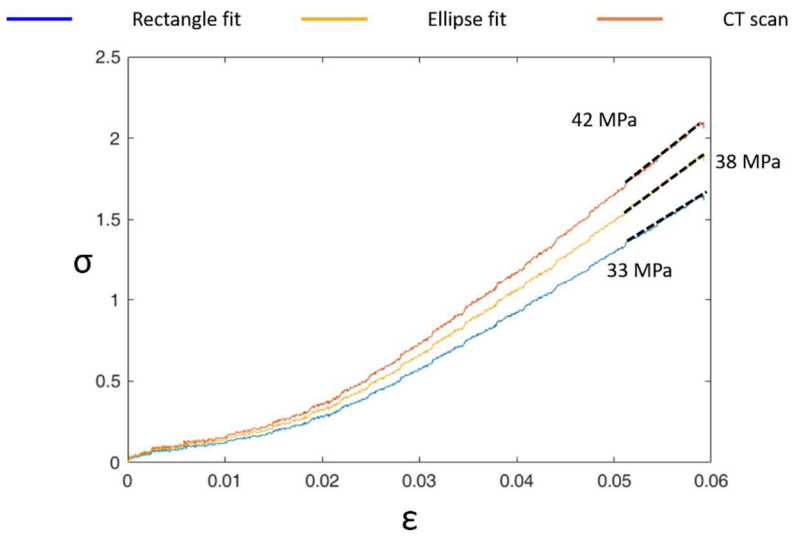

Figure 28: A comparison of the variations in modulus (black dotted line) for a representative 0.5 Hz triangle waves using the IL estimate to attain a 6% strain level.

2.4.3 Peak Force and Hysteresis

Ligament peak force and hysteresis increased by 80% and 250% respectfully, for displacement levels generated by the CL as compared to both LL and IL (Table 1). Stiffness did not notably change with variations in loading frequency or length estimation.

2.4.4 Automation System Performance

Each ligament was mechanically tested for approximately 16 hours without interruption, during which time temperature changed within ± 1.3 ^{o}C of the target temperature (37 ^{o}C). After examining the ligament before and after testing, the saline sprayers maintained specimen moisture comparable to ligaments wrapped in saline soaked gauze and sprayers were interrupted during high-speed video recordings. Load, actuator displacement, marker trajectories, high-speed video, and temperature data was recorded successfully for all trials.

2.4.5 Ligament Alignment

The partially dissected weighted foot ligament pose differed from the potted ligament pose by an average of about 23^{o} (± 6.6^{o}) and differed in length by about 1.4 mm (± 4.13 mm). Specimen alignment in the mechanical testing machine was very close to the vertical alignment between insertions. There was a vertical offset of no more than 10^{o} between ligament position and actuator motion measured via fiducial marker tracking. Therefore, the load applied was within 10^{o} of the longitudinal axis of the ligament.

2.5 DISCUSSION

2.5.1 Summary of work

Due to their small size, wrapping orientation, and complex 3D geometries, ligaments of the foot and ankle require unique testing considerations to generate accurate measurements. Ligament fiber orientation dictates boarder definitions which determine ligament morphology (Figure 29). The surface concavities and wrapping orientation make the measurements of shape definitions challenging, thereby effecting cross-sectional area and anatomical length estimation. The CL estimate is a commonly used technique [35], [36] based on estimates of the outer ligament fibers and might not represent the collagen fibers engaged during physiological ligament loading. The LL and IL estimates consider the ligament length between insertion centroids in a way that considers anatomical orientation while the ankle is in neutral position (approximately 90^{o} to the lower leg). The IL estimate builds on the LL estimate in that it takes a path along the center of the ligament and therefore considers ligament wrapping. While it is common to fit either an ellipse or

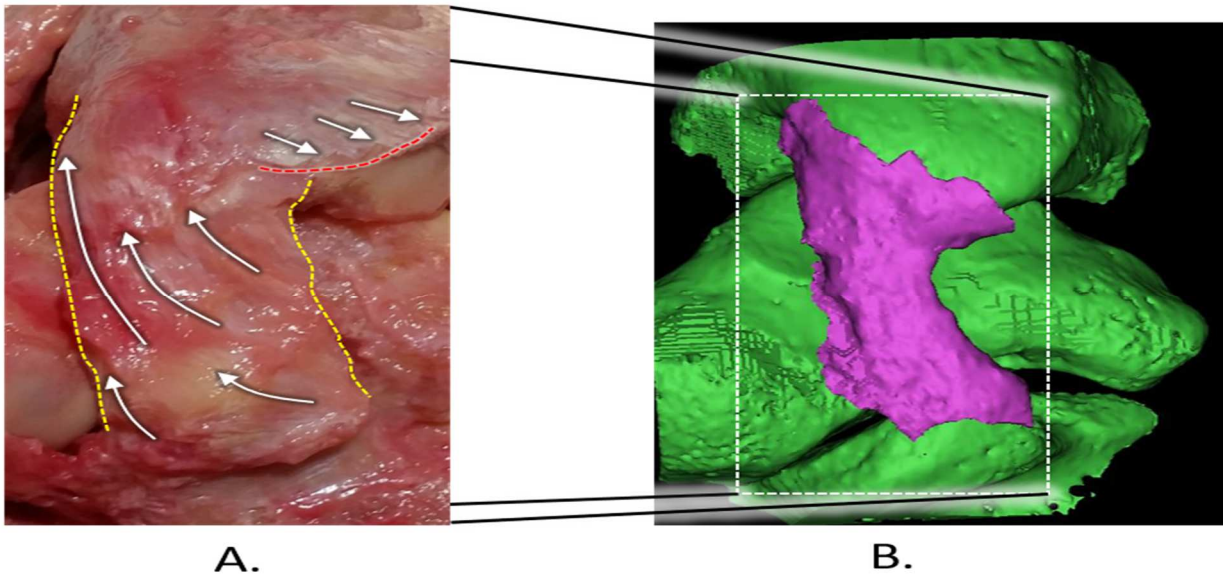

Figure 29: An example of ligament morphological complexity: (A) Dissection photo of the tibiocalcaneal ligament with fiber orientation indicated by white arrows. Ligament borders (yellow dotted line) are determined by collagen fiber direction. Fibers that are not in alignment with insertions are cut (red dotted line). The borders are reestablished during segmentation (B) shown here with ligament (purple) and bone (green) masks.

rectangle to width and thickness measurements [37], [40], [41], [98], these methods can be poor estimates of the true cross-sectional area and as a result the mechanical characteristics varied as compared to the CT measure of cross-sectional area.

Ligament hydration and temperature can influence the material properties and contribute to variability in mechanical characteristics. Therefore, the temperature was kept within 37 ± 1.3 ^{o}C, and the sprayer was applied at regular intervals. Regulating these variables helps to improve precision and ensure that the experiments are repeatable.

2.5.2 Ligament isolation and measurement

Ligament borders were defined during dissection by visually tracing ligament fiber paths to insertion points (Figure 29A). Unlike more clearly defined ligaments such as the anterior and posterior cruciate ligaments, many of the ligaments in the foot and ankle have diffuse insertions with collagen fibers in many orientations [2]. Therefore, discretion was used when making determinations of ligament borders. These border definitions at the insertions influence the caliper measurements and insertion surface definitions which define subsequent length definitions (CL, LL, and IL). Border definitions at the mid-substance define the cross-sectional area by measuring the tissue (either with calipers or with digital tools) after dissection. Further, cross-sectional area measurements are determined by tissue hydration, with dehydrated tissues exhibiting smaller cross-sectional areas than hydrated tissues. Considerations with border definitions continued when segmenting DICOM images of ligament and bone tissues.

2.5.3 Ligament Surface

Segmented DICOM data provided details of the bone and ligament surface meshes used to make measurements (Figure 29B). Very few duplicate or internal points or vertices were found (< 10) and least squares subdivision [106] smoothed but did not demonstrably change the shape of the ligament surface (Figure 19). The uniformly spaced points refined ligament definitions and aided bone-insertion centroid and cross-sectional centroid determinations. The refined mesh surface might have also aided in early convergence of the IL estimate (≤ 3 bidirectional iterations) due to consistent surface definitions when applying alpha shapes. Adapting methods from Kindig

et al. (2013) [109], an alpha shape radius ($\alpha = 0.3$) was maintained for all ligaments based on a pilot ligament specimen. Additionally, the improved surface definitions informed insertion centroid and length estimation since its location was refined based on the location of the neighboring cross-sectional centroids during IL estimation (Figure 30) [109], [110].

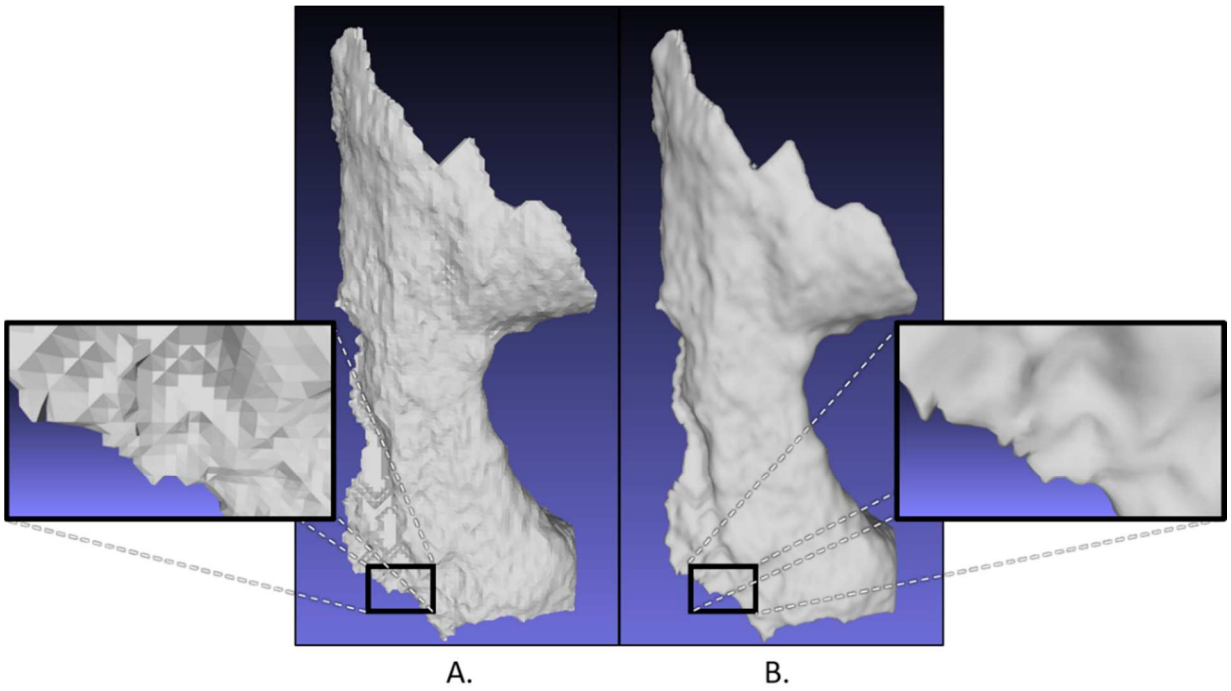

Figure 30: Mesh generated from a segmented DICOM image of the tibiocalcaneal ligament before (A) and after (B) removing duplicate faces, duplicate vertices, and smoothing using least squares subdivision surfaces. Surface details are shown in outer frames.

2.5.4 Ligament Mechanical Response

The variations in length and cross-sectional area estimates changed the hysteresis, peak load, and modulus (Figure 31 & Figure 28). However, the changes in morphological estimates did not dramatically change the stiffness. At higher triangle wave frequencies, the actuator was not able to reach the commanded strain level. This most likely due to the inertial effects of the potting (specimen was about 8% of the weight of the potting), the fact that the machine was operating within about 3% of its stroke (< 2mm strain target; 60mm stroke), and was tuned with a load cell that was operating within about 2% of its capacity (≤ 100 N load; 5kN load cell). It is also possible that the displacement targets set by the different length estimates remained between the toe region and the yielding region and therefore exhibited minimal variation. However, the variations across cross-sectional area measurements influenced the stress and strain relations according to the relationship A^{-1}, where A is the cross-sectional area determined by measurement variability resulting in large changes in modulus. From these data we can conclude that the modulus decreases as the cross-sectional area increases and the relationship is not linear. It also stands to reason that if the cross-sectional area measurement is refined, the mechanical properties from previously reported data might also be refined. Similar relationships can be established with the peak force and hysteresis properties, however more than one displacement level would be necessary due to the non-linear viscoelastic behavior of these tissues [27].

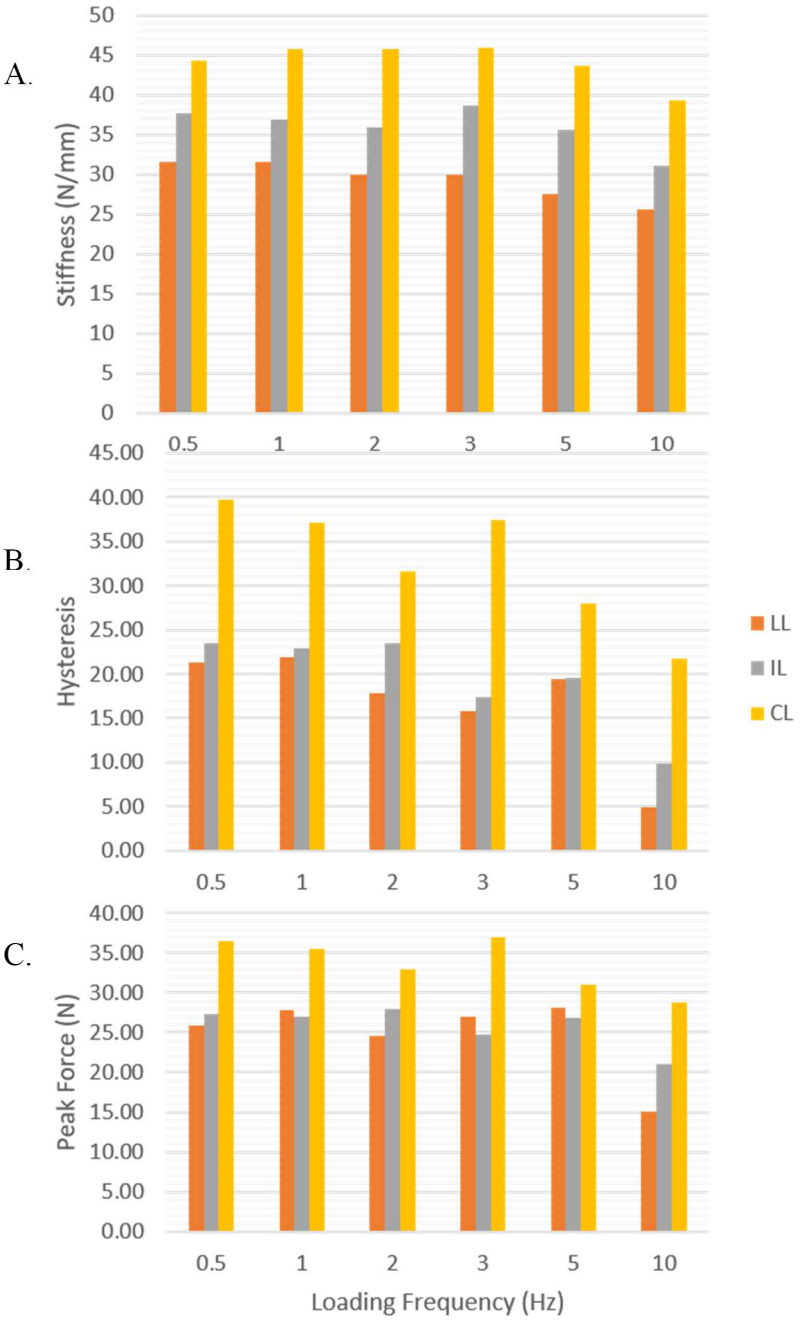

Figure 31: Variations in average stiffness (A), hysteresis (B) and peak force (C) resulting from changes in measurement length and loading frequency.

2.6.1 Limitations

While these results illuminate the importance of accurate ligament morphology measurements and environmental chamber maintenance, this study had several inherent limitations. First, excised ligaments from cadaveric foot specimens are continuously degrading in the absence of an active circulatory system. Additional degradation likely occurs with the three-freeze-thaw cycles and approximate 13 hours at room temperature and 12 hours at physiologic temperatures with almost 2,000 triangle wave cycles. This fact might influence the mechanical characteristics of the ligaments throughout testing. While the results from testing were consistent, the sample size was relatively small (n=8) and should be considered when interpreting the data. As mentioned earlier, a certain amount of discretion was taken by the experimenter in defining ligament morphology during dissection and segmentation (Figure 29). Exact measures of length and cross-sectional area are ultimately defined by the experimenter, beginning with dissection and removal of bone-ligament-bone specimen and continuing with accurate segmentation. Further to this point, the alpha shape radius and mesh smoothing will also influence the morphology characteristics. These all contribute to the determinations of length and cross-sectional area as well as ligament alignment in the mechanical testing machine. Additionally, ligament position between the partially dissected weighted foot and the excised ligament were variable based on foot anatomy. Weighting the foot caused a small amount of calcaneal eversion that resulted in position changes between the weighted foot CT scan and the excised ligament which was fixed and removed in an unweighted position. Pes planus (flat feet) in at least one specimen caused calcaneal eversion to be exaggerated in the weighted foot pose. Additionally, it is possible that there was some movement in the rigid external brace consisting of wire and a tongue depressor used to fix the foot pose during ligament extraction. It would be ideal to fix the foot pose and excise the

ligaments while the foot was weighted, but our loading jig design did not allow for this. Rigidity of the wood brace could also be improved with additional wood or alternative material that does not scatter X-ray. Future design improvements might also be applied to the temperature controller which was a bang-bang controller in this study and could be improved with a PID or similar controller.

2.6.2 Previous Work

Many of the methods in this study are novel improvements over techniques reported in the literature. Some of the most notable improvements presented here are the morphological ligament characteristics. While previous attempts have been made to use specialized area micrometers [35], imaging tools [45], [93], [97], [99], molding and casting [45], [95], calipers [37], [40], [41], [98], and laser scanners [43], [44], [52], [92], [111] to measure length and cross-sectional area, few have shown the effects of ligament morphology measurement variations. In a study by Noguchi et al. [93], the cross-sectional areas of rabbit ACL, MCL, and Achilles tendon were measured in two ways: one using ultrasonography, and the other a rectangular fit from caliper width and thickness measurements. The study showed no significant difference between cross-sectional areas. However, these results are likely specific to those tissues tested and do not consider the wrapping that some ligaments exhibit. We have demonstrated the limitation of calipers and primitive shape fits to ligament cross sectional area. In this study, the use of alpha shapes and iterative length estimation yield area and length measures which better take into account unique ligament shape and course. In the work presented in this study, we improved upon this issue by maintaining ligament *in situ* loaded pose, even after ligament removal from the specimen.

The LL, IL, and cross-sectional area techniques are capable of measuring ligaments that are relatively flat and rectangular in shape, as well as ligaments that fan out to broad insertions different directions or have a complex path between insertion sites. It is also important to note that the techniques used to determine LL, IL and cross-sectional areas are likely usable for any 3D renderings of a bone-ligament-bone sample generated by any imaging modality (such as MRI), however this has not yet been tested. These techniques for morphology measurement are substantial and novel improvements upon prior technique in literature.

In addition to measuring ligament morphology, the need to maintain physiological pose during mechanical testing is a reported limitation in studies [45], [95]. While many studies have excised bone-ligament-bone samples and visually align the specimen during potting or mechanical testing, our technique fixes the anatomical pose during ligament removal and potting to ensure that the ligament is loaded in a way that resembles *in vivo* loading during mechanical tests. Misalignments between the longitudinal axis of the fixed bone-ligament-bone sample and the actuator trajectory can be measured using fiducial marker tracking of the insertion positions during mechanical tests.

In addition to maintaining physiological positions, other studies have maintained ligament temperature and hydration in a way that mimics the *in vivo* environment. To achieve this, studies have submerged ligaments in a variety of solutions including paraffin, polyethylene glycol (PEG), phosphate buffered saline (PBS), and different concentrations of saline in water. Most of these studies show that the solution concentration and the duration of exposure have the greatest impact on mechanical properties due to the osmotic drive changing initial stress by changing tissue composition. This study used a solution concentration (0.9 g/L) that has been shown to exhibit minimal effect on mechanical properties [47] and to spray rather than submerge the ligament in

the solution in an effort to minimize the exposure to the solution while still maintaining tissue hydration. Ligaments are typically sprayed manually and therefore require constant observation which can limit the duration of mechanical testing [36], [90]. The automated mechanical testing system presented in this study allows for a more exhaustive battery of tests to be performed.

Although the methods outlined above require additional labor, this study demonstrates methods for ligament morphology measurement and preparation that are reliable and repeatable. We have demonstrated that variations in measured lengths and cross-sectional areas have considerable influence on mechanical properties. While there is some time investment in mechanical testing automation, the testing procedures can be expedited, and exhaustive testing can be performed while minimizing variability due to experimental procedures. Therefore, ligament morphology and environmental conditions should be carefully considered when designing a ligament mechanical testing procedure.

Chapter 3. MECHANICAL CHARACTERISTICS

3.1 INTRODUCTION

3.1.1 Ankle Ligament Function

Ligaments are collagen structures that connect bones to provide joint alignment and function. The foot and ankle consist of over 30 joints which articulate bony segments that bear the weight of the body and are essential for gait. Ligaments wrap around bony anatomy and contain fibers that insert into bones in multiple directions, allowing these tissues to endure loads from multiple directions. The collateral ankle ligaments provide lateral stability of the ankle joint during pivoting and cutting maneuvers. Therefore, high loads and relatively large range of motion can cause ligament injury. Ankle sprains are numerous with more than half a million cases per year and accounting for approximately 20% of all single-sports injuries [65], [66], [79]. Approximately 25% of those who sprain their ankles are unable to attend school or work for about 1 week following the injury. In some cases, ligament laxity from repeated ankle sprains can lead to ankle joint instability. Repeated ankle sprains and long-term malalignment can detrimentally affect joint health and may even accelerate ankle arthritis [83]. The tibiocalcaneal ligament crosses the ankle and subtalar joints and limits calcaneal inversion. Therefore, this ligament was mechanically tested for this study.

The mechanical properties of ligaments have been studied in detail, especially the properties of the anterior cruciate ligament [40], [43], [112] and medial collateral ligament [113]. However, ankle ligament properties have mostly focused on quantifying the ultimate strength characteristics of the tissues. In these studies, bone-ligament-bone specimens have been loaded in

a variety of displacement rates ranging from quasi-static (~0.5mm/s) [35], [87] to dynamic (10cm/s) [114]. A few studies have presented ankle ligament stiffness properties modelled as linear springs [35], [114], even though non-linear viscoelastic properties have been observed in ankle ligaments [114]. There have also been studies that present ankle ligament viscoelastic properties using multiple strain levels at a variety of physiological loading rates [19], [30]. These studies show somewhat of an increase in stiffness at higher strain levels and strain rates however this was not enough to demonstrate that the ligament is largely rate sensitive. It has been demonstrated that a loading rate dependent response is exhibited by other viscoelastic materials [115], [116]. Therefore, the viscoelastic characteristics of ankle ligaments have primarily considered the failure and relaxation properties. The non-destructive properties including the viscoelastic mechanical response to a variety of loading rates, provide an important understanding of the physiological response that ankle ligaments exhibit.

3.1.2 Viscoelastic Theory

Ligaments exhibit both a time-dependent and strain-dependent response to an applied load and are therefore classified as viscoelastic materials. Fung's quasi-linear viscoelastic (QLV) model is one of the most widely used theories in soft tissue biomechanics. The theory assumes that the tissue response can be separated by their strain-dependent and time-dependent components [27]. The QLV elastic and time-dependent properties use a linear combination of non-linear terms to estimate the resultant stress (Eq. 1), where the time-dependent stress response to a sustained strain is given by the reduced relaxation function $G(t)$, and the strain-dependent stress response to a step input in strain is given by the instantaneous elastic function $\sigma(\varepsilon)$. The reduced relaxation function

$G(t)$ can be used to calculate the force response of a linear viscoelastic material over an arbitrary strain history by applying Boltzman's super position principle (Appendix C), resulting in the hereditary integral [30]:

$$\sigma(t) = \int_0^t G(t-\tau)\frac{d\sigma}{d\varepsilon}\frac{d\varepsilon(\tau)}{d\tau}d\,\tau \tag{3.1}$$

A common viscoelastic model that approximates the ligament force-relaxation behavior is the generalized standard linear model (Appendix A), which consists of a combination of springs and dashpots that exhibit both the elastic and viscous components of the material (Figure 32). In practice, the instantaneous stress response and relaxation response are obtained by curve fitting the functions to experimental data. The time it takes to reach the strain level is disregarded in the reduced relaxation function, therefore it is important to minimize this period by loading the tissue

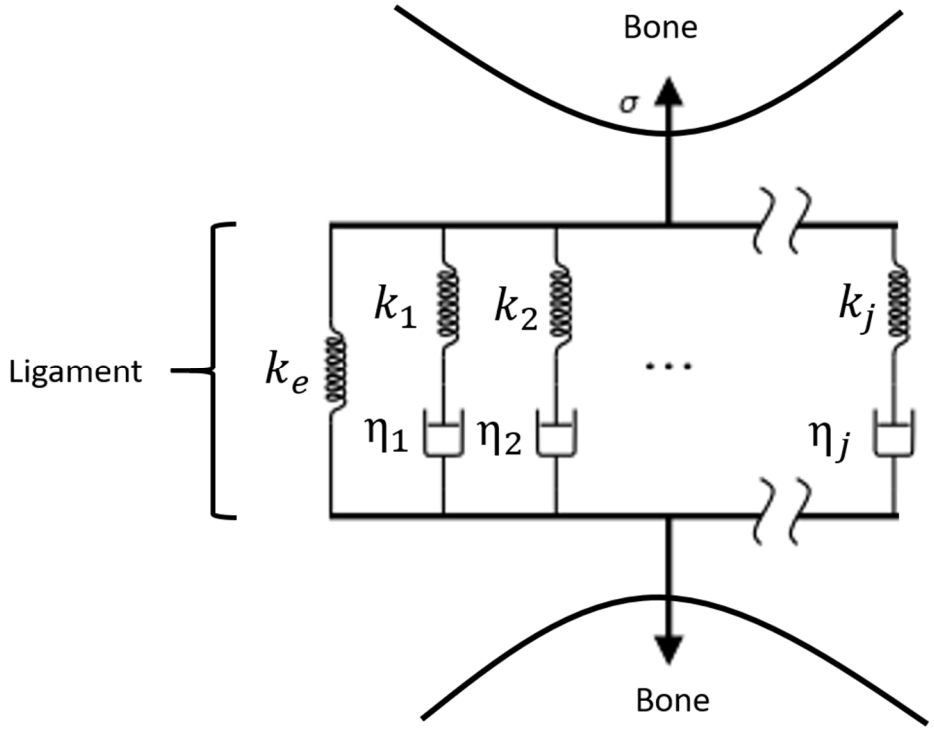

Figure 32: the generalized standard linear model represented as springs and dashpots. For this study, a total of 4 terms were used to express the viscoelastic behavior (j=4).

rapidly. The relaxation function begins at the target strain and continues for a period of time that is assumed to produce a stress steady state.

The instantaneous elastic function $\sigma(\varepsilon)$ is approximated by curve fitting an exponential function (Eq. 2) to experimental data. The rapid loading rate is used in place of a step function to displace the ligament to the target strain and the instantaneous elastic function $\sigma(\varepsilon)$ is determined from the stress verses strain response. One function that is commonly used [117] takes the form

$$\sigma(\varepsilon) = A(e^{B\varepsilon} - 1) \tag{3.2}$$

The QLV model has the advantage of more accurately representing viscoelastic materials than standard linear models yet simplified from fully non-linear models. Therefore, an experimental testing and analysis protocol was developed to characterize the viscoelastic properties of ankle ligaments so that they may improve the biofidelity of ankle ligament mechanical models.

3.2 METHODS

3.2.1 Ligament Preparation

To evaluate ankle ligament mechanical characteristics, the middle portion of the tibiocalcaneal ligament was harvested from eight fresh frozen cadaveric foot specimens (3 male/5 female, 57 ± 11.5 years, 168.7 ± 33.5 lbs., 26.3 ± 6.3 BMI). The specimens remained frozen (-20^{o}C) until 24 hours prior to mechanical testing. As previously described in chapter 2, the cadaveric foot was partially dissected (ligaments exposed to air on all sides) and partially weighted (~50lbs) for the duration of a computed tomography (CT) scan. Following the scan, the ankle was unloaded and placed in a neutral positioned with the foot 90^{o} to the lower leg and fixed with a rigid

external fixture before excising bone-ligament-bone specimens. Next, the specimen was placed into a 10 cm diameter packaging tube and mounted with polyester putty and polyester resin (2:1) (Bondo; 3M, Maplewood MN). Fiducial markers were fixed to each potted end and CT scanned (second CT scan) for later registration to bone-ligament insertion points. Ligament length was determined using the iterative length estimation (IL) previously described.

3.2.2 Mechanical Testing

Once the potted ligament specimen was fixed in the mechanical testing machine (E3000 Instron, Norwood, MA), specimens was tuned using a single constant loading rate for an initial estimate of stiffness. A 2 Hz cyclic triangle wave was applied to the specimen so that tuning gain factors could be adjusted to better fit the ligament to the strain targets. A battery of non-destructive ligament mechanical tests were performed for a set of strain levels (4%, 6%, 8% strain) and each test was followed by 15 minutes of zero strain (Figure 33). First, ligaments were subjected to 34 cycles of triangle waves at physiological frequencies (0.5, 1, 2, 3, 5, 10 Hz) in a randomized order. Following the triangle wave tests, 30 cycles of preconditioning preceded a ramp (~200 mm/s) to the target strain which was maintained for 10 minutes so that stress relaxation could be measured. The first triangle wave of the randomized set was repeated followed by a series of triangle waves at 6 randomized frequencies (0.5, 1, 2, 3, 5, 10 Hz). Each test was followed by 15 min of zero strain and this process was repeated for 4%, 6%, and 8% strain level. Data were recorded at 1000 Hz for all mechanical tests. Environmental temperature (37^{o}C) and specimen hydration (2 seconds 0.9% NaCl saline every 15 minutes) was maintained with an analog/digital BNC breakout (BNC 2090; National Instruments, Austin TX), custom LabView software, and relay-controlled

hardware previously described. Fiducial markers were tracked with a 6-camera motion capture system (240 Hz; OptiTrack, Corcallis, OR) during actuator motion. The fiducial markers were registered to ligament insertions which allowed the angle between the long axis of the ligament to be compared to the linear motion of the actuator.

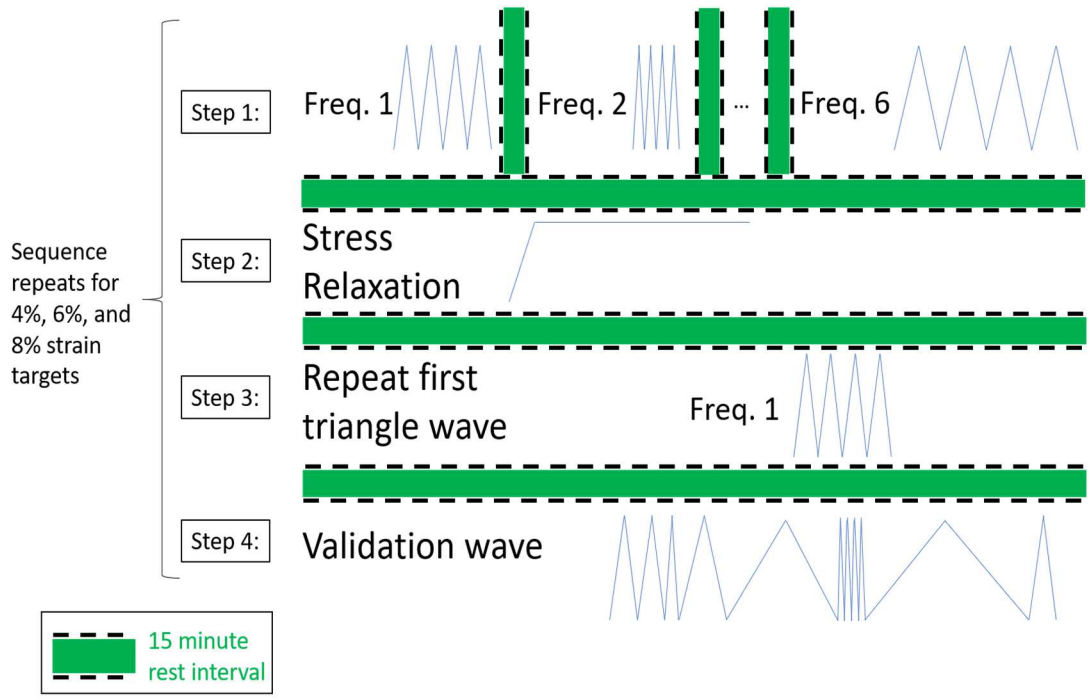

Figure 33: Schematic illustration of mechanical testing battery applied to all ligament specimens. Step 1 is a randomized order of cyclic tests, followed by stress relaxation at step 2, then the first cyclic test is repeated from step 1 to evaluate the effects of the testing battery on the tissue, and finally a random multifrequency validation waveform in step 4 which is used to test the fit of the QLV model.

3.2.3 Data Processing

The coefficients of the reduced relaxation function $G(t)$ (Eq. 2) and instantaneous stress function $\sigma(\varepsilon)$ (Eq. 3) were determined by curve fitting to normalized experimental data using least squares optimization (Appendix B). The relaxation function consisted of a four term (j=4) generalized linear model,

$$G(t) = k_1 e^{-\frac{t}{\eta_1}} + k_2 e^{-\frac{t}{\eta_2}} + k_3 e^{-\frac{t}{\eta_3}} + k_4 e^{-\frac{t}{\eta_4}} + G_\infty \tag{3.3}$$

The instantaneous elastic function $\sigma(\varepsilon)$ (Eq. 2) and this reduced relaxation function (Eq. 3) were applied to Fung's QLV model (Eq. 1) yielding the time-dependent and strain-dependent constitutive model for the ligament behavior. This model was tested with the time and strain data from a validation waveform consisting of previously tested triangle wave frequencies in a randomized order and at a single strain level. Differences between the model predicted stress and the experimentally measured stress were compared by taking the difference of the integrals over the duration of the measurement (error reported as $\pm \sigma t$ for relaxation fit and $\pm \sigma\varepsilon$ for instantaneous stress response).

The loading and relaxation coefficients were used to compare the effects of varying strain levels. A second order polynomial function was fit to the stress strain relationship of each of the last three triangle waves and their derivatives were solved for the last strain point to determine tangent modulus (E_T). Stiffness was measured as a linear fit to the last 30% of the load elongation curve and hysteresis was measured by integrating the loading and unloading of those three waves.

3.3 RESULTS

Data from six of the eight prepared ligaments were used. One ligament (specimen 5) was excluded due to very low loads measured during testing (< 5N for most tests). One of the tibiocalcaneal specimens (specimen 8) was excluded due to an insertion site fractured at some point during preparation but before mechanical testing. The pretesting CT scan confirmed a fracture of the distal bone and therefore the specimen was excluded from the study. During mechanical testing the target strain level was not achieved for higher frequency triangle waves. For the 10 Hz triangle waves the strain was as little as 50% of the commanded strain level, and about 60-80% of the target strain level for stress relaxation tests. However, differences in mechanical response are described below.

3.3.1 Curve Fitting

The instantaneous elastic response $\sigma(\varepsilon)$ was found to have a very good fit (< 0.0005 $\sigma\varepsilon$) to the experimental data (Figure 34 and Figure 35A). The elastic response to strain varied for the A coefficient (~± 50% average change) and B coefficient (~± 75% average change) among 4%, 6%, and 8% strain levels (strain levels were based on IL estimations) (Table 3). While testing specimen 3, the rapid actuator motion did not always reach the strain level at a constant loading rate allowing for additional relaxation during loading (Figure 37B). This resulted in a poor characterization of the relaxation response.

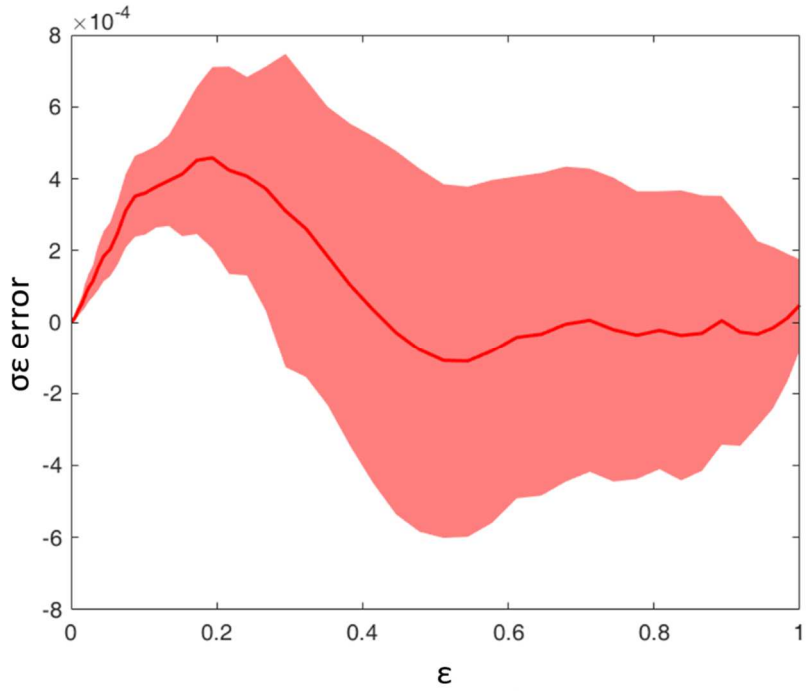

Figure 34: Model error during the rapid loading of the ramp and hold test. The error was quantified by subtracting the integral of the stress strain data from the integral of the predicted stress strain ($\Delta\sigma\varepsilon$) for each strain interval

The reduced relaxation function fit to the experimental data of individual ligaments had good agreement with an average peak underestimation error (-0.13 σt) occurring at 2 milliseconds into relaxation and reducing to almost zero (± 0.002 σt) within 1 second (Figure 36 and Figure 35B). The long time behavior showed very little relaxation modeling error (< ± 0.005 σt). In some tests, the actuator controller was not able reach the strain level at a constant strain rate, resulting in additional relaxation before the target strain was reached (Figure 37). Nevertheless, mean reduced relaxation functions varied by < 50% between strain level tests as shown in (Table *4*). The relaxation was between 52% and 76% of the peak force for the six ligaments tested. The time constants for the reduced relaxation function demonstrated approximately an order of magnitude difference between the first two terms and between the second and fourth terms (approximately 5 s, 50 s, 100 s, and 500 s) but the third term was not an order of magnitude from the second term

(Table *4*). This might indicate that the data could be represented with three terms instead of four. The relaxation constant G_∞ was about 60% of peak force and did not appear to change as the strain level increased.

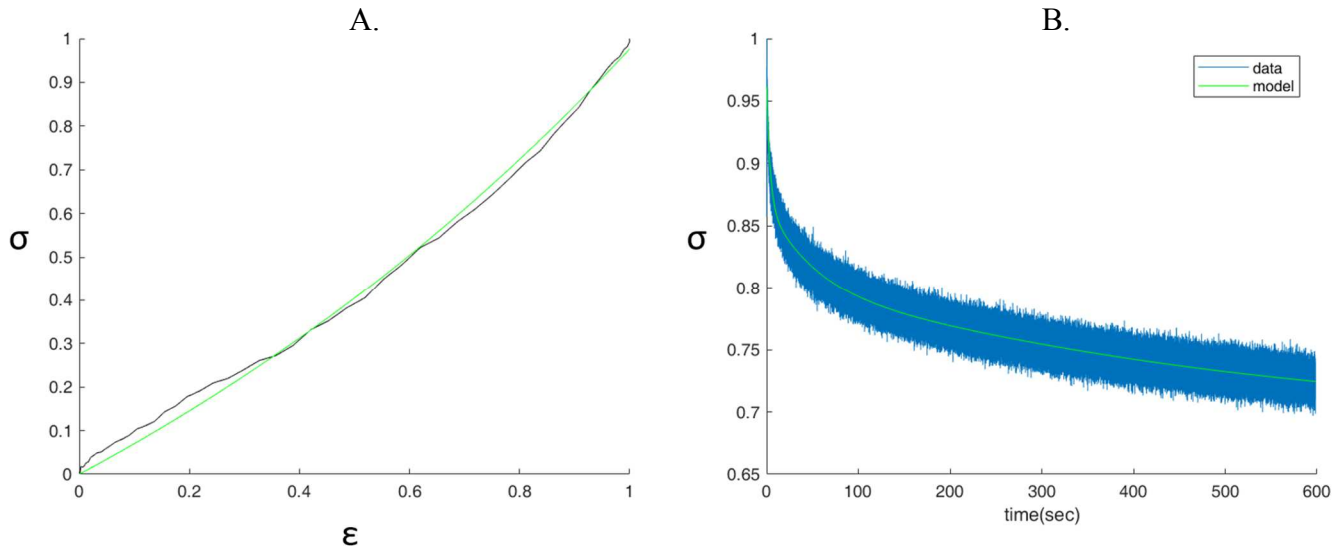

Figure 35: The results from fitting the (A) instantaneous stress model and (B) reduced relaxation model to experimental data from a representative ligament sample.

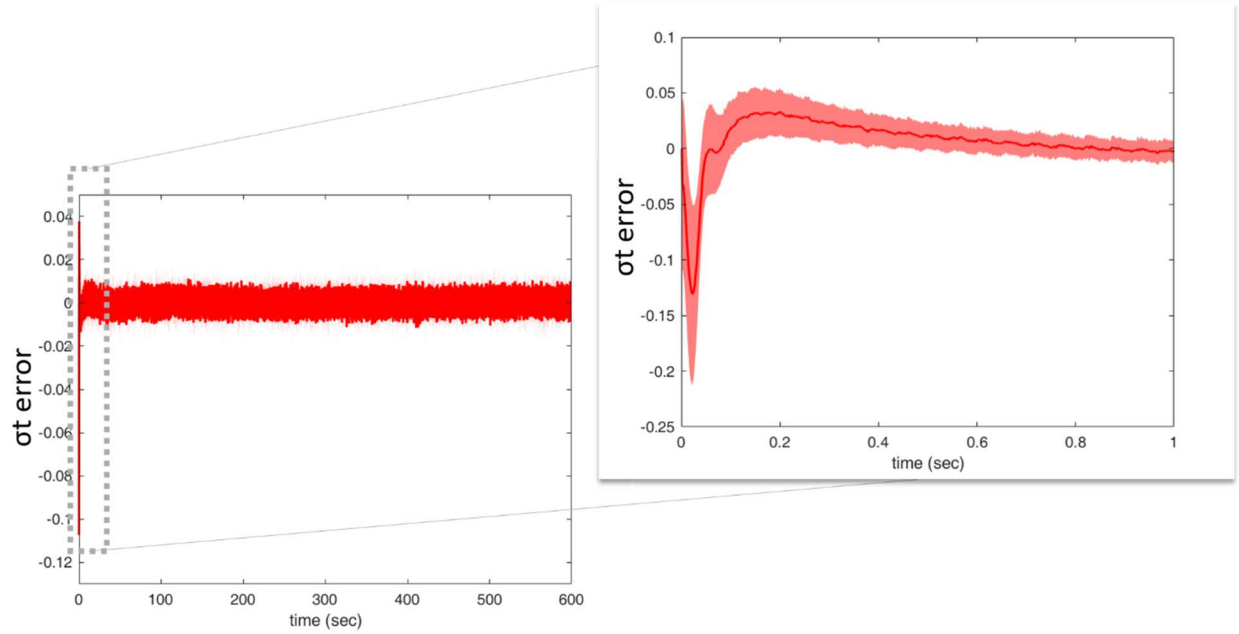

Figure 36: Model error during the relaxation period. The error was quantified by subtracting the integral of the stress time experimental data from the integral of the predicted stress time integral ($\Delta\sigma t$) for each time interval.

Strain Level	A	B
4%	6.037 ± 2.544	0.189 ± 0.105
6%	3.337 ± 2.764	0.460 ± 0.325
8%	3.063 ± 5.196	0.779 ± 0.383

Table 4: Instantaneous elastic function constants $\sigma(\varepsilon)$ fit to experimental data (n=6)

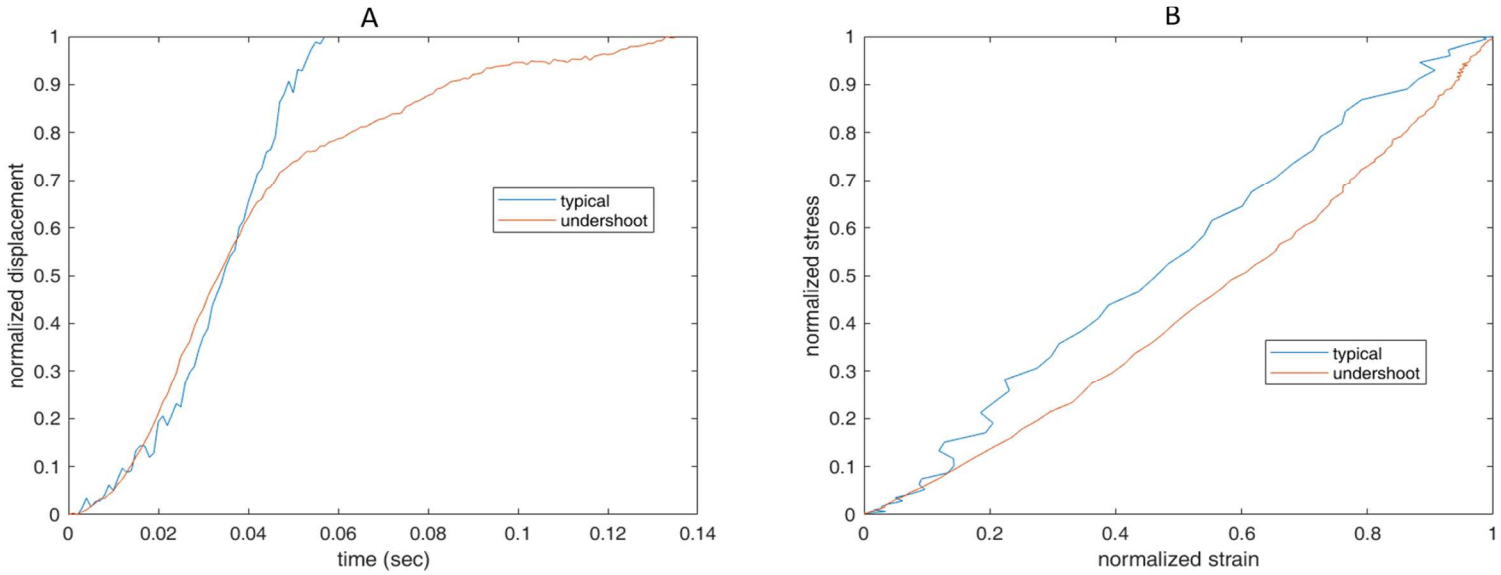

Figure 37: A representative comparison of a ramp preceding a hold test. (A) The displacement of a tuned specimen (blue) reaches the displacement level in a shorter period of time than the poorly tuned specimen (red). (B) The relaxation response resulting from the slower ramp response.

Strain Level	η_1	η_2	η_3	η_4	G_∞
4%	5.10 ± 3.33	79.01 ± 24.54	144.36 ± 41.49	407.75 ± 143.64	0.64 ± 0.06
6%	3.17 ± 1.09	58.88 ± 27.27	90.58 ± 25.91	340.43 ± 79.57	0.64 ± 0.07
8%	2.70 ± 1.69	44.15 ± 32.43	85.48 ± 46.37	250.34 ± 27.14	0.60 ± 0.05

Table 3: Reduced relaxation constants $G(t)$ from curve fit data (n=6)

3.3.2 Constitutive Model Validation

The time and strain data from the validation waveform was applied to the QLV model derived from the instantaneous elastic response $\sigma(\varepsilon)$ and reduced relaxation function $G(t)$, resulting in a predict stress that was compared to measured stress. When the rapid loading of the stress relaxation was performed at a constant loading rate as fast as the mechanical testing machine can safely achieve, the relaxation response was accurately captured, and the reduced relaxation function was able to accurately predict the stress response. In these cases, there was good agreement at lower stresses levels but the peak stress were underestimated by approximately 10%. (Figure 38A). However, if the loading during the stress relaxation test was not performed rapidly, the tissue had time to relax during the ramp (Figure 37) and therefore the QLV underpredicted the relaxation response. This occurred in three tests and resulted in an overestimation of ligament stress when applying the constitutive model to the validation waveform (Figure 38B).

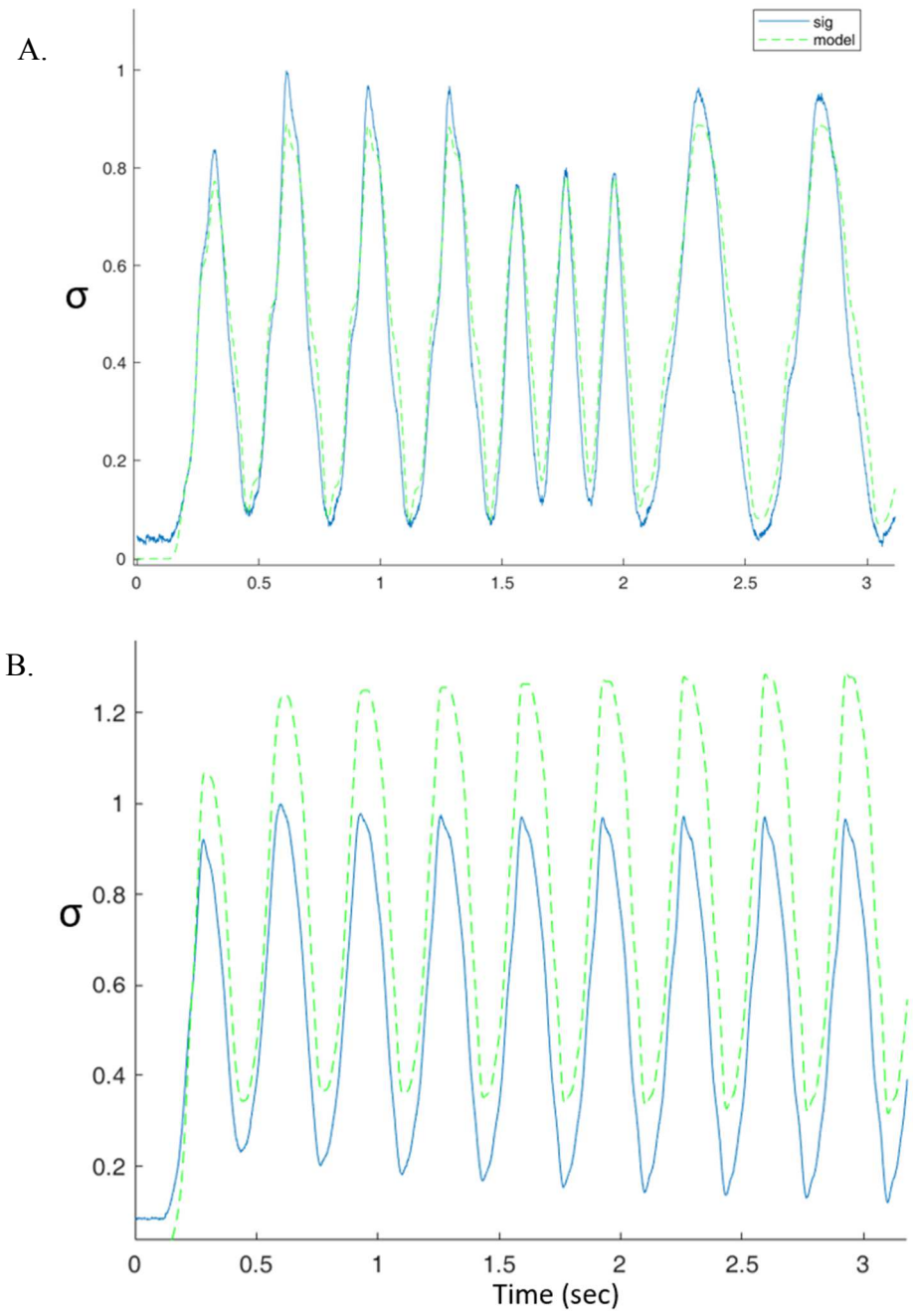

Figure 38: two representative examples of a constitutive model stress estimates (green dotted lines) compared to the measured stress (blue line) of a random triangle waveform. (A) Predicted stress (green dotted line) of a QLV model fit to a well-tuned stress relaxation test shows good agreement with the measured stress (blue line) but is not able to match the measured stress (blue line) at higher loads. (B) Predicted stress (green dotted line) of a QLV model fit to a poorly tuned (slowly loaded) stress relaxation test does not adequately characterize the relaxation response and therefore overpredicts the stress as compared to the measured stress (blue line).

3.3.3 Additional Mechanical Properties

The stress strain response shows a strain rate dependent modulus of elasticity despite variations in strain level (Figure 39). At lower strain levels there is a relative rate-insensitivity that consistent with ligament mechanical response at small strain levels [117]. However, as the strain increases the stress response becomes more sensitive to strain rate. Additionally, the stiffness did not change considerably throughout the duration of mechanical testing as demonstrated by the repeated first triangle wave test (Figure 40). The peak force and hysteresis both decreased in response to increases in loading rate, however this was due to lower strain levels and not due to a loading rate response. In general, there was little change in the stiffness (37.4 ± 20.9 N/mm), modulus (27.7 ± 22.5), peak force (38.5 ± 21.9 N), or hysteresis (39.8 ± 24.9) in response to increasing triangle wave frequency (Table 5).

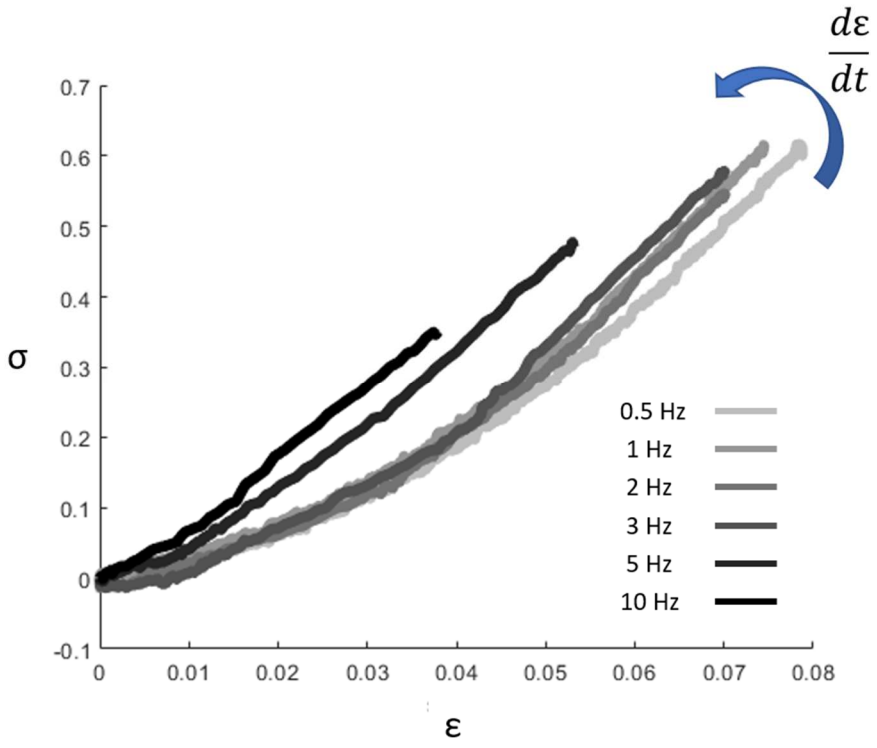

Figure 39: Stress strain response to the loading portion of a triangle wave test at various physiological frequencies (0.5, 1, 2, 3, 5, 10 Hz) causing a change in strain rate $\frac{d\varepsilon}{dt}$.

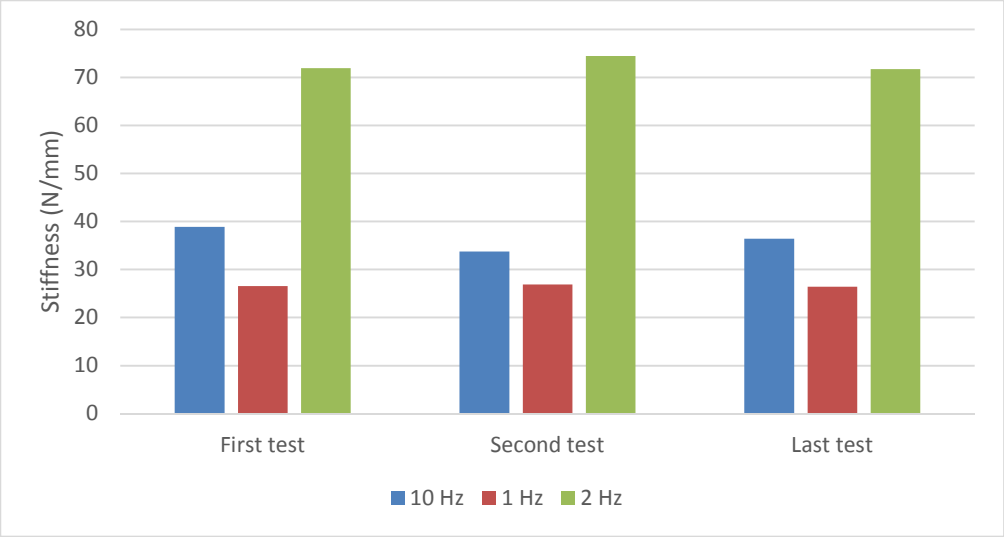

Figure 40: Stiffness changes of 3 ligaments (red and blue) during the duration of testing. The very first triangle wave test was repeated following each strain level test.

Hz	Stiffness (N/mm)	Modulus	Peak Force (N)	Hysteresis
0.5	38.0 ± 18.5	28.4 ± 22.5	42.6 ± 25.4	50.1 ± 34.1
1	38.8 ± 19.5	29.0 ± 23.0	42.2 ± 24.4	47.6 ± 30.8
2	38.4 ± 19.3	28.5 ± 22.5	39.9 ± 22.6	42.6 ± 26.9
3	38.1 ± 21.4	28.3 ± 22.9	39.5 ± 22.1	41.4 ± 25.5
5	36.7 ± 22.0	27.1 ± 22.1	36.1 ± 19.2	34.1 ± 17.3
10	34.3 ± 24.8	25.1 ± 21.8	30.5 ± 17.5	22.8 ± 14.6

Table 5: Mean values and standard deviations of the mechanical characteristics from triangle waves at an 8% strain level

3.4 DISCUSSION

3.4.1 Summary of Findings

This study characterized the viscoelastic properties of the tibiocalcaneal ligament at various strain levels and loading rates. A stress-strain relationship was observed for strain rate dependent modulus. Minimal differences were found in stiffness, modulus, hysteresis, or peak force as a function of triangle wave frequency. The peak force slightly decreased with increases in triangle wave frequency due to reduced strain and not as a result of strain rate. The minimal hysteresis differences between triangle wave tests are likely a result of loading and unloading that occurred at different strains and therefore cannot be characterized as a strain rate dependent response. The stiffness and modulus exhibit a similar displacement rate and strain rate dependent responses. However, these are trends that might be exhibited at higher strains but requires further testing to determine definitively. Additionally, the relaxation constant G_∞ did not change with increases in strain which is consistent with a study examining the characteristics of the ankle ligaments relaxation [30].

Data from the stress relaxation test agreed to the model fit of the instantaneous stress function (< 0.0005 σε) and the long-time behavior of the reduced relaxation function (< ± 0.005 σt). However, at the beginning of relaxation the reduced relaxation function underestimated the stress (-0.13 σt). Errors in the short time period of relaxation will result in underestimation of the stress during rapid elongation when less time history has developed. This is likely to explain some of the underestimation of the peak stress during model validation.

The constitutive model developed from experimental data was able to accurately predict stress responses, however it consistently underestimated the peak stress responses. The cause of this is likely due to the experimental and modeling limitations described below. However, when the strain level target was not reached quickly during the stress relaxation test, the ligament was allowed time to relax during loading and that relaxation could not be measured in the relaxation test and is not part of the reduced relaxation model fit. Therefore, the constitutive model that utilizes this reduced relaxation function will underestimate ligament relaxation and overpredict the stress response. It is generally understood that all constitutive models are approximations of the actual mechanical behavior in biological systems.

3.4.2 Limitations

This study is subject to experimental limitations in both mechanical testing and mathematical modeling. Accurate mechanical properties are predicated on appropriate strain level (engaging the collagen fibers without yielding the tissue) and consideration of mechanical testing order (incrementally increasing the strain levels and randomizing the loading rate).

Strain targets

The strain levels for this experiment were chosen based on pilot testing (n=1) which replicated some of the experimental conditions described above. The specimen was subjected to triangle waves at increasing strain levels (2% strain intervals) from 2% strain until failure with 15 minutes of rest between tests. Ligament length was determined using the average value of three caliper measurements of the outer ligament fibers and the testing was conducted at room temperature with the ligament wrapped in a 0.9% saline soaked paper towel. Both the length

estimation and the environmental conditions in the pilot study varied from the methods in this study. However, this provided an estimate of how the ligaments would behave under testing conditions. Data from this pilot test informed the choice of strain levels that were about 4-6% below the yielding point to ensure that the ligament would not be destructively damaged during testing. While the mechanical characteristics reported here are within the range of previously reported data [30], [35], these strain levels might have been too conservative resulting in strains that did not engage a majority of collagen fibers for all ligaments. For one of the specimens the loads measured from the strain levels never exceeded 5 N resulting in the exclusion of this ligament from the study. After reviewing the video data from this test, the specimen remained buckled during triangle wave testing.

Material testing system sensitivity and tuning

Ligament mechanical testing requires careful actuator tuning in order to maintain target trajectories. The inability to reach strain levels in this study is an indication that tuning was not adequate and will need to be improved in future work. It is possible that programmed overshoot can be determined from a representative ligament sample or that tuning can be repeated for each strain level. For the duration of testing in this study (> 8 hours), several factors can influence the effectiveness of the actuator tuning. One notable concern involved the changes in potting conditions during testing. The hydration system used in this experiment consisted of a sprayer aimed at the ligament used to periodically hydrated the tissue with saline. The overspray caused the outer potting (cardboard packaging tube) to absorb saline and increase in mass. The inertial effects from this would likely be enough to alter the pre-test tuning, however, this was compounded by the fact that the load cell was mounted on the actuator. This arrangement was not only likely to influence actuator control, but also effect the 5 N preload applied to the ligament. In one instance

the potting absorbed enough saline to apply a 5 N load to the load cell when the ligament was visibly slack, requiring the experimenter to tare the load cell and restart the test. Ligaments were allowed time to acclimate in the environmental chamber for approximately 1 hour before the load cell was tared and testing commenced. This also allowed time for the potting to absorb saline before the test began.

Idealized modeling vs limits of testing

The limitations of mechanical testing can result in modeling errors. The accuracy of the short and long time constants are based on approximating a step response and sustaining that strain for a sufficient period of time to measure a stress steady state as a result of tissue relaxation. It is considered physically impossible to achieve a step response in practice since it takes some time for the actuator to move from one position to another. Despite making efforts to keep this period very brief still allows for some tissue relaxation. Additionally, the amount of time needed to accurately measure the relaxation effect is a limitation that has also been previously addressed [18], [30]. It is possible that the specimen has not reached a true minimum stress state in the sustained strain period. Additionally, the considerations of a slow ramped step response and a premature ending to the sustained strain would tend to underestimate the instantaneous elastic response and overestimate the relaxation stress. This might help to explain the inability of the constitutive model to approximate the higher stresses and peak stress when applied to the validation triangle waveforms.

3.4.3 Previous Work

The properties of ankle ligaments have mostly focused on single loads to failure [35], [87], [114] with very few articles examining the viscoelastic properties of ankle ligaments [30], [118]. Given the differences in experimental procedures between these studies, it can be challenging to interpret and compare findings. While these studies tested bone-ligament-bone samples, applied many of the same mechanical testing protocols, and used similar analysis techniques, the studies differ from the experimental methods of this study in several ways. This study controlled for temperature and hydration throughout testing while previous studies have tested ankle ligaments at room temperature using a saline gauze for hydration. It has been shown that temperature and hydration influence material properties and should therefore be controlled during mechanical tests [47], [48], [101], [119]. Additionally, the testing battery of this study was much longer (> 8 hours) than those of previous studies (< 3 hours) and are therefore vulnerable to degradation which in turn can influence the actuator controller. Nevertheless, the stiffness, elastic modulus, and hysteresis behavior measured from this study compare to previous findings [19], [30], [34], [87]. Additionally ligament stiffness and hysteresis have not been found to be strain rate dependent at low strain levels [30], [117]. However, some of these studies were performed at very slow loading rates (0.01%/s, 0.1%/s, 1.0%/s) and in most cases a strain dependent response in hysteresis and stiffness was observed as a trend but has not be statistically measured.

The upper bound of the modulus measured in this study related to the lower bound of previously reported moduli [35]. This could be due to the discrepancies in cross-sectional area measurements which were performed with a custom micrometer as compared to the measurement from CT used in this study. As previously described the discrepancy in cross-sectional area

measurements can cause an increase in modulus if the cross-sectional area is underestimated. Further, the variations in loading rate (~0.5mm/s to ~1000mm/s) and temperature differences (about 21^{o}C in previous studies [35], [114] and 37^{o}C in this study) have been shown to influence the viscous component of the tissue resulting in decreases in peak force as temperature increases [101]. Other studies have shown that the stiffness and hysteresis increase with higher strain levels and strain rates [19], [30], [117], although no studies have demonstrated a statistical differences in ankle ligament stiffness and hysteresis with changes in loading rate.

The relaxation response of the ligaments tested also agrees with previously reported data. Others have shown a relaxation constant within approximately 60% of the peak force during a stress relaxation test [19], [30]. The same generalized linear model has been used by others to derive the reduced relaxation function shown in this study [30]. While it is possible to fit a four term reduced relaxation function to ankle ligament data [30], there were five terms used in this study with each time constant η_i was shown to change by an order of magnitude from the previous constant. Results from this study indicate that if the third time constant was removed each of the time constants would change by approximately an order of magnitude (Table 4). This might indicate that the reduced relaxation model could be represented with these data using as few as four terms since exponential decay behavior can be modelled with logarithmically spaced nodes. Additionally, the relaxation response in ankle ligaments characterized thus far has been done at room temperature and without preconditioning cycles [19], [30]. There is some debate about preconditioning cycles and their influence on relaxation response. While it is true that preconditioning results in some tissue relaxation, it also serves to emulate the response of the tissue *in vivo* and allows for more repeatable experimental conditions. Without preconditioning, there is

no guarantee that the tissue will not be damaged during the rapid loading required for the stress relaxation test.

There are differences in mechanical testing methods used to characterize ankle ligament material properties. For one, the non-destructive triangle wave testing battery used in this study compares to non-destructive square wave testing seen in other studies [19], [30], [117]. The inertial effects from abruptly stopping the actuator can cause a ringing in the load signal and require additional interpretation [30]. Additionally, some mechanical tests load ankle ligaments to decreasing strain levels which can degrade the tissues for subsequent tests [19], [30]. Finally, the number and duration of mechanical tests has been limited to experimenter availability to this point. Therefore, before now an exhaustive battery of strain rates and stress relaxation tests has not been feasible.

3.4.4 Conclusions

This study has produced data for modeling the behavior of the tibiocalcaneal ligament in a variety of strains and strain rates. This study shows that the tibiocalcaneal ligaments demonstrate rate sensitive trend for the strain levels tested. All ligaments exhibited non-linear viscoelastic behavior and therefore are well suited to the QLV model presented in this study. The results from this paper serve to improve the biofidelity of ankle ligament computational models. The products generated from this work are: (a) a QLV model for multiple strain targets that is validated against an independent experimental test not used to generate the model, (b) a representation of the mechanical behavior with changes in strain rate, models generated with (c) mechanical test that were performed under environmentally controlled conditions (i.e., constant temperature and

hydration), and (d) anatomical ligament pose, all of which are (e) controlled with an automated mechanical testing system.

Chapter 4. DISCUSSION

4.1 LIMITATIONS IN LIGAMENT TESTING

Modeling ligament mechanical behavior is technically difficult and prone to errors beginning with specimen preparation and continuing with mechanical testing and analysis. Measurements of ligament morphology must be faithfully measured in a way that considers the anatomy and *in vivo* function. These considerations must also be applied to mechanical testing such that ligament pose and specimen environment is maintained, and physiological loading conditions are applied. Finally, theoretical modeling limitations and experimental repeatability must be considered when analyzing mechanical data. The work presented here has addressed these considerations by developing specialized techniques to improve our understanding of ankle ligament mechanical function.

4.1.1 Preparation limitations

Many methods have been used to mechanically test ligaments in a way that imitates the physiological conditions. An effort has been made to mechanically test partially dissected joints [8], [35], cut the ligament into uniform samples [88], [120], or visually align excised bone-ligament-bone samples [30], [32], [34]. While these experiments can provide valuable information about ligament function, they do not control both the anatomical position/function of the ligament and the loading direction. When testing partially dissected joint ligament mechanics must be inferred only after they have been cut. By cutting ligaments to a uniform size the ability to capture

the enthesis (the region of ligament that connects to the bone) is lost. Additionally, this technique poses challenges with gripping the soft tissue in a reliable way. Finally, it is difficult to ensure alignment of ligament fibers due to the irregular shape of ligament and bone surfaces. Once in position this technique offers no certainty that the orientation of the potted ligament is relevant to *in vivo* loading conditions.

The methods introduced in this work propose ways imitate physiological conditions. Methods to maintain anatomical orientation within a known certainty (~23° and ± 4.13 mm) using external fixation to excise ligaments with the foot in a specific pose. This method allows for mechanical testing to be conducted with the ligament in a known orientation which is tracked throughout mechanical testing and can be related back to the *in situ* position. This is an improvement to the current conventions used in mechanical testing today.

Techniques for measuring initial length and cross-sectional areas also differ between experiments. This is an important step when conducting any mechanical test since it is the initial length that is often used to determine the displacement magnitude during the test and it is the cross-sectional area that is used to generalize the material response. However, it is extremely difficult to measure length and cross-sectional area experimentally. Therefore, it is common to measure ligament length by averaging caliper measurements of the outer ligament fibers [19], [30], [34]. For some anatomical structures (including some ligaments) this might be viable method, however small irregularly shaped ligaments such as those tested in this work pose a challenge due to lack of uniformity along their length. Cross-sectional area estimates on the other hand are estimated in several ways. Some studies measure the thickness and width using calipers and fit the measurements to a rectangle [40], [41], or an ellipse [37]. However, these methods simplify

ligament geometry and have been shown in this work to often underestimate the true cross-sectional area.

This work introduces methods for determining ligament length and cross-sectional area with the foot in a repeatable pose. The effects of mischaracterizing the length and cross-sectional area are outlined Chapter 2. Length is derived in a way that considers the wrapping orientation of the ankle ligament as in a partially weighted pose. The length estimate tool uses ligament borders defined by segmented CT scans that are compared to dissection photos. Once the ligament has been dissected and the CT images have been segmented, the method for determining length are repeatable and represent the ligament anatomy. Ligament cross-sectional area is determined using the same segmented CT images and are therefore also representative of the ligament anatomy and can be determined in a repeatable way.

4.1.2 Mechanical Testing Limitations

The majority of ligament mechanical tests are conducted at room temperature with saline used to regularly hydrate the tissue [19], [30], [35], [87], while others maintain a constant temperature by submerging the ligament in a solution for the duration of the test. Hydration [47] and temperature [101], [103] can influence mechanical properties of the tissues and should therefore be controlled during mechanical testing. However, long-term exposure (> 8 hours) can cause solutes from the buffer to diffuse into the tissue and interact with its structure and mechanics [47]. Therefore, it is necessary to maintain hydration while minimizing the tissue's exposure to a solution and simultaneously maintain a constant environmental temperature.

The environmental temperature and hydration was maintained during all mechanical tests presented in this study. A custom insulated chamber was constructed so that temperature could be maintained within < ± 2ºC of body temperature (37ºC) and saline was sprayed at regular intervals. This is an improvement over reported testing procedures where ligaments are "regularly bathed" in saline solutions [19], [30], [34] because both the ligament hydration and exposure to solution are known throughout testing. Additionally, this system was maintained using automation which allows exhaustive batteries of tests to be conducted and a range of previously infeasible mechanical testing experiments to be conducted. In the event that a ligament needs to be re-tested, the time required by the experimenter to conduct such a test is minimal.

Maintaining ligament *in situ* pose during potting was attempted in this study. However, the results of this effort did not achieve close alignment with the weighted foot specimen with an angle offset of about 23º (± 6.6º) and a length difference of about 1.4 mm (± 4.13 mm). This is likely the result of calcaneal eversion during the partially dissected foot weighting. The calcaneus everts based on the forefoot position (i.e. pes cavus, pes planus), native ligament laxity, and positioning in the loading jig. It would be ideal to secure the ligament position with a rigid external fixture while the foot is weight bearing, however, this was not possible with the current loading jig. Additionally, if such a loading jig were to be constructed, special considerations would need to be made to ensure that the stored energy due to foot loading doesn't become hazardous when drilling and cutting into the bone.

4.2 SUMMARY OF FINDINGS

The results from chapters 2 and 3 summarize the products from this study. In chapter 2 the methods introduced are compared to some of the current conventions for ligament testing. These results highlighted the challenges of testing small irregularly shaped ligaments by demonstrating the length variability (~25% between CL, LL, and IL) and cross-sectional area variability (~80% between fitting a rectangle to caliper measurements and CT scans). This work also showed that specimen temperature and hydration can be maintained for > 15 hours of continuous testing. Although these methods require additional work, they are reliable and repeatable while minimizing the burdens to the experimenter who must orchestrate an exhaustive battery of tests without making mistakes. Combined with the ligament morphology methods, mechanical testing automation can improve the tests performed and therefore our understanding of ankle ligament function.

In addition to addressing limitations to mechanical testing methodology, this study characterized the viscoelastic properties of the tibiocalcaneal ligament at various strain levels and loading rates. The instantaneous stress and reduced relaxation functions were fit to the stress relaxation data. While there was good agreement between the model and experimental data overall, it is important to note that the predominate error was found at the beginning of relaxation where the model reliably underestimated the stress (-0.13 σt). From this work a QLV model was developed which was applied to a validation waveform and evaluated for fit. The validation waveform was an independent mechanical test consisting of random triangle waves at a constant amplitude. These random triangle waves were not used to build the model and therefore serve as an independent validation. Results from testing showed good agreement between predicted and

measured stress (RMSE < 0.1) Additionally, the relaxation constant G_∞ was found to be relatively constant with increases in strain. Although the strain targets were not reached for all conditions, the stress-strain relationship, and relaxation behavior, were verified with results from previous findings [30], [34].

4.3 FUTURE WORK

The methods for determining the mechanical properties of the tibiocalcaneal ligament as presented in this work, will be repeated for additional ligaments of the foot and ankle. These ligaments include: calcaneonavicular, calcaneofibular, tibiocalcaneal, and tibiofibular. Each of these ligaments contribute to the function of the high ankle joint, ankle joint, subtalar joint, and medial longitudinal arch of the foot. With this data set complete, a relationship between mechanical function and anatomical location and a sensitivity analysis can be evaluated. However, before additional testing can begin several limitations illuminated by this study should be overcome. First, ligament tuning procedures will need to be improved so that strain targets during cyclical non-destructive testing and stress relaxation testing can be attained. This will provide information about how the ligaments respond to a repeated strain for direct comparison. Additionally, improvements in tuning will ensure that strain targets are achieved during the loading portion of the stress relaxation tests which will improve the fit of the QLV model and resulting stress predictions. Finally, model validation tests should include preconditioning cycles to replicate the testing conditions and emulate *in vivo* loading conditions.

There are some additional goals that are intended for future studies and therefore have not been explored in this work. The high-speed video data of the speckled ligament is also registered

to the fiducial marker clusters and can therefore be used to measure the ligament 2D strain field and map it back to the anatomical plane. Some improvements can be made to the process of registering the ligament potted pose to the weighted foot ligament pose. One such improvement is to explore shape fitting to anatomical regions on the bone fragment so that 3D insertion bone positions can be determined. This in combination with strain field analysis from high speed video can be used to inform the application of a constitutive model developed from mechanical testing data. Finally, while an effort has been made to measure the ligament cross-sectional area in a weighted foot specimen, there was not an attempt to measure the ligament cross-section in loaded conditions. However, using methods adapted from the length and cross-sectional area measurements a method can be developed to estimate the cross-sectional area under loading conditions outside the mechanical testing machine. If this can be achieved it could improve stress estimations during mechanical testing. It is my hope and intention to continue the work of this study so that it may be shared further within the scientific community.

BIBLIOGRAPHY

[1] M. Benjamin and J. R. Ralphs, "Tendons and ligaments--an overview," *Histol. Histopathol.*, vol. 12, no. 4, 1997.

[2] P. Golanó *et al.*, "Anatomy of the ankle ligaments: a pictorial essay," *Knee Surgery, Sport. Traumatol. Arthrosc.*, vol. 24, no. 4, pp. 944–956, 2016.

[3] Y. (Yuan-C. Fung, *Biomechanics Mechanical Properties of Living Tissues*, 2nd Editio. New York: Springer-Verlag, 1993.

[4] S. A. Norkus and R. T. Floyd, "The Anatomy and Mechanisms of Syndesmotic Ankle Sprains," *J. Athl. Train.*, vol. 36, no. 1, pp. 68–73, 2001.

[5] A. Katznelson, E. Lin, and J. Militiano, "Ruptures of the ligaments about the tibio-fibular syndesmosis.," *Injury*, vol. 15, no. 3, pp. 170–2, 1983.

[6] T. Brosky, J. Nyland, A. Nitz, and D. N. M. Caborn, "The Ankle Ligaments: Considerations of Syndesmotic Injury and Implications for Rehabilitation," *J. Orthop. Sport. Phys. Ther.*, vol. 21, no. 4, 1995.

[7] P. K. Levangie and C. C. Norkin, *Joint Structure and Function: A Comprehensive Analysis*. F.A. Davis Company, 2005.

[8] H. B. Kitaoka, Z. P. Luo, K. N. an, E. S. Growney, and L. J. Berglund, "Material Properties of the Plantar Aponeurosis," *Foot Ankle Int.*, vol. 15, no. 10, pp. 557–560, 1994.

[9] *Foot and ankle core knowledge in orthopaedics*. Philadelphia, Pa.]: Elsevier Mosby, 2007.

[10] B. G. Castelucci *et al.*, "Time-dependent regulation of morphological changes and cartilage differentiation markers in the mouse pubic symphysis during pregnancy and postpartum recovery," *PLoS One*, vol. 13, no. 4, pp. 1–17, 2018.

[11] M. Sakane, H. Mutsuzaki, S. Hattori, H. Nakajima, and N. Ochiai, "Time dependence of changes of two cartilage layers in anterior cruciate ligament insertion after resection on chondrocyte apoptosis and decrease in glycosaminoglycan," *BMC Sports Sci. Med. Rehabil.*, vol. 1, no. 1, 2009.

[12] J. Apostolakos *et al.*, "The enthesis: a review of the tendon-to-bone insertion.," *Muscles. Ligaments Tendons J.*, vol. 4, no. 3, pp. 333–42, 2014.

[13] D. Subit, C. Masson, C. Brunet, and P. Chabrand, "Microstructure of the ligament-to-bone attachment complex in the human knee joint," *J. Mech. Behav. Biomed. Mater.*, vol. 1, no. 4, pp. 360–367, 2008.

[14] M. Z. Ilic, P. Carter, A. Tyndall, J. Dudhia, and C. J. Handely, "Proteoglycans and catabolic products of proteoglycans present in ligament," *Biochem. J.*, vol. 385, no. 2, pp. 381–388, 2005.

[15] D. R. Eyre, "Collagen: molecular diversity in the body's protein scaffold," *Science*, vol. 207, no. 4437, 1980.

[16] S. Hsu, R. Liang, and S. L. Y. Woo, "Functional tissue engineering of ligament healing," pp. 1–10, 2010.

[17] R. A. Hauser, E. E. Dolan, H. J. Phillips, A. C. Newlin, R. E. Moore, and B. A. Woldin, "Ligament Injury and Healing : A Review of Current Clinical Diagnostics and Therapeutics," pp. 1–20, 2013.

[18] J. A. Weiss and J. C. Gardiner, "Computational Modeling of Ligament Mechanics," vol.

29, no. 4, pp. 1–70, 2001.
[19] A. M. Butler and W. R. Walsh, “Mechanical response of ankle ligaments at low loads.,” *Foot ankle Int. / Am. Orthop. Foot Ankle Soc. [and] Swiss Foot Ankle Soc.*, vol. 25, no. 1, pp. 8–12, 2004.
[20] P. Berillis, A. Environment, A. Envi-, and N. Ionia, “SM Gr up Marine Collagen : Extraction and,” no. Figure 1, pp. 1–13, 2015.
[21] D. W. Urry and T. M. Parker, “Section: Extracellular matrix proteins; Mechanics of elastin: molecular mechanism of biological elasticity and its relationship to contraction,” *J. Muscle Res. Cell Motil.*, vol. 23, no. 5–6, pp. 543–559, 2002.
[22] M. C. Kirby, T. A. Sikoryn, D. W. L. Hukins, and R. M. Aspden, “Structure and mechanical properties of the longitudinal ligaments and ligamentum flavum of the spine,” *J. Biomed. Eng.*, vol. 11, no. 3, pp. 192–196, 1989.
[23] H. B. Henninger, W. R. Valdez, S. A. Scott, and J. A. Weiss, “Elastin governs the mechanical response of medial collateral ligament under shear and transverse tensile loading,” *Acta Biomater.*, vol. 25, pp. 304–312, 2015.
[24] T. J. Lujan, C. J. Underwood, N. T. Jacobs, and J. A. Weiss, “Contribution of glycosaminoglycans to viscoelastic tensile behavior of human ligament,” *J. Appl. Physiol.*, vol. 106, no. 2, pp. 423–431, 2009.
[25] S. Reese and J. A. Weiss, “Tendons and Ligaments: Current State and Future Directions,” in *Multiscale Modeling in Biomechanics and Mechanobiology*, Springer London, 2015, pp. 159–206.
[26] S. P. Reese, S. A. Maas, and J. A. Weiss, “Micromechanical models of helical superstructures in ligament and tendon fibers predict large Poisson’s ratios,” *J. Biomech.*, vol. 43, no. 7, pp. 1394–1400, 2010.
[27] Y. C. B. Fung, “Elasticity of soft tissues in simple elongation ’,” no. 6, 1967.
[28] S. Hund, M. Kameneva, and J. Antaki, “A Quasi-Mechanistic Mathematical Representation for Blood Viscosity,” *Fluids*, vol. 2, no. 1, p. 10, 2017.
[29] M. A. Meyers, “Mechanical behavior of materials.” Prentice Hall, Upper Saddle River, N.J., 1999.
[30] J. R. Funk, G. W. Hall, J. R. Crandall, and W. D. Pilkey, “Linear and Quasi-Linear Viscoelastic Characterization of Ankle Ligaments,” *J. Biomech. Eng.*, vol. 122, no. 1, pp. 15–22, 2000.
[31] S. L.-Y. Woo, G. A. Johnson, and B. A. Smith, “Mathematical modeling of ligaments and tendons. (Special Issue: 20th Anniversary Biomechanics Symposium),” *J. Biomech. Eng.*, vol. 115, no. 4A B, 1993.
[32] J. A. W. van Dommelen *et al.*, “Characterization of the Rate-Dependent Mechanical Properties and Failure of Human Knee Ligaments.” 2005.
[33] R. C. Haut, “Age-dependent influence of strain rate on the tensile failure of rat-tail tendon,” *J. Biomech. Eng.*, vol. 105, no. 3, 1983.
[34] S. Siegler, J. Block, and C. D. Schneck, “The Mechanical Characteristics of the Collateral Ligaments of the Human Ankle Joint,” *Foot Ankle Int.*, vol. 8, no. 5, pp. 234–242, 1988.
[35] S. Siegler, D. Ph, and C. D. Schneck, “The Mechanical Characteristics of the Collateral Ligaments of the Human Ankle Joint *,” pp. 234–242, 1988.
[36] J. R. Funk, G. W. Hall, J. R. Crandall, and W. D. Pilkey, “Linear and quasi-linear viscoelastic characterization of ankle ligaments,” *J. Biomech. Eng.*, vol. 122, no. 1, 2000.
[37] D. P. Pioletti, L. R. Rakotomanana, and P. F. Leyvraz, “Strain rate effect on the

mechanical behavior of the anterior cruciate ligament-bone complex," *Med. Eng. Phys.*, vol. 21, no. 2, pp. 95–100, 1999.
[38] L. Bertozzi, R. Stagni, S. Fantozzi, and A. Cappello, "Knee model sensitivity to cruciate ligaments parameters: A stability simulation study for a living subject," *J. Biomech.*, vol. 40, no. SUPPL. 1, pp. 38–44, 2007.
[39] K. H. Bloemker, "Computational Knee Ligament Modeling Using Experimentally Determined Zero-Load Lengths," *Open Biomed. Eng. J.*, vol. 6, no. 1, pp. 33–41, 2012.
[40] M. K. Kwan, T. H. C. Lin, and S. L. Y. Woo, "On the viscoelastic properties of the anteromedial bundle of the anterior cruciate ligament," *J. Biomech.*, vol. 26, no. 4–5, pp. 447–452, 1993.
[41] J. Hewitt, F. Guilak, R. Glisson, and T. P. Vail, "Regional material properties of the human hip joint capsule ligaments," *J. Orthop. Res.*, vol. 19, no. 3, pp. 359–364, 2001.
[42] J. Hashemi, N. Chandrashekar, C. Cowden, and J. Slauterbeck, "An alternative method of anthropometry of anterior cruciate ligament through 3-D digital image reconstruction," vol. 38, pp. 551–555, 2005.
[43] Y. Fujimaki, E. Thorhauer, Y. Sasaki, P. Smolinski, S. Tashman, and F. H. Fu, "Quantitative in Situ Analysis of the Anterior Cruciate Ligament," *Am. J. Sports Med.*, vol. 44, no. 1, pp. 118–125, 2016.
[44] G. Tajima *et al.*, "Morphology of the tibial insertion of the posterior cruciate ligament," *J. Bone Jt. Surg. - Ser. A*, vol. 91, no. 4, pp. 859–866, 2009.
[45] K. H. Schmidt and W. R. Ledoux, "Quantifying ligament cross-sectional area via molding and casting.," *J. Biomech. Eng.*, vol. 132, no. 9, p. 091012, 2010.
[46] W. Han, N. Nerurkar, L. Smith, N. Jacobs, R. Mauck, and D. Elliott, "Multi-scale Structural and Tensile Mechanical Response of Annulus Fibrosus to Osmotic Loading," *Ann. Biomed. Eng.*, vol. 40, no. 7, pp. 1610–1621, 2012.
[47] B. N. Safa, K. D. Meadows, S. E. Szczesny, and D. M. Elliott, "Exposure to buffer solution alters tendon hydration and mechanics," *J. Biomech.*, vol. 61, pp. 18–25, 2017.
[48] A. H. Hoffman, D. R. Robichaud, J. J. Duquette, and P. Grigg, "Determining the effect of hydration upon the properties of ligaments using pseudo Gaussian stress stimuli," *J. Biomech.*, vol. 38, no. 8, pp. 1636–1642, 2005.
[49] J. M. Dorlot, M. Ait Ba Sidi, G. M. Tremblay, and G. Drouin, "Load elongation behavior of the canine anterior cruciate ligament," *J. Biomech. Eng.*, vol. 102, no. 3, 1980.
[50] S. L.-Y. Woo, C. A. Orlando, J. F. Camp, and W. H. Akeson, "Effects of postmortem storage by freezing on ligament tensile behavior," *J. Biomech.*, vol. 19, no. 5, pp. 399–404, 1986.
[51] P. Clavert, J.-F. Kempf, F. Bonnomet, P. Boutemy, L. Marcelin, and J.-L. Kahn, "Effects of freezing/thawing on the biomechanical properties of human tendons," *Surg. Radiol. Anat.*, vol. 23, no. 4, pp. 259–262, 2001.
[52] D. K. Moon, S. L.-Y. Woo, Y. Takakura, M. T. Gabriel, and S. D. Abramowitch, "The effects of refreezing on the viscoelastic and tensile properties of ligaments," *J. Biomech.*, vol. 39, no. 6, pp. 1153–1157, 2006.
[53] S. Pai and W. R. Ledoux, "The shear mechanical properties of diabetic and non-diabetic plantar soft tissue," *J. Biomech.*, 2012.
[54] S. D. Abramowitch and S. L. Woo, "An Improved Method to Analyze the Stress Relaxation of Ligaments Following a Finite Ramp Time Based on the Quasi-Linear Viscoelastic Theory," *J. Biomech. Eng.*, vol. 126, no. 1, p. 92, 2004.

[55] T. J. A. Mommersteeg, L. Blankevoort, R. Huiskes, J. G. M. Kooloos, and J. M. G. Kauer, "Characterization of the mechanical behavior of human knee ligaments: A numerical-experimental approach," *J. Biomech.*, vol. 29, no. 2, pp. 151–160, 1996.
[56] L. Blankevoort, J. H. Kuiper, R. Huiskes, and H. J. Grootenboer, "Articular contact in a three-dimensional model of the knee," *J. Biomech.*, vol. 24, no. 11, 1991.
[57] H. B. Henninger, S. A. Maas, J. H. Shepherd, S. Joshi, and J. A. Weiss, "Transversely isotropic distribution of sulfated glycosaminoglycans in human medial collateral ligament: A quantitative analysis," *J. Struct. Biol.*, vol. 165, no. 3, pp. 176–183, 2009.
[58] J. A. Weiss, J. C. Gardiner, B. J. Ellis, T. J. Lujan, and N. S. Phatak, "Three-dimensional finite element modeling of ligaments: Technical aspects," *Med. Eng. Phys.*, vol. 27, no. 10, pp. 845–861, 2005.
[59] M. A. Baldwin, P. J. Laz, J. Q. Stowe, and P. J. Rullkoetter, "Efficient probabilistic representation of tibiofemoral soft tissue constraint," *Comput. Methods Biomech. Biomed. Engin.*, vol. 12, no. 6, pp. 651–659, 2009.
[60] J. Wismans, F. Veldpaus, J. Janssen, A. Huson, and P. Struben, "A three-dimensional mathematical model of the knee-joint," *J. Biomech.*, vol. 13, no. 8, pp. 677,679-681,685, 1980.
[61] J. Shin, N. Yue, and C. Untaroiu, "A Finite Element Model of the Foot and Ankle for Automotive Impact Applications," *Ann. Biomed. Eng.*, vol. 40, no. 12, pp. 2519–2531, 2012.
[62] K. M. Hamdia, M. Marino, X. Zhuang, P. Wriggers, and T. Rabczuk, "Sensitivity analysis for the mechanics of tendons and ligaments: investigation on the effects of collagen structural properties via a multiscale modelling approach.," *Int. j. numer. method. biomed. eng.*, no. April, p. e3209, 2019.
[63] L. Li *et al.*, "Using value of information methods to determine the optimal sample size for effectiveness trials of alcohol interventions for HIV-infected patients in East Africa," *BMC Health Serv. Res.*, vol. 18, no. 1, pp. 1–9, 2018.
[64] N. M. Laird, M. C. Weinstein, and W. B. Stason, "Sample-size estimation: a sensitivity analysis in the context of a clinical trial for treatment of mild hypertension," *Am. J. Epidemiol.*, vol. 109, no. 4, 1979.
[65] K. S. Sung and J. M. Park, "Acute ankle sprains," *Arthrosc. Orthop. Sport. Med.*, vol. 3, no. 1, pp. 11–17, 2016.
[66] B. R. Waterman, P. J. Belmont, K. L. Cameron, T. M. Deberardino, and B. D. Owens, "Epidemiology of ankle sprain at the United States Military Academy.," *Am. J. Sports Med.*, vol. 38, pp. 797–803, 2010.
[67] R. F. Wallace, M. M. Wahi, M. A. J. O. T. Hill, and A. B. Kay, "Rates of Ankle and Foot Injuries in Active-Duty U . S . Army Soldiers , 2000 – 2006," vol. 176, no. March, pp. 2000–2006, 2011.
[68] L. Bulathsinhala, M. P. H. O. T. Hill, D. E. Scofield, T. F. Haley, and J. R. Kardouni, "From Service in US Army Soldiers," vol. 45, no. 6, pp. 477–484, 2015.
[69] J. Suyama *et al.*, "Comparison of Public Safety Provider Injury Rates," vol. 3127, 2009.
[70] S. Shah, A. Thomas, J. Noone, C. M. Blanchette, and E. A. Wikstrom, "Incidence and Cost of Ankle Sprains in United States Emergency Departments," vol. 8, no. 6, pp. 547–552, 2016.
[71] M. M. Gosselin, J. A. Haynes, J. J. McCormick, J. E. Johnson, and S. E. Klein, "The Arterial Anatomy of the Lateral Ligament Complex of the Ankle: A Cadaveric Study,"

Am. J. Sports Med., vol. 47, no. 1, pp. 138–143, 2019.
[72] C. Frank, S. L.-Y. Woo, D. Amiel, F. Harwood, M. Gomez, and W. Akeson, "Medial collateral ligament healing: A multidisciplinary assessment in rabbits," *Am. J. Sports Med.*, vol. 11, no. 6, pp. 379–389, 1983.
[73] B. W. Oakes, "Acute soft tissue injuries: nature and management," *Aust. Fam. Physician*, vol. 10, no. 7 Suppl, 1981.
[74] J. A. Weiss, S. L. Woo, K. J. Ohland, S. Horibe, and P. O. Newton, "Evaluation of a new injury model to study medial collateral ligament healing: Primary repair versus nonoperative treatment," *J. Orthop. Res.*, vol. 9, no. 4, pp. 516–528, 1991.
[75] C. Frank, D. Mcdonald, and N. Shrive, "Collagen Fibril Diameters in the Rabbit Medial Collateral Ligament Scar: A Longer Term Assessment," *Connect. Tissue Res.*, vol. 36, no. 3, pp. 261–269, 1997.
[76] S. L. Y. Woo, S. D. Abramowitch, R. Kilger, and R. Liang, "Biomechanics of knee ligaments: Injury, healing, and repair," *J. Biomech.*, vol. 39, no. 1, pp. 1–20, 2006.
[77] C.-Y. Lin, Y.-W. Shau, C.-L. Wang, H.-M. Chai, and J.-H. Kang, "Quantitative evaluation of the viscoelastic properties of the ankle joint complex in patients suffering from ankle sprain by the anterior drawer test," *Knee Surgery, Sport. Traumatol. Arthrosc.*, vol. 21, no. 6, pp. 1396–1403, 2013.
[78] H. Tropp, "Commentary: Functional Ankle Instability Revisited," *J. Athl. Train.*, vol. 37, no. 4, 2002.
[79] M. A. Freeman, "Instability of the foot after injuries to the lateral ligament of the ankle," *J. Bone Joint Surg. Br.*, vol. 47, no. 4, 1965.
[80] A. Miller and S. M. Raikin, "Lateral Ankle Instability," *Oper. Tech. Sports Med.*, vol. 22, no. 4, pp. 282–289, 2014.
[81] J. de Vries, R. Krips, I. Sierevelt, and L. Blankevoort, "Interventions for treating chronic ankle instability," *Cochrane Database Syst. Rev.*, no. 4, 2006.
[82] J. A. Buckwalter and T. D. Brown, "Joint Injury , Repair , and Remodeling," no. 423, pp. 7–16, 2004.
[83] D. Blalock, A. Miller, M. Tilley, and J. Wang, "Clinical Medicine Insights : Arthritis and Musculoskeletal Disorders Joint Instability and Osteoarthritis," pp. 15–23, 2015.
[84] T. Onur, R. Wu, S. Chu, W. Chang, H. Kim, and A. Dang, "JointInstabilityPosttraumaticOsteoarthritisMouseModel.pdf." 2013.
[85] "Osteoarthritis," *National Institutes of Health*, 2016. [Online]. Available: https://www.niams.nih.gov/health-topics/osteoarthritis.
[86] F. Galbusera *et al.*, "Material Models and Properties in the Finite Element Analysis of Knee Ligaments: A Literature Review," *Front. Bioeng. Biotechnol.*, vol. 2, no. November, pp. 1–11, 2014.
[87] A. Beurner, W. L. W. Van Hemert, B. A. Swierstra, and L. E. Jasper, "A Biomechanical Evaluation of the Tibiofibular and Tibiotalar Ligaments," *Foot Ankle Int.*, pp. 426–429, 2003.
[88] E. C. Schmidt, M. Chin, J. T. Aoyama, T. J. Ganley, K. G. Shea, and M. W. Hast, "Mechanical and Microstructural Properties of Pediatric Anterior Cruciate Ligaments and Autograft Tendons Used for Reconstruction," *Orthop. J. Sport. Med.*, pp. 1–12, 2019.
[89] J. A. Weiss and L. E. Paulos, "Mechanical testing of ligament fixation devices," *Tech. Orthop.*, vol. 14, no. 1, pp. 14–21, 1999.
[90] B. Nie, J. L. Forman, M. B. Panzer, A. R. Mait, J. P. Donlon, and R. W. Kent, "Fiber-

based modeling of in situ ankle ligaments with consideration of progressive failure," *J. Biomech.*, vol. 61, pp. 102–110, 2017.
[91] J. H. Wang *et al.*, "Measurement of the end-to-end distances between the femoral and tibial insertion sites of the anterior cruciate ligament during knee flexion and with rotational torque," *Arthrosc. - J. Arthrosc. Relat. Surg.*, vol. 28, no. 10, pp. 1524–1532, 2012.
[92] M. Ferretti, M. Ekdahl, W. Shen, and F. H. Fu, "Osseous Landmarks of the Femoral Attachment of the Anterior Cruciate Ligament: An Anatomic Study," *Arthrosc. J. Arthrosc. Relat. Surg.*, vol. 23, no. 11, pp. 1218–1225, 2007.
[93] M. Noguchi, T. Kitaura, K. Ikoma, and Y. Kusaka, "A method of in-vitro measurement of the cross-sectional area of soft tissues, using ultrasonography," *J. Orthop. Sci.*, vol. 7, no. 2, pp. 247–251, 2002.
[94] M. Honal, C. Lovell-Smith, M. Vicari, E. Weitzel, K. Izadpanah, and M. Weigel, "Accurate semiautomatic assessment of ligament length variations from MRI data," *Med. Phys.*, vol. 40, no. 9, 2013.
[95] K. H. Schmidt, "Foot Ligament Mechanical Properties," 2009.
[96] J. a Weiss and J. C. Gardiner, "Computational modeling of ligament mechanics.," *Crit. Rev. Biomed. Eng.*, vol. 29, no. 3, pp. 303–371, 2001.
[97] R. Thein *et al.*, "The ACL Graft Has Different Cross-sectional Dimensions Compared with the Native ACL," *Am. J. Sports Med.*, vol. 44, no. 8, pp. 2097–2105, 2016.
[98] A. F. Anderson, D. C. Dome, S. Gautam, M. H. Awh, and G. W. Rennirt, "Correlation of anthropometric measurements, strength, anterior cruciate ligament size, and intercondylar notch characteristics to sex differences in anterior cruciate ligament tear rates," *Am. J. Sports Med.*, vol. 29, no. 1, pp. 58–66, 2001.
[99] M. Dienst *et al.*, "Correlation of intercondylar notch cross sections to the ACL size: a high resolution MR tomographic in vivo analysis," *Arch. Orthop. Trauma Surg.*, vol. 127, no. 4, pp. 253–260, 2007.
[100] D. Chimich, N. Shrive, C. Frank, L. Marchuk, and R. Bray, "Water content alters viscoelastic behaviour of the normal adolescent rabbit medial collateral ligament," *J. Biomech.*, vol. 25, no. 8, 1992.
[101] S. L. Woo, T. Q. Lee, M. A. Gomez, S. Sato, and F. P. Field, "Temperature dependent behavior of the canine medial collateral ligament," *J. Biomech. Eng.*, vol. 109, no. 1, p. 68, 1987.
[102] T. C. Lam, C. G. Thomas, N. G. Shrive, C. B. Frank, and C. P. Sabiston, "The effects of temperature on the viscoelastic properties of the rabbit medial collateral ligament," *J. Biomech. Eng.*, vol. 112, no. 2, pp. 147–152, 1990.
[103] X. Zhang and R. Z. Gan, "Dynamic properties of human stapedial annular ligament measured with frequency-temperature superposition," *J. Biomech. Eng.*, vol. 136, no. 8, pp. 1–7, 2014.
[104] M. L. Williams, R. F. Landel, and J. D. Ferry, "The Temperature Dependence of Relaxation Mechanisms in Amorphous Polymers and Other Glass-forming Liquids," *J. Am. Chem. Soc.*, vol. 77, no. 14, pp. 3701–3707, 1955.
[105] P. Cignoni, M. Callieri, M. Corsini, M. Dellepiane, F. Ganovelli, and G. Ranzuglia, "MeshLab: An open-source mesh processing tool," *6th Eurographics Ital. Chapter Conf. 2008 - Proc.*, pp. 129–136, 2008.
[106] S. Boyé, G. Guennebaud, and C. Schlick, "Least Squares Subdivision Surfaces," *Comput.*

Graph. Forum, vol. 29, no. 7, pp. 2021–2028, 2010.
[107] H. Edelsbrunner and D. G. Kirkpatrick, "On the Shape of a Set of Points in the Plane," vol. I, 1983.
[108] M. Palanca, G. Tozzi, and L. Cristofolini, "The use of digital image correlation in the biomechanical area: a review," *Int. Biomech.*, vol. 3, no. 1, pp. 1–21, 2016.
[109] M. W. Kindig and R. W. Kent, "Characterization of the centroidal geometry of human ribs," *J. Biomech. Eng.*, vol. 135, no. 11, 2013.
[110] V. S. Cheong and A. M. J. Bull, "Short communication A novel specimen-speci fi c methodology to optimise the alignment of long bones for experimental testing," *J. Biomech.*, vol. 48, no. 16, pp. 4317–4321, 2015.
[111] H. Zhao and Z. Wang, "Motion measurement using inertial sensors, ultrasonic sensors, and magnetometers with extended kalman filter for data fusion," *IEEE Sens. J.*, vol. 12, no. 5, pp. 943–953, 2012.
[112] J. A. W. Van Dommelen *et al.*, "Characterization of the Rate-Dependent Mechanical Properties and Failure of Human Knee Ligaments," *SAE Tech. Pap. Ser.*, vol. 1, 2010.
[113] K. M. Quapp and J. A. Weiss, "Material characterization of human medical collateral ligament," *J. Biomech. Eng.*, vol. 120, no. 6, p. 757, 1998.
[114] D. E. Attarian, D. P. Devito, and W. Garrett, "Biomechanical Characteristics of Human Ankle Ligaments," no. December 2014, 1985.
[115] K. M. Pawelec, A. A. White, and S. M. Best, "Viscoelastic Material," in *Bone Repair Biomaterials (second edition)*, 2019, pp. 65–102.
[116] J. McElhaney, " Biomechanics . Mechanical Properties of Living Tissues by Y. C. Fung ," *Med. Phys.*, vol. 9, no. 5, pp. 788–789, Sep. 1982.
[117] S. L. Woo, M. A. Gomez, and W. H. Akeson, "The time and history-dependent viscoelastic properties of the canine medical collateral ligament," *J. Biomech. Eng.*, vol. 103, no. 4, p. 293, 1981.
[118] A. M. Butler, D. Ph, W. R. Walsh, and D. Ph, "Mechanical Response of Ankle Ligaments at Low Loads," pp. 8–12, 2004.
[119] N. Kucher and M. Zarazovskii, "Evaluation of the strenth of unidirectional carbon-fiber-reinforced epoxy laminates," *Strength Mater.*, vol. 38, no. 6, 2006.
[120] C. Bonifasi-lista, S. P. Lake, M. S. Small, and J. A. Weiss, "Viscoelastic properties of the human medial collateral ligament under longitudinal , transverse and shear loading," vol. 23, pp. 67–76, 2005.

APPENDIX A: RELAXATION FUNCTION DEVELOPMENT FOR STANDARD LINEAR MODEL

Mechanical models are often used to describe viscoelastic behavior of materials. In this thesis, the standard linear model (Figure A1) is used, consisting of constant springs E_1 and E_2 and a dashpot η_1. The linear spring undergoes a deformation directly proportional to the load F (i.e., $F = E$) while the dashpot is deformed at a velocity proportional to the load (i.e., $F = \eta\dot{u}$.) For the standard linear model in Figure A1, the following equations can be inferred:

$$\varepsilon = \varepsilon_1 + \varepsilon_2 \qquad (a1)$$

$$\sigma = \sigma_1 + \sigma_2 \qquad (a2)$$

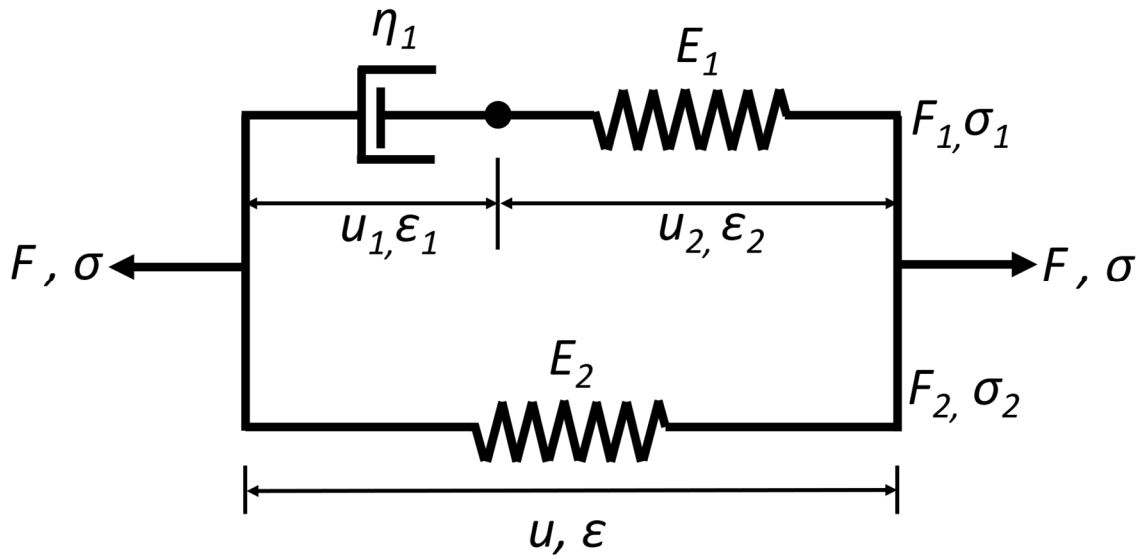

Figure A1: Standard linear model consisting of constant springs E_1 and E_2 with a dashpot η_1. In this configuration displacement (u) and strain (ε) are constant for both parallel units. The force (F) and stress (σ) vary based on the properties of the springs and dashpot.

$$\sigma_2 = E_2\varepsilon \qquad (a3)$$

$$\sigma_1 = E_1\varepsilon_2 = \eta_1\dot{\varepsilon_1} \qquad (a4)$$

By combining equations $(a3)$ and $(a4)$ into $(a1)$ we get

$$\dot{\varepsilon} = \frac{\dot{\sigma_1}}{E_1} + \frac{\sigma_1}{\eta_1} \tag{1}$$

It is also possible to arrange equation $(a2)$ and $(a3)$ to get

$$\sigma_1 = \sigma - \sigma_2 = \sigma - E_2\varepsilon \tag{2.1}$$

$$\dot{\sigma_1} = \dot{\sigma} - E_2\dot{\varepsilon} \tag{2.2}$$

After substituting equation (2.1) and (2.2) into equation (1) we get

$$\dot{\varepsilon} = \frac{\dot{\sigma} - E_2\dot{\varepsilon}}{E_1} + \frac{\sigma - E_2\varepsilon}{\eta_1}$$

Then we can arrange the stress (σ) on one side and the strain (ε) on the other side,

$$\dot{\varepsilon} = \frac{\dot{\sigma}}{E_1} - \frac{E_2\dot{\varepsilon}}{E_1} + \frac{\sigma}{\eta_1} - \frac{E_2\varepsilon}{\eta_1}$$

$$\dot{\varepsilon} + \frac{E_2\dot{\varepsilon}}{E_1} + \frac{E_2\varepsilon}{\eta_1} = \frac{\dot{\sigma}}{E_1} + \frac{\sigma}{\eta_1}$$

$$\frac{E_2\varepsilon}{\eta_1} + \left(1 + \frac{E_2}{E_1}\right)\dot{\varepsilon} = \frac{\dot{\sigma}}{E_1} + \frac{\sigma}{\eta_1} \tag{3}$$

Equation (3) represents the governing equation for a standard viscoelastic model. We can then consider the effects of the unit step function, also known as the Heaviside function, for a constant strain. The Heaviside function is defined as:

$$H(t) = 1 \quad when\, t > 0 \quad and\ \mathrm{H}(t) = 0 \quad when\, t < 0$$

Then under constant strain of magnitude 1 we can write the Heaviside function as:

$$\varepsilon(t) = H(t) \text{ and } \dot{\varepsilon}(t) = \delta(t)$$

where δ(t) is the Dirac delta function, i.e.,

$$\delta(t) = \infty \quad when\, t = 0 \quad and\ \ \delta(t) = 0 \quad when\, t \neq 0$$

The governing equation (3) can be written as follows:

$$\frac{E_2}{\eta_1} H(t) + \left(1 + \frac{E_2}{E_1}\right) \delta(t) = \frac{\dot{\sigma}}{E_1} + \frac{\sigma}{\eta_1} \tag{4}$$

We can rewrite this so that the stress response resembles a differential equation in standard form and consider the behavior of this function for the time before the unit step is applied when $\delta(t) = H(t) = 0$. Under these conditions,

$$\dot{\sigma} + \frac{E_1}{\eta_1} \sigma = (E_1 + E_2)\delta(t) + \frac{E_1 E_2}{\eta_1} H(t) \tag{5}$$

$$\dot{\sigma} + \frac{E_1 \sigma}{\eta_1} = 0$$

The solution to this homogeneous differential equation, and its derivative, is

$$\sigma(t) = A(t)e^{-\frac{E_1}{\eta_1}t} \tag{6}$$

The elastic response function, $A(t)$, can be solved in the following steps

$$\dot{\sigma}(t) = \dot{A}(t)e^{-\frac{E_1}{\eta_1}t} - \frac{E_1}{\eta_1}A(t)e^{-\frac{E_1}{\eta_1}t} \tag{7}$$

We can substitute equations (6) and (7) into equation (5) to get

$$\dot{A}(t)e^{-\frac{E_1}{\eta_1}t} - \frac{E_1}{\eta_1}A(t)e^{-\frac{E_1}{\eta_1}t} + \frac{E_1}{\eta_1}A(t)e^{-\frac{E_1}{\eta_1}t} = (E_1 + E_2)\delta(t) + \frac{E_1E_2}{\eta_1}H(t)$$

$$[\dot{A}(t) - \cancel{\frac{E_1}{\eta_1}A(t)} + \cancel{\frac{E_1}{\eta_1}A(t)}]\, e^{-\frac{E_1}{\eta_1}t} = (E_1 + E_2)\delta(t) + \frac{E_1E_2}{\eta_1}H(t)$$

$$\dot{A}(t) = (E_1 + E_2)\delta(t)e^{\frac{E_1}{\eta_1}t} + \frac{E_1E_2}{\eta_1}H(t)e^{\frac{E_1}{\eta_1}t} \tag{8}$$

Equation (8) can be integrated with respect to time from just before the step strain to the current time step.

$$A(t) = (E_1 + E_2)\int_0^t \delta(t')e^{\frac{E_1}{\eta_1}t'}dt' + \frac{E_1E_2}{\eta_1}\int_0^t H(t')e^{\frac{E_1}{\eta_1}t'}\,dt'$$

$$A(t) = (E_1 + E_2) + \frac{E_1E_2}{\eta_1}\frac{\eta_1}{E_1}\left[e^{\frac{t'E_1}{\eta}}\right]_{t'=0}^{t'=t}$$

$$A(t) = (E_1 + E_2) + E_2\left(e^{\frac{E_1}{\eta_1}t} - 1\right) \tag{9}$$

We can obtain the relaxation function $G(t)$ by substituting equation (9) into equation (6)

$$\sigma(t) = G(t) = \left((E_1 + E_2) + E_2\left(e^{\frac{E_1}{\eta_1}t} - 1\right)\right)e^{-\frac{E_1}{\eta_1}t}$$

$$G(t) = (E_1 + E_2)e^{-\frac{E_1}{\eta_1}t} + E_2\left(1 - e^{-\frac{E_1}{\eta_1}t}\right)$$

$$G(t) = E_2 + (E_1 + E_2 - E_2)e^{-\frac{E_1}{\eta_1}t}$$

$$G(t) = E_2 + E_1 e^{-\frac{E_1}{\eta_1}t} \tag{10}$$

This relaxation function (equation 10) has two major components, the first term (E_2) describes the (time-invariant) relaxation of the parallel component with only the spring while the second term ($E_1 e^{-\frac{E_1}{\eta_1}t}$) describes the time-dependent relaxation of the parallel component with the spring and dashpot (Figure A1). It is also important to consider that when $t \to \infty$ the second term approaches zero and therefore the long term modulus behavior defined by this relaxation function $G(t)$ will be described by E_2.

Additionally, this function can be expanded with additional parallel spring and dashpot components. By adding and tuning these components it is possible to use this model to represent the mechanical properties of the material. Adding additional parallel spring and dashpot components is mathematically equivalent to adding further exponential terms to equation (10). Such a series of decaying exponentials, known as a Prony series, is commonly used to describe the response to a sudden strain sustained over a period of time (i.e. stress/relaxation or ramp and hold). After reviewing some preliminary data, it was determined that a five term Prony series had the fewest terms to provide the best fit to the data presented in this thesis. Therefore, the

schematic of this model can be represented with five parallel components (Figure A2) and represented as the following,

$$G(t) = k_1 e^{-\frac{t}{\eta_1}} + k_2 e^{-\frac{t}{\eta_2}} + k_3 e^{-\frac{t}{\eta_3}} + k_4 e^{-\frac{t}{\eta_4}} + G_\infty$$

Where the eight coefficients $a - l$ represent the spring stiffnesses and dashpot viscosities for each of the parallel components and σ_{min} represents the spring component that determines the long term modulus.

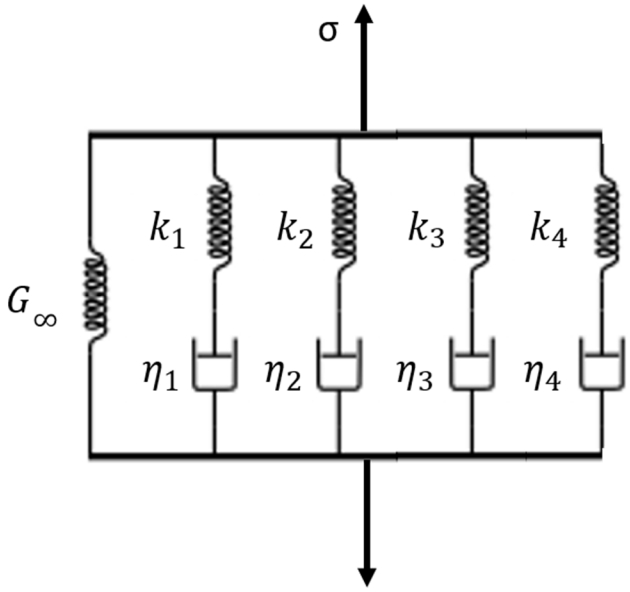

Figure A2: Schematic of the expanded standard linear model with four parallel spring and dashpot elements.

APPENDIX B: CURVE FITTING

The following describes the process by which the modelling coefficients were determined from the collected data. A least squares optimization routine from Matlab's optimization toolbox was used to minimize the final difference between the data and the model. First, an initial guess of the model constants is made in a process often referred to as "seeding the optimizer". This can improve the accuracy of the model fit during optimization.

The model is fit to data from the stress relaxation test which consists of loading to a strain target and sustaining that strain while measuring the load response. The loading response is separated from the relaxation response at t_0 (Figure A 3) and each component is fitted to separate functions.

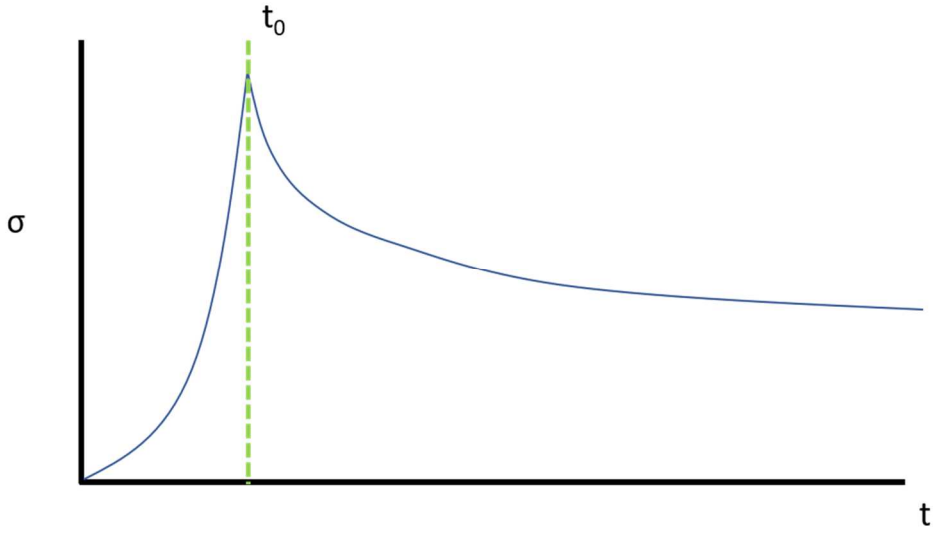

Figure A 3: Generalized stress relaxation response. A strain is applied over a very short period of time (0 to t_0) , and then sustained for a long period (t_0 to t).

The Instantaneous Stress Response

The loading portion of the stress relaxation response is commonly modelled as [31]

$$\sigma(\varepsilon) = A(e^{B\varepsilon} - 1) \tag{1}$$

To start, the time and stress collected from experimental data is normalized. The first attempt at determining the A coefficient was to fit a line to the first and last points in the data set. Therefore, the initial estimate of A is

$$A_{est} = \frac{\sigma_{last} - \sigma_0}{\varepsilon_{last} - \varepsilon_0} \tag{2}$$

To estimate the B coefficient, a log transform was performed on equation 1.

$$e^{B\varepsilon} = \frac{\sigma}{A} + 1$$

$$B\varepsilon = log\left(\frac{\sigma}{A} + 1\right)$$

Since the data is normalized, the slope (A) is approximately 1. Therefore,

$$B_{est} = \frac{log(\sigma_0 + 1)}{\varepsilon_0} \tag{3}$$

Then the least squares function is minimized using the Matlab function *fminunc.* Equations (2) and (3) are applied to the least squares function,

$$min(\sigma_{data} - \left(A_{est}(e^{B_{est}\varepsilon} - 1)\right)^2$$

Relaxation Function

The relaxation function from appendix A is used to model the relaxation response,

$$G(t) = k_1 e^{-\frac{t}{\eta_1}} + k_2 e^{-\frac{t}{\eta_2}} + k_3 e^{-\frac{t}{\eta_3}} + k_4 e^{-\frac{t}{\eta_4}} + G_\infty \tag{3}$$

Note that the exponential constants (η_i) can be adjusted so that one term dominates the function at a specific point in time. As before, the constants are estimated to improve the efficiency of the least square's optimizer.

First, the minimum stress was used to estimate G_∞ and the stress data was corrected by subtracting the minimum stress (σ_{min}) and dividing by the max stress (σ_{max}),

$$\sigma_{corrected} = \frac{\sigma_{data} - \sigma_{min}}{\sigma_{max}}$$

Next, a log transform is then applied to the corrected stress data ($\sigma_{corrected}$) so that the data approximates a linear function, and a line is fit to this transformation. The reciprocal of this slope provides an estimate of the long time behavior (η_4 in equation (3)).

$$Y = log(\sigma_{norm}) = mx + b$$

$$\eta_{4_{est}} = \frac{1}{m}$$

The ligament relaxation response occurs very quickly following the initial strain, requiring short intervals between estimates of the first few constants. The exponential constant of the second term in equation (3) (η_2) was set to the time at which

$$\sigma(t_2) = \sigma_0 e^{-1}$$

$$\eta_{2_{est}} = t_2$$

Where σ_0 is the initial stress at relaxation ($\sigma(t_0)$) and therefore the y-intercept and t_2 is the time at which the measured stress fits this function. The $\sigma(t_2)$ is arbitrarily chosen to represent early relaxation response. However, this time point didn't capture some of the earlier stress behavior and after reviewing the data, 10% of this time was chosen to estimate η_1. The third time coefficient (η_3) was estimated to be halfway between η_2 and η_4.

The leading coefficients (k_i) were estimated to be equivalent,

$$k_i = \frac{e^{\sigma_0}}{4}$$

Equation (3) was updated with estimates of the constant terms (k_1 and η_i) and used in the least squares function

$$min(\sigma_{data} - k_1 e^{-\frac{t}{\eta_1}} + k_2 e^{-\frac{t}{\eta_2}} + k_3 e^{-\frac{t}{\eta_3}} + k_4 e^{-\frac{t}{\eta_4}} + G_\infty)^2$$

APPENDIX C: VISCOELASTIC CONSTITUTIVE MODEL

Appendix B presents the optimization method that was used to determine the model coefficients representing the relaxation and instantaneous stress functions described in Appendices A and B. We can see from the functions outlined in the previous sections that the stress behavior of a viscoelastic material over time is a function of the stress relaxation function and the strain. Using Boltzmann's superposition principle we can generalize these observations by asserting that the stress in a material at a time t, $(t > \tau)$ is dependent on the incremental strain $\Delta\varepsilon$ at a previous time τ ($\tau = t_0, t_1, t_2$, etc.), the stress relaxation over the time $t > \tau$, and the accumulated stress prior to that time $(0 \leq t \leq \tau)$ (Figure A1).

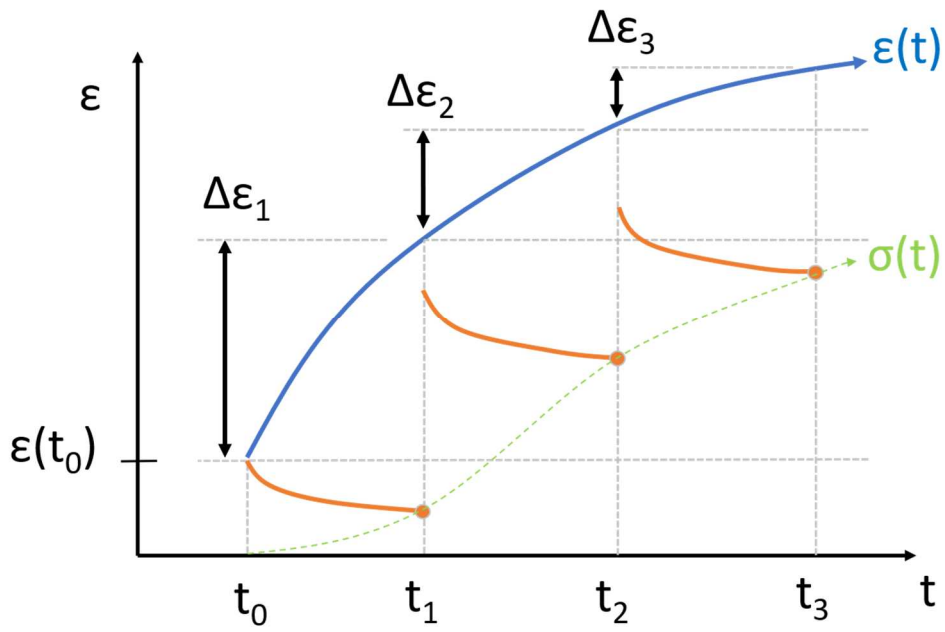

Figure A 4: graphical representation of Boltzmann superposition. As the strain ε(t) (blue line) changes over a time step Δt, the stress $\sigma(t_i\text{-}t_{i-1})$ response over the time period (red line) relaxes. The accumulative stress σ(t) response is then derived (green dotted line).

For the first time point t_0 an initial strain $\varepsilon(0)$ is applied to the material resulting in a nonlinear elastic response that relaxes over that interval $t - t_0$. For each new time step Δt_i, the strain rate $\frac{d\varepsilon}{dt}$ is determined and applied to the next time interval from $t_0 - t_1$. The function describing this behavior for n strain increments can be described as follows:

$$\sigma(t) = \frac{\Delta d\varepsilon_0}{\Delta t_0}|_{t=t_0}\Delta t_0 G(t-t_1)\frac{\Delta\sigma_{ins}(\Delta\varepsilon_0)}{\Delta\varepsilon_0} + \frac{\Delta\varepsilon_1}{\Delta t_1}|_{t=t_1}\Delta t_1 G(t-t_2)\frac{\Delta\sigma_{ins}(\Delta\varepsilon_1)}{\Delta\varepsilon_1} + \cdots$$

$$\sigma(t) = \sum_{i=0}^{n}\frac{\Delta\varepsilon_i}{\Delta t_i}|_{t=t_i}\Delta t_i G(t-t_{i+1})\frac{\Delta\sigma_{ins}(\Delta\varepsilon_i)}{\Delta\varepsilon_i}$$

where $\Delta\sigma_{ins}(\Delta\varepsilon_i)$ is the stress increment produced due to the strain increment $\Delta\varepsilon_i$. Taking the limit as $n \to \infty$ and $\Delta t_i \to 0$, this response can be summarized as the following hereditary integral,

$$\sigma(t) = \int_0^t G(t-\tau)\frac{d\sigma}{d\varepsilon}\frac{d\varepsilon(\tau)}{d\tau}d\,\tau$$

where $G(t-\tau)$ is the relaxation applied over the interval $t-\tau$, and $\frac{d\varepsilon(\tau)}{d\tau}$ is the derivative of the instantaneous stress response function. To illustrate how the function works in practice, recall the relaxation function derived in Appendix A,

$$G(t) = ae^{-\frac{t}{b}} + ce^{-\frac{t}{d}} + ge^{-\frac{t}{h}} + ke^{-\frac{t}{l}} + \sigma_{min}$$

Substituting t for $t-\tau$ to represent the time intervals,

$$G(t-\tau) = ae^{-\frac{t-\tau}{b}} + ce^{-\frac{t-\tau}{d}} + ge^{-\frac{t-\tau}{h}} + ke^{-\frac{t-\tau}{l}} + \sigma_{min}$$

For the instantaneous nonlinear elastic response, a common function was used (Fung, 1967):

$$\sigma_{ins}(\varepsilon) = A(e^{B\varepsilon} - 1)$$

Therefore, the hereditary integral from equation (1) can be re-written as

$$\sigma(t) = \int_0^t \left(ae^{-\frac{t-\tau}{b}} + ce^{-\frac{t-\tau}{d}} + ge^{-\frac{t-\tau}{h}} + ke^{-\frac{t-\tau}{l}} + \sigma_{min}\right)\left(A(e^{B\varepsilon} - 1)\right)\frac{d\varepsilon}{d\tau}\, d\tau$$

where t is the time taken to reach the target strain during a ramp and hold test used to determine the relaxation model $G(t)$ and instantaneous stress model $\sigma_{ins}(\varepsilon)$. The instantaneous stress model is applied over a finite ramp, γ. Therefore, for each time step the measured stress was:

$$\sigma(t) = 2A\gamma\sigma_{min}t_0 e^{\frac{B\varepsilon}{2}} sinh\left(\frac{B\varepsilon}{2}\right) + 2Acd\gamma(e^{\frac{B\varepsilon}{2}-\frac{t}{d}})sinh\left(\frac{B\varepsilon}{2}e^{\frac{t_0}{d}} - 1\right)$$
$$+ 2Agh\gamma(e^{\frac{B\varepsilon}{2}-\frac{t}{h}})sinh\left(\frac{B\varepsilon}{2}e^{\frac{t_0}{h}} - 1\right) + 2Akl\gamma(e^{\frac{B\varepsilon}{2}-\frac{t}{l}})sinh\left(\frac{B\varepsilon}{2}e^{\frac{t_0}{l}} - 1\right)$$
$$+ 2Aab\gamma(e^{\frac{B\varepsilon}{2}-\frac{t}{b}})sinh\left(\frac{B\varepsilon}{2}e^{\frac{t_0}{b}} - 1\right)$$